Aus dem

Department für Augenheilkunde Tübingen
Universitäts-Augenklinik

Shedding light on the immune response to AAV gene therapy

Thesis submitted as requirement to fulfill the degree ,,Doctor of Philosophy" in *Experimental Medicine* (PhD)

at the
Faculty of Medicine
Eberhard Karls Universität
Tübingen

by

Rodríguez Bocanegra, Eduardo David

2022

Dean: Professor Dr. B. Pichler

First reviewer: Professor Dr. M. D. Fischer
Second reviewer: Privatdozent Dr. H. Schmidt

Date of oral examination: 07.06.2022

Dedication

To my parents,

Table of contents

Abbreviations

AAP	assembly activating protein
AAV	adeno-associated virus
ABCA4	ATP-binding cassette transporter 4
ANOVA	analysis of variance
AMD	age-related macular degeneration
AMP	adenosine monophosphate
ATP	adenosine triphosphate
ATP-RO	RO model of ATP-induced retinal damage
BRB	blood-retinal barrier
BSS	balance salt solution
Casp-3	Caspase-3
CD	cluster of differentiation
cDNA	complementary DNA
cgAAV	clinical grade AAV
cGAS	cGMP-AMP synthase
cGMP	cyclic guanosine monophosphate
CMV	cytomegalovirus (promoter)
CNGA3	cyclic nucleotide gated channel subunit alpha 3
CNS	central nervous system
DAMP	damage-associated molecular pattern
DC	dendritic cell
ddPCR	droplet digital PCR
dHS	donated HS
DKK3	dickkopf 3
DNA	deoxyribonucleic acid
DNase I	deoxyribonuclease I
eGFP	enhanced green fluorescent protein
ELISA	enzyme-linked immunosorbent assay
ELM	external limiting membrane
EMA	European Medicines Agency
ETDRS	early treatment diabetic retinopathy study
FACS	fluorescence activated cell sorting
FAF	fundus autofluorescence
FBS	foetal bovine serum
FDA	US Food and Drug Administration
FGFR	fibroblast growth factor receptor
GCL	ganglion cell layer
GLP	good laboratory practice
GMP	good manufacturing practice
HCl	hydrochloric acid
HCP	host cell protein
HEK293	human embryonic kidney 293 (cell line)
HGFR	hepatocyte growth factor receptor
hiFBS	heat-inactivated FBS
hLG3BP	human Galectin-3-binding protein
hPDE6A	human phosphodiesterase 6A subunit
HRF	hyperreflective foci
HS	human serum

HSD	honestly significant difference
HSPG	heparan sulphate proteoglycan
H&E	haematoxylin and eosin
ICC	interclass correlation coefficient
IFN	interferon
IHC	immunohistochemistry
IL	interleukin
INL	inner nuclear layer
IPL	inner plexiform layer
iPSC	induced pluripotent stem cell
IR	infrared
IRBP	interphotoreceptor retinoid-binding protein
IRD	inherited retinal disease
IRF	interferon-regulatory factor
IS	inner photoreceptor segment
ITR	inverted terminal repeat
LamR	laminin receptor
LCA	Leber congenital amaurosis
LOQ	limit of quantification
LPS	lipopolysaccharide
LRAT	lecithin-retinol acyltransferase
MACS	magnetic activated cell sorting
MDA5	melanoma differentiation associated gene-5
MOI	multiplicity of infection
mRNA	messenger RNA
MyD88	myeloid differentiation primary response 88
NDS	normal donkey serum
NF-κB	nuclear factor κB
NFL	nerve fibre layer
NHP	non-human primate
NK cell	natural killer cell
NOD	nucleotide-binding and oligomerization domain
ODN	oligonucleotide
ONL	outer nuclear layer
OPL	outer plexiform layer
ORF	open reading frame
OS	outer photoreceptor segment
PAMP	pathogen-associated molecular pattern
PBS	phosphate buffered saline
PCR	polymerase chain reaction
pDC	plasmacytoid dendritic cell
PFA	paraformaldehyde
PMA	phorbol 12-myristate 13-acetate
polyA	polyadenylation signal
PR	photoreceptors
PRR	pattern recognition receptor
PTM	post-translational modification
qRT-PCR	quantitative real-time PCR
rAAV	recombinant AAV
RDH5	all-trans-retinol dehydrogenase 5

RK	rhodopsin kinase (promoter)
RNA	ribonucleic acid
RO	retinal organoid
RP	retinitis pigmentosa
RPE	retinal pigment epithelium
RPE65	retinoid isomerohydrolase
RT	room temperature
Sf	*Spodoptera frugiperda*
SD	standard deviation
SD-OCT	spectral domain-optical coherence tomography
ss	single stranded
STGD	Stargardt's disease
TBS	tris-HCl buffered saline
TLR	toll-like receptor
TNF	tumour necrosis factor
vg	vector genomes
VP	viral protein
VR	variable region
μRO	RO with microglia cells

List of Tables

List of Figures

1. Introduction

1.1. The retina

The retina is a highly organized and differentiated tissue located in the posterior segment of the eye and it is considered an extension of the central nervous system (CNS)[1]. The central region of the retina is the macula which contains the area with the highest visual acuity, the fovea. The function of the retina is to convert light energy, that enters the eye through the pupil and the lens, into changes in membrane potential and transmit these signals to the brain through the optic nerve.

1.1.1. Anatomy

There are two different compartments in the retina: the retinal pigment epithelium (RPE) and the neural retina. The RPE is bordering the outer parts of the neural retina as a highly polarized single layer of cuboidal epithelial cells. This monolayer functions as the outer blood-retinal barrier (BRB) together with the Bruch membrane and the choriocapillaris. The neural retina can be further divided in 3 main cellular layers that consist of the outer nuclear layer (ONL), the inner nuclear layer (INL) and the ganglion cell layer (GCL), and they are interconnected through synapses (synaptic plexiform layers) located in between these layers (**Figure I.1.**). The cell bodies of the photoreceptors (cones and rods) are densely packed forming the ONL, while the outer and inner segments of the photoreceptors extend from the ONL towards the RPE. The ONL and the photoreceptor segments together form the photoreceptor layer. Between the ONL and the INL there is a synaptic area named outer plexiform layer (OPL) where the synapses of the photoreceptors are formed with the dendrites of bipolar and horizontal cells[2]. These synaptic connections allow the signal transmission from the photoreceptors to second-order neurons of the retina. In the INL reside the cell bodies of interneurons such as horizontal, amacrine, and bipolar cells that are organized into multiple circuits that converge onto the ganglion cells through the inner plexiform layer (IPL). The body of the ganglion cells are contained in the GCL and their axons merge towards the optic nerve forming the nerve fibre layer (NFL)[3]. The retina also contains Müller glia and microglia cells, considered the resident immune cells of the CNS. While the Müller glia span the retina from the

inner to the outer limiting membrane, microglia are typically located in the OPL, and INL[4].

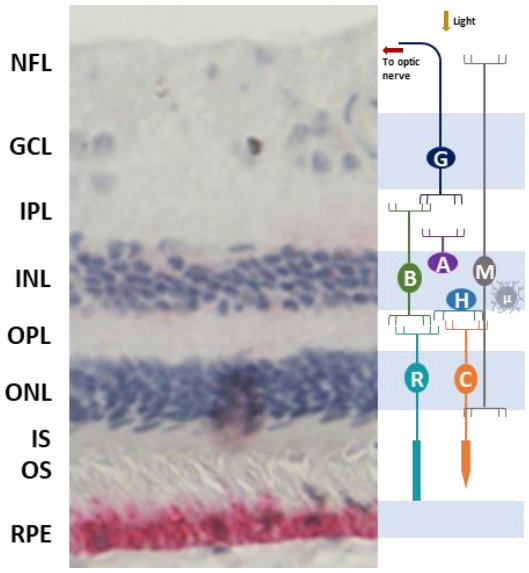

Figure I.1. Sagittal section of the retina layers and schematic representation of its constituent cells. RPE: retinal pigment epithelium; OS: outer segments; IS: inner segments; ONL: outer nuclear layer; OPL: outer plexiform layer; INL: inner nuclear layer; IPL: inner plexiform layer; GCL: ganglion cell layer; NFL: nerve fibre layer; R: rod; C: cone; B: bipolar cell; A: amacrine cell; H: horizontal cell; M: Müller cell; μ: microglia cell; G: ganglion cell.

1.1.2. Function: Phototransduction and the retinoid cycle

One of the principal roles of the photoreceptors is the phototransduction (**Figure I.2.**). This biochemical process enables cones and rods to convert the light stimuli into electrochemical signals which are transmitted into the brain and constitute vision[5]. Rhodopsin, transducin and phosphodiesterase (PDE) are key proteins that mediate the activation of the light responses in the disc membrane of rod photoreceptors' outer segments (OS). Rhodopsin is formed by an 11-*cis*-retinal attached to an opsin and it becomes active by the absorption of a photon. This causes a photoisomerization of 11-*cis*-retinal to all-*trans*-retinal leading to its release from the opsin. Once rhodopsin enters the activated state, it is capable to activate transducin (a heterotrimeric G-protein, G_t), which binds to the C-terminal end of rhodopsin. Likewise, PDE6 is also activated and starts the hydrolysis of cyclic guanosine monophosphate (cGMP) in the cytoplasm leading to the closure of the cGMP-dependent Na^+ channels and the hyperpolarization of the cell. The hyperpolarization of the photoreceptors results in a decrease in the release of glutamate (the neurotransmitter at the photoreceptors' synaptic

terminals), thus transmitting the signal to the brain through the second-order neurons[6].

With the release of the all-*trans*-retinal after light-activation of the rhodopsin the retinoid cycle begins (**Figure I.2.**). This process is another key function that photoreceptors together with RPE cells carry out in order to regenerate the visual chromophore (11-*cis*-retinal) necessary for the phototransduction. To do so, part of the released all-*trans*-retinal is transported from the intradiscal face to the cytosolic face of the photoreceptor's disk membranes by the adenosine triphosphate (ATP)-binding cassette transporter 4 (ABCA4). There, it is reduced to all-trans-retinol and it finds its way into the RPE cell through the interphotoreceptor retinoid-binding protein (IRBP), where it is esterified to all-*trans*-retinyl esters by lecithin-retinol acyltransferase (LRAT). The RPE cells are able to convert back these esters into 11-*cis*-retinol by the retinoid isomerohydrolase (RPE65) and further oxidised into 11-*cis*-retinal by NADPH-dependent all-trans-retinol dehydrogenase 5 (RDH5). The cycle is complete once the 11-cis-retinal finds its way back from the RPE to the photoreceptor OS and recombines with opsins to form rhodopsin[7,8]. In addition to the re-isomerization of all-*trans*-retinal back into 11-*cis*-retinal, the RPE is responsible for the delivery of nutrients such as glucose and fatty acids from the blood to the photoreceptors, but also for the transport of water, metabolic end products and ions from the retina to the blood, while its tight junctions build an important part of the blood retina barrier[8].

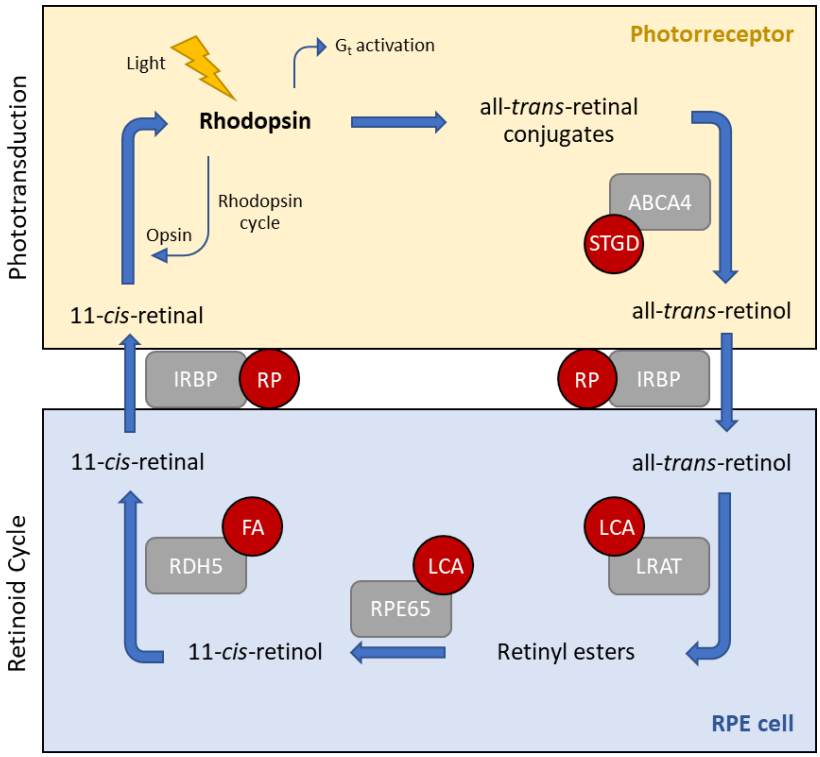

Figure I.2. Phototransduction and retinoid cycle. Red circles represent some inherited retinal diseases caused by mutations in proteins involved in the phototransduction processes and in the retinoid cycle. LCA: Leber congenital amaurosis; RP: retinitis pigmentosa; FA: fundus albipunctatus; STGD: Stargardt's disease.

1.1.3. Gene therapy for inherited retinal diseases

Given the importance of the phototransduction and the retinoid metabolic pathways, it is not unexpected that many types of retinopathies are due to mutations in genes that encode proteins involved in the visual cycle that result in monogenic inherited forms of blindness (**Figure I.2**). Some examples are: mutations in the PDE6 subunits (*PDE6A* and *PDE6B* genes) that cause 2-4% of cases of autosomal recessive retinitis pigmentosa[9]; defects in the *RPE65* gene that cause around 6% of all cases of Leber congenital amaurosis (LCA)[10]; or mutations in the *ABCA4* gene that cause Stargardt's disease (STGD) with an incidence of 1:10.000[11]. These diseases belong to the large group of inherited retinal diseases (IRDs) which are genetically and clinically heterogeneous disorders typically characterized by severe vision loss[12].

For most IRD cases, there is no treatment available and supportive management (low vision aids etc) is considered best practice. Nevertheless, preclinical research and clinical trials are currently underway for several IRD subtypes using

gene therapy[13]. Gene therapy refers to a treatment method that involves delivering nucleic acid-based products such as DNA, RNA or oligonucleotides to a target tissue in order to generate a therapeutic effect. One of the most promising gene delivery system for retinal gene therapy and gene therapy in general are recombinant variants of the adeno-associated viral (AAV) vector.

AAV-mediated retinal gene therapy aims to address the underlying cause of IRDs in which a mutation has induced a dysfunctional protein by exploiting the capacities of AAV viral vectors[14]. For 15 years, IRDs have been an attractive target for AAV-mediated gene therapy as the eye is considered an enclosed compartment and a relatively immune privileged organ due to the blood-retina barrier[15]. This treatment is usually applied either by intravitreal injection or subretinal injection. The intravitreal injection is a minimally invasive procedure whereby the medicinal product is injected into the vitreous cavity and thus can access different tissues of the eye including the retina, and ultimately the systemic circulation[15]. On the other hand, the subretinal injection requires a surgical procedure in which the viral suspension is injected between the photoreceptors and the RPE layer. This is the most common way to deliver the AAV-based treatment in IRDs that are characterized by degeneration of photoreceptors and RPE cells, such as retinitis pigmentosa (e.g. NCT04611503) or LCA (e.g. NCT02781480) among others.

Many clinical studies based on AAV-mediated retinal gene therapy have taken place in the last two decades[15,16]. One of the great successes of gene therapy for IRDs was the approval of the first AAV-mediated gene therapy for RPE65 mutation-associated retinal dystrophies with *voretigene neparvovec* (Luxturna, AAV2-hRPE65v2), by the US Food and Drug Administration (FDA) in 2017[17].

1.2. Adeno-associated virus

Since its discovery in 1965[18], AAVs have become one of the most popular viral vectors in research due to its advantageous features such as transduction efficiency of post-mitotic cells and long-term transgene expression.

1.2.1. Biology and structure of AAV

AAVs belong to the family Parvoviridae and are members of the *Dependoparvovirus* genus[19]. To complete a productive replication cycle, viruses from this genus require coinfection with a helper virus such as an adenovirus[20], and this relationship explains its name “adeno-associated virus”. Wild type AAVs are one of the smallest known viruses (24-26 nm in diameter) and consist of a non-enveloped icosahedral capsid that contains a 4.7 kb long single-stranded DNA genome. Both ends of the AAV genome have identical inverted GC-rich terminal repeats (ITRs) forming a hairpin-shaped secondary structure through its internal palindromic sequence. This results in 145-nucleotide sequences of double-stranded DNA that contain *cis*-elements necessary for productive infection[21,22]. The ITRs flank two open reading frames (ORFs) that encode the *rep* and the *cap* genes for AAV replication and capsid formation, respectively, including the assembly activating protein (AAP). The first ORF, *rep*, encodes four proteins which are involved in genome replication, site specific integration and transcription regulation. The second ORF, *cap*, encodes the three structural proteins that constitute the icosahedral capsid of the AAV: viral protein-1 (VP1), VP2 and VP3 in a 1/1/10 stoichiometric distribution, respectively[23,24]. AAV genes are expressed under the control of three different promoters (p5, p19 and p40) and share a unique polyadenylation signal (polyA).

The capsid dictates the gene delivery properties of the AAV as it contains channels for the release of the viral genome and protrusions with variable regions (VRs). The VRs determine the viral tropism of the AAV serotypes, are responsible for their cell adherence and internalization, and are involved in the immunogenicity of the AAV viral capsids[15,25,26].

1.2.2. The viral cycle

AAVs need cellular attachment factors for the infection. Depending on the serotype, these cellular attachments factors differ from each other. For instance, to attach to the host cell, AAV serotype 8 (AAV8) requires the 37/67-KDa laminin receptor (LamR), while AAV2’s primary receptor is heparan sulphate proteoglycan (HSPG)[27,28]. Once the first attachment is completed, AAVs require a subsequent binding to a cellular co-receptor such as integrin αvβ5, hepatocyte

growth factor receptor (HGFR) or fibroblast growth factor receptor (FGFR) among others, in order to enter the cell[27,29,30]. Upon binding to its respective receptors, AAV is internalized in an endocytic vesicle in the cytoplasm.

AAV stays in the vesicular system until the endosome in which it is contained reaches the perinuclear region of the cell. There, the acidification of the endosomal compartment facilitates the escape of the AAV to the cytoplasm[31]. The AAV particles use the nuclear pores to enter the nucleus of the cell and start the release of the viral genome[32]. However, as noted above, AAV needs a co-infection with a helper virus in the same host cell to complete the viral cycle. When a helper virus is not present, AAV establishes a dormant infection in the host cell by repressing the expression of *rep* genes. Depending on the cell cycle and on the cell type, the AAV genome is either integrated in the host cell DNA[33], specifically on the chromosome 19, or it remains as a circular episome[34]. When a helper virus such as an adenovirus is present and co-infecting the cell, the productive replication of AAV is re-activated. The assembly of the viral proteins of the capsid is assisted by the protein AAP which facilitates the morphogenesis of the capsids in the nucleolus[35]. AAV also uses viral proteins of the helper virus such as E1A (from adenovirus) to initiate the transcription of *rep* genes by activating the AAV promoters[36]. The replication of the viral DNA generates multiple single- and double-stranded (ss, ds)DNA molecules that are subsequently packaged into the viral progeny capsids and used as templates for a constant replication, respectively[37].

1.2.3. Recombinant AAV vectors

Viral vectors are efficient tools to deliver genes of interest into their target cells or tissues. In our case, recombinant AAVs are the most popular viral vectors for retinal gene therapy due to their ability to transduce all key retinal cell populations. Recombinant AAV vectors are obtained by genetic modifications of the wild type AAV viruses. The viral *rep* and *cap* genes are removed and substituted by a transgene cassette, that encodes for a protein of interest, together with a promoter and a polyA signal flanked by the remaining ITRs[38] (**Figure I.3.**). Therefore, the AAV genome loses the capacity of site-specific integration in the DNA of the host cell and for replication even in the presence of a helper virus.

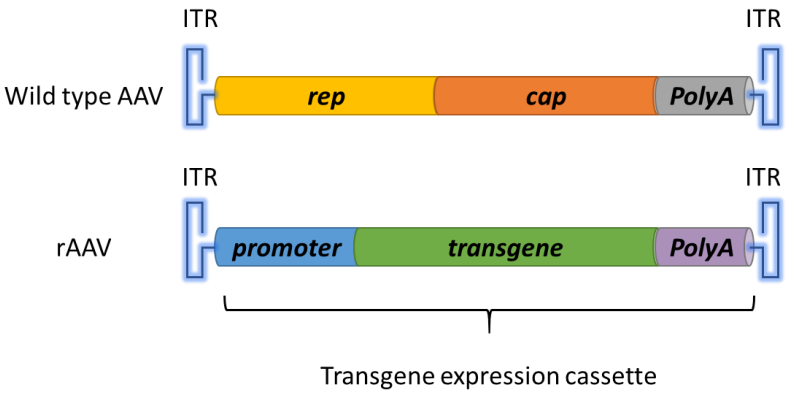

Figure I.3. Genome organization of wild type and recombinant AAVs. Wild type viral genes are replaced by transgene expression cassette.

In order to exploit the different tissue tropism of the wild type AAV serotypes, a cross-packaging or pseudotyping process is required in recombinant AAVs[39]. In this process, a recombinant AAV genome (usually originating from serotype 2) is packaged into a capsid from another AAV serotype. Therefore, the user is able to select the most convenient capsid to target the tissue of interest. In retinal gene therapies for diseases affecting the photoreceptors, the therapeutic transgene cassette can be flanked by the AAV2 ITRs and loaded into a capsid from an AAV8 (denoted as AAV2/8), as serotype 8 has tissue tropism for photoreceptors and such a pseudotype would specifically increase transduction of the photoreceptor target cell population. For example, the study NCT04611503 is a Phase I/II study for the treatment of PDE6A-associated retinitis pigmentosa that uses AAV2/8-hPDE6A as viral vector.

1.2.4. Production systems

One of the challenges for AAV vectors is creating scalable and cost-effective vector production. Currently, there is a growing number of institutions and companies that are using different production platforms to generate AAV vectors for basic research and clinical trials. The production of AAV vectors is mainly based on either transient transfection of mammalian cells with (two or three) expression plasmids or on a permanent infection of insect cells with a recombinant baculovirus (**Figure I.4.**).

The transient plasmid transfection of mammalian cells is the most widely used production platform for AAV viral vectors[40]. This platform builds on the co-

transfection of human embryonic kidney 293 (HEK293) cell line with two or three DNA plasmids[41]. The DNA plasmids contain the components that are required to the production of the AAV: *rep*/*cap* genes, adenoviral-helper genes and the transgene cassette flanked by the ITRs (**Figure I.4.a.** shows the classical approach with 3 plasmids; packaging and helper plasmid sequences are sometimes combined in one plasmid). This approach not only eliminates helper virus contamination in AAV preparations but also increases the adaptability in terms of altering serotype or transgene, and it is suitable for producing clinical grade vectors[42]. However, while the production rate of this production platform has shown to be suitable for early clinical studies and might provide marketable product for limited patient population purposes, the platform's limited scalability remains a serious constraint.

The use of baculoviral vectors in insect cells is an alternative to the use of plasmid transfected mammalian cell lines. This production platform consists on the co-infection of *Spodoptera frugiperda* (*Sf9*) insect cell line with two baculoviral vectors carrying the *rep*/*cap* genes and the transgene cassette flanked by the ITRs (**Figure I.4.b.**). In contrast to the transient plasmid transfection of mammalian cells, this platform has an enormous potential of scalability by the use of bioreactors[43]. Nevertheless, impurities (defined as any component present in the purified AAV vector suspension other than the desired product such as baculoviral DNA or cell lysates[44]) that can be found packaged in the final product, as well as the fact that AAV vectors obtained from this platform may be less potent than mammalian-produced AAV vectors, are two potential limitations of this system[45].

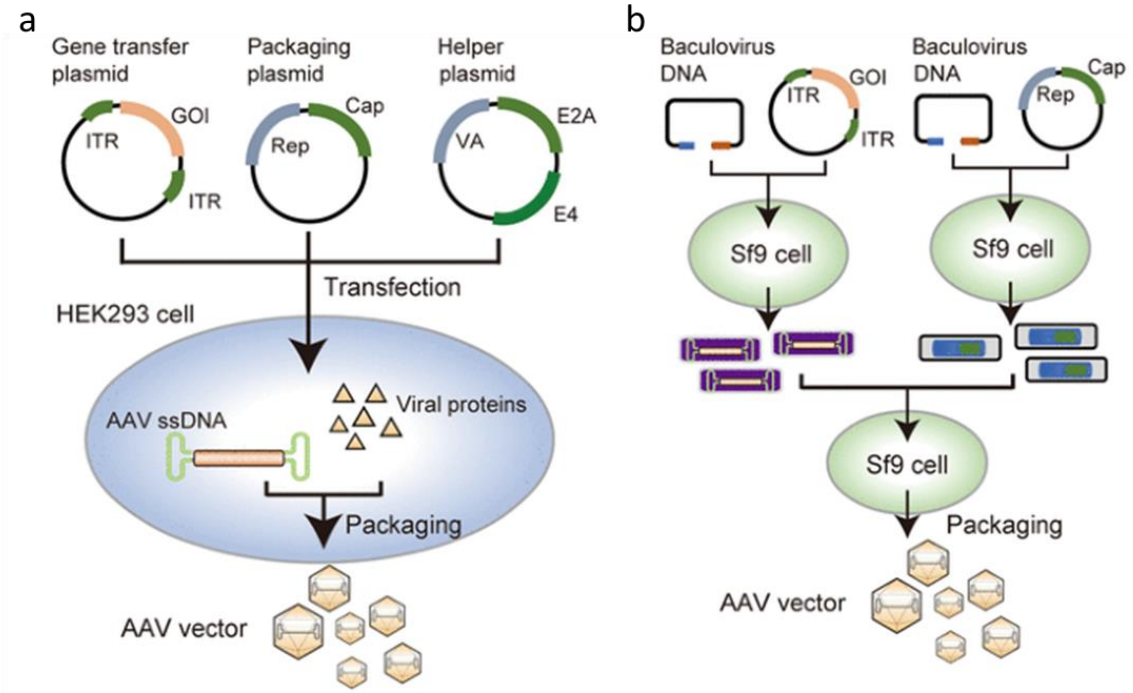

Figure I.4. AAV production systems. (a) Transient triple transfection of HEK293 cells and (b) baculoviral infection of *Sf9* cells. GOI: gene of interest. Adapted from Ohmori et al (2018)[46].

1.3. Immune responses to AAV vectors

Despite the fact that there has been tremendous interest in the development of new AAV-mediated strategies for both basic research and clinical applications over the last decade[47–49], an increasing number of scientists report data indicating immune responses following AAV administration in pre-clinical and clinical studies[15,50–52]

1.3.1. Host innate immune responses against AAV vectors

Innate immunity is considered the first line of defence against infections since it is able to react quickly as it does not require adaption to the pathogens. The detection of pathogen-associated molecular patterns (PAMPs) and damage-associated molecular patterns (DAMPs) by pattern recognition receptors (PRRs) is essential for any innate immune response[53]. Innate immune cells such as monocytes, macrophages, natural killer cells (NK cells), and dendritic cells (DCs) express PRRs, although certain PRRs are also found on adaptive immune cells[54] and even in cells not typically described as immune-competent cells in tissues such as the retina[15,55,56]. When PRRs recognize viral nucleic acids or membrane

glycoproteins, the nuclear factor κB (NF-κB) and interferon-regulatory factor (IRF) are activated. These transcription factors play key roles in the expression of immune mediators such as pro-inflammatory cytokines/chemokines or type I interferons (IFNs), respectively[57], which in turn, are crucial in inflammation and the development of adaptive immune responses[58,59]. Important pro-inflammatory cytokines and chemokines include interleukin-1 (IL-1), IL-6, IL-8, tumour necrosis factor (TNF-α) or macrophage inflammatory protein-1 (MIP-1), which have important roles in the promotion of inflammation, vascular permeability, recruitment of immune cells and antigen presenting cell maturation/activation[60]. On the other hand, biological activities of type I IFNs, specifically IFN-α and IFN-β, include antiviral, antiproliferative and immunomodulatory effects in the host response to viral infection such as enhance of antigen presentation, support the effector functions of viral-specific B and T cells and promote survival activated T cells[61] (**Figure I.5.**).

Toll-like receptors (TLRs) belong to the PRRs group and are transmembrane proteins located on the cell surface or within endosomal compartments. They consist of extracellular/extravesicular domains for the recognition of PAMPs and DAMPs, transmembrane domains and intracellular/intravesical toll-IL-1 receptor (TIR) domains[62]. TLR activation promotes the recruitment of adaptor proteins by the TIR domains like the myeloid differentiation primary response 88 (MyD88), that are needed for downstream signal transduction pathway activation. The primary differences amongst the ten members of the human TLR family (TLR1-10) include ligand selectivity, signal transduction mechanisms, and subcellular location[63]. For instance, TLR2, located on the cell membrane, is a sensor of numerous PAMPs including AAV viral capsid proteins[64]. To determine this, primary human Kupffer cells and liver sinusoidal endothelial cells were stimulated with AAV vectors resulting in an increase of inflammatory cytokines via TLR2 and NF-κB activation. On the other hand, TLR9, located in endosomal compartments, also responds to AAV, not to the capsid, but to the viral DNA[65]. According to Zhu et al. the viral DNA of AAV2 was able to induce the production of type I IFNs by activating the TLR9 pathway in plasmacytoid dendritic cells (pDCs) (**Figure I.5.**). When PAMPs and DAMPs are located in the cytoplasm, they are detected by cytosolic PRRs such as nucleotide-binding and oligomerization domain (NOD)-like receptors (NLRs), absent in melanoma 2 (AIM2)-like receptors (ALRs),

intracellular sensors of DNA like cGMP-AMP synthase (cGAS), retinoic acid-inducible gene I (RIG-I-like) receptors (RLRs) and melanoma differentiation associated gene-5 (MDA5) receptors. Until recently, the role of the cytosolic PRRs in immune responses induced by AAV vectors was not clear (**Figure I.5.**). However recent studies suggest a potential involvement of these receptors in the recognition of the AAV vectors. In a pre-clinical study carried by Reichel et al., a significant upregulation of RLR and AIM2/NLR pathway components was revealed in non-human primates after AAV-mediated retinal gene therapy[50]. In addition, those animals also presented retinal immune infiltrates and retinal inflammation when examined/sectioned at 28 days after AAV vector administration. Shao et al. showed that infection of primary human and mouse hepatocytes with AAV vectors led in late overexpression of MDA5 and RIG-I, as well as enhanced type I IFN expression[66]. In AAV-transduced cells, blocking MDA5 (viral sensors expressed ubiquitously in the cytoplasm) also reduced late type I IFN expression and enhanced transgene expression. Furthermore, investigations of Chandler et al., revealed the involvement of the cGAS receptor showing that this cytosolic PRR decreases the efficacy of AAV transduction in fibroblasts from mouse embryos[67]. They also hypothesised that retinal inflammation following AAV-mediated retinal gene therapy may be related to cGAS activation on retinal microglia cells[68].

Collectively, the release of inflammatory cytokines and type I IFNs by activation of PRRs upon AAV vector stimulation, results in the promotion of adaptive immune responses including capsid/transgene-specific $CD4^+$ and CD8+ T cells as well as capsid-specific antibodies (**Figure I.5.**)[15].

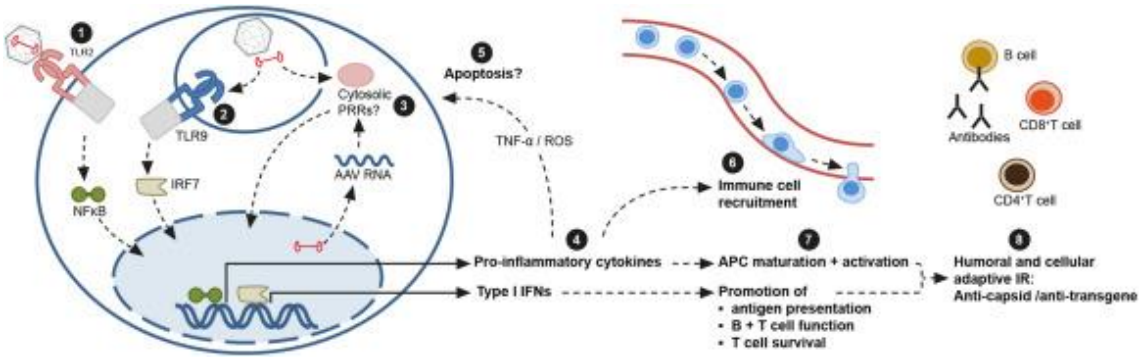

Figure I.5. Innate and adaptive immune responses following the recognition of AAV vector particles. (1) AAV capsid recognition by TLR2. (2) Viral DNA recognition by TLR9. (3) Potential

recognition of viral DNA or RNA from transgene by cytosolic PRRs. (4) Induction of pro-inflammatory-cytokines and type I IFNs. (5) TNF-α and reactive oxygen species-mediated apoptosis. (6) Recruitment of immune cells. (7) Pro-inflammatory cytokines induce activation and maturation of APCs while type I IFNs induces the promotion of antigen presentation, B and T cell functions and survival of activated T cells. (8) Promotion of adaptive immune responses. Obtained from Bucher et al (2020)[15].

1.3.2. AAV vector- and AAV production system-dependent factors that modulate vector immunogenicity

The immunogenicity of AAV vectors, which reflects the interactions of the vector with the host immune system, is probably of the highest importance due to its influence on treatment results and safety. As mentioned above, AAV vectors are constituted by different components such as the viral capsid or the viral DNA, that can potentially trigger an immune response[64,65]. It is known that certain sections of the vector genome, such as the ITR regions' short double-stranded DNA sequences[67], the promoter, and/or the transgenic sequence[69], may also have a unique impact on the immunological response. In addition, after successful transduction, the transgenic RNA[70] and transgene products[71] are another potentially immunogenic components (**Figure I.6.a.**)[15].

Structural variations across serotypes may influence immune responses by changing the vector's antigenic characteristics, tropism, entry mechanism or transduction rate. Different AAV serotypes' protein capsids have structural variations that impact transgene expression and the activation of cellular anti-capsid and anti-transgene immune responses, and those differences in immunogenicity across serotypes have been ascribed to differences in the VP3 capsid protein[72].

Immune responses after AAV application might also be triggered by production system-derived impurities in the vector suspension[15,45]. Components of the culture medium, chemicals used to purify AAV vectors, endotoxins, residual host cell proteins (HCP), residual host cell DNA and residual baculoviral or plasmid DNA are impurities that are routinely checked in clinical grade AAV preparations. On the other hand, because experimental non-clinical grade AAV vectors are not utilized in clinical trials, they are often subject to less stringent quality controls. However, as some of these variables may have a substantial influence on

preclinical outcomes, even non-clinical AAV products are also subject to purification steps to eliminate extra-viral DNA, endotoxins and residual HCPs (**Figure I.6.b.**)[69,73,74].

Another factor that potentially modulate AAV vector immunogenicity is the post-translational modifications (PTMs) present on the AAV capsids due to the production systems (HEK293 or *Sf9*)[45]. Capsids of AAV vectors produced in HEK293 cells, for example, have different PTMs than capsids of AAV vectors produced in *Sf9* insect cells. These differences may result in distinct immunological responses once AAV vectors are applied.

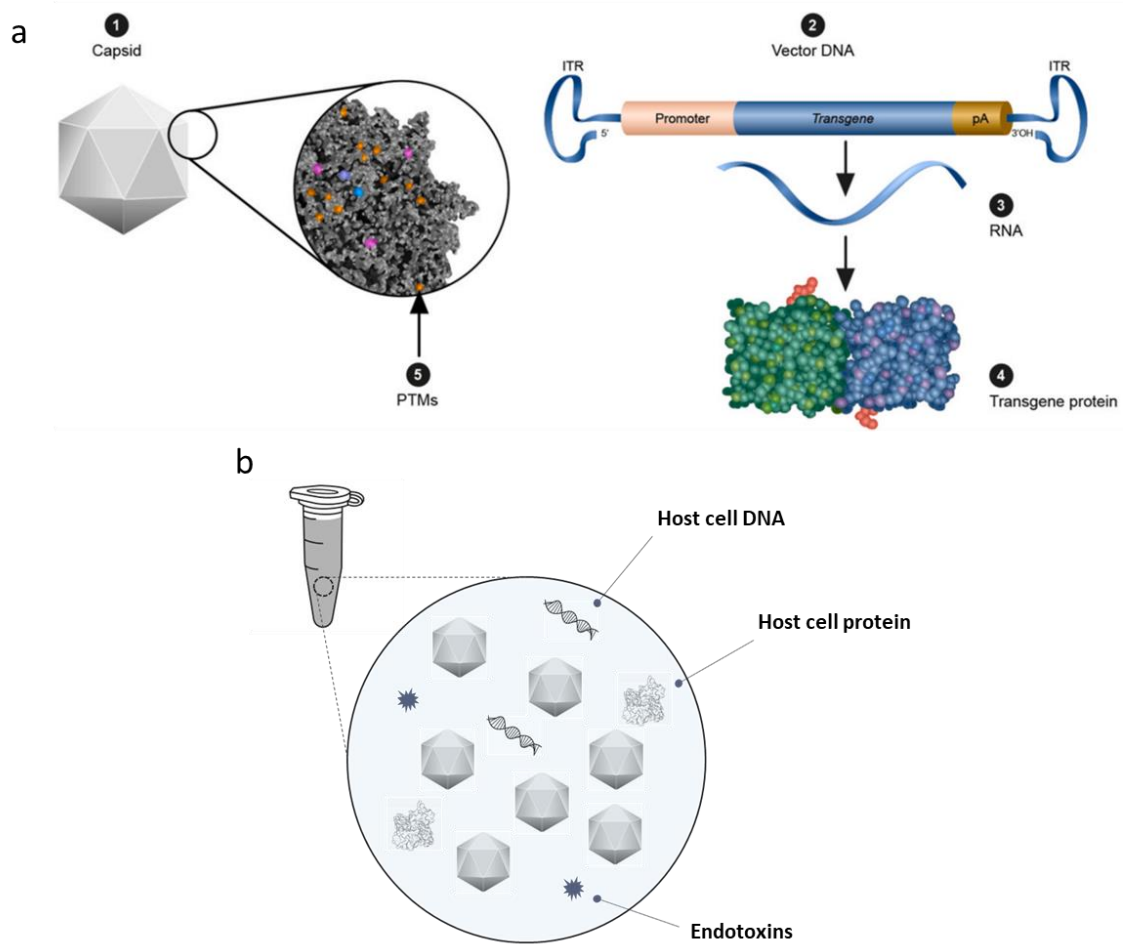

Figure I.6. AAV vector- and AAV production system-dependent factors that modulate vector immunogenicity. (a) AAV vector components that can potentially trigger an immune response: (1) viral capsid, (2) vector DNA, (3,4) Transgene RNA and protein following transduction, and (5) PTMs of the capsid. Obtained from Bucher et al (2020)[15]. (b) Schematic representation of some production system-derived impurities in the AAV vector suspension.

1.4. Models to study immune responses to AAV

In vitro and *in vivo* models are often used by investigators to explore biological responses and processes relevant to human health and disease. These models can range from basic cell-based systems to more sophisticated specialized cells, tissues, organs and living animal models. To investigate immune responses to AAV-mediated gene therapy several *in vitro* and *in vivo* models can be used. For instance, immunocompetent cell models are required to study the vector-dependent factors that may modulate the immunogenicity of AAV. Also, specialized cell types can be used to study the transduction efficiency and potential immune responses to AAV in the target cell or tissue. Ultimately, animal models are employed to determine efficacy and safety of AAV vectors understanding the overall host innate and adaptive immune responses of the organism. Here we introduce different models that may help us to shed light on the immune responses to AAV vectors to improve safety and efficacy of retinal gene therapy

1.4.1. Immunocompetent cell models to study vector-dependent factors that modulate AAV vector immunogenicity

To understand how AAV vectors are recognized by the innate immune system, immunocompetent *in vitro* cell models expressing PRRs are required. Deciphering the receptors and pathways involved in the recognition of either the viral capsid or the viral DNA using these *in vitro* models, could result in potential strategies that might improve the safety of AAV vectors for future gene therapies in humans.

THP-1 cells. Monocytes and macrophages are members of the innate immune system. The THP-1 acute monocytic leukaemia cell line has morphological and functional features similar to primary monocytes. After differentiation with phorbol 12-myristate 13-acetate (PMA)[75] or other stimuli such as 25-dihydroxyvitamin D3 (vD3)[76] or macrophage colony-stimulating factor (M-CSF)[77], THP-1 cells acquire a macrophage-like phenotype. These cells have been used to study immune responses due to their ability to detect foreign pathogens, such as bacteria and viruses, via PRRs and produce pro-inflammatory cytokines and chemokines. For instance, Zaiss et al.[73] showed that complement opsonization of the capsid enhances AAV uptake into differentiated macrophage-like THP-1 cells. Capsid

opsonization was achieved in the presence of serum with active complement. They observed that the enhanced uptake coincided with increased macrophage activation resulting in the promotion of NF-κB-dependent genes such as MIP-1β, MIP-2, IL-1β and IL-8 in a serum-dependent manner.

On the other hand, recognition of weak stimuli by THP-1 cells can be challenging. It has been described that unwanted consequences of THP-1 macrophage *in vitro* differentiation, such as up-regulation of specific genes while PMA incubation, may mask the moderate effect of specific stimuli. As AAV vectors can be considered to have low immunogenicity, optimized THP-1 differentiation protocols are required[75].

Plasmacytoid dendritic cells. Plasmacytoid dendritic cells (pDCs) are a unique subset of dendritic cells that play an important function in antiviral immunity as they are specialised in secreting high levels of type I IFNs upon viral infections. Apart from IFNs, pDCs also secrete pro-inflammatory cytokines and chemokines. The secretion of these immune mediators is mainly mediated through the activation of the double stranded (ds)DNA receptor, TLR9[78]. The use of pDCs as immunocompetent *in vitro* cell model has allowed to more accurately study the role of TLR pathways in innate immune responses generated by AAV vectors[65]. Zhu et al. first described the involvement of the TLR9 pathway in the recognition of viral DNA from AAV8 and AAV2 using mouse pDCs[65]. They showed that pre-treatment with the TLR9 antagonist, H154, blocked the induction of pro-inflammatory cytokines and type I IFNs upon AAV stimulation.

Although pDCs is the best model to study antiviral innate immunity, it also presents minor limitations such as the limited availability of pDCs in human blood (0.2-0.8% of peripheral blood mononuclear cells)[79], or the poorly transduction efficiency by AAV vectors[80,81].

1.4.2. Retinal cell models to study transduction efficiency and potential immune responses to AAV in the target tissue

To investigate how the target tissue and its constituent cells behave upon AAV infection, *in vitro* models of the target tissue are used due to its high degree of similarity or complexity to the *in vivo* tissue. In case of AAV-mediated retinal gene therapy, *in vitro* models of RPE and neural retina could be used to investigate not

only the transduction efficiency of different recombinant AAV vectors, but also the potential innate immune responses generated by the different retinal cells.

Retinal pigment epithelium. RPE cells have been considered an important regulatory cell within the retina due to its role in maintaining physiological and structural balance in the tissue. *In vitro* cultured RPE cells from either cell lines[82], primary retinal tissue[83] or from induced pluripotent stem cells (iPSC)[84] retain many characteristics found *in vivo*. These cell models can be used to determine the transduction efficiency of AAV vectors. Studies showing the capability of AAV vectors to transduce RPE demonstrated that RPE cells were the preferred target of AAV2/5 and AAV5/5, as well as the primary target of AAV2/1[85]. Thereafter, novel capsids have been developed in order to increase the transduction efficiency of AAV in RPE cells such as AAV2-7m8, which resulted to be more efficient than the other AAV vectors tested under identical conditions[86].

However, the nature of the RPE cells that sense AAV vectors and initiate innate immune responses is still unknown. It is thought that the RPE may play an important role in innate and adaptive immune responses in the retina to invading organisms and potentially to AAV-derived antigens as they express different TLRs (TLRs 1-7, 9 and 10)[55]. In addition, it has been reported that RPE cells act as antigen presenting cells in the retina expressing MHC class II in ocular inflammation[87].

On the other hand, as it is an artificial system, RPE cell models also have clear drawbacks. As cultured cells lack their natural microenvironment, they might initiate cell cycle, differentiation and apoptosis[82], which could also have an impact when analysing results after AAV transduction.

Retinal organoids. Apart from RPE, the development of a physiologically appropriate *in vitro* model capable of mimicking the biology of the human neural retina is also important to study how this tissue responds to AAV vectors. Retinal organoids (ROs) are structures that mimic primitive optic vesicle-like structures with retinal layering similar to that seen *in vivo*[88,89], for that reason ROs can be used to investigate the efficacy, kinetics and cell tropism of different serotypes of AAV vectors[90].

Innate immune receptors such as TLRs are also known to be expressed in the cells that constitute the neural retina. This indicates that the innate immune response to AAV vectors could be activated by a variety of retinal cell types:

ganglion cells, amacrine cells, horizontal cells, bipolar cells, Müller glia, and photoreceptors[91–93]. In addition, these cells types are also present in ROs, making the use of this complex *in vitro* model potentially useful for studying innate immune responses to AAV.

The main current limitations of ROs for modelling and treating IRDs are the absence of vasculature[94], the lack of RPE monolayer around the RO and its interaction with the photoreceptors[95] and the lack of bone marrow derived/tissue resident immune cells[96]. However, recent studies demonstrate that these drawbacks can be addressed. For instance, Achberger et al. demonstrated for the first time that by merging ROs and organ-on-a-chip technology it is possible to provide vasculature-like perfusion to the organoids[88]. Akhtar et al. showed that by co-culturing ROs with RPE cells the differentiation of the photoreceptors present in the RO can be accelerated[97]. An also, Chichagova et al. has shown that by applying microglia cells to the ROs the immune function is enhanced[98].

1.4.3. Non-human primates to study efficacy and safety of AAV vectors.

Animal models, ranging from small animals such as mice or rats to large animals such as pigs or non-human primates (NHPs), are being explored for AAV-mediated retinal gene therapy. These animal models are used to investigate the biodistribution, cell tropism, and transduction efficiency of AAV vectors, as well as to test alternative surgical techniques and administration routes and to investigate dosage thresholds and vector-induced immune response and toxicity[15].

Because only primates have a macula[99], NHP models are critical not only for elucidating biological mechanisms behind vision, but also for developing AAV-mediated retinal gene therapy treatments. Therefore, the NHP eye is the most appropriate model to investigate a response to a new AAV product in the absence of specific disease criteria. On the other hand, natural occurring or engineered mutations have provided useful other animal models (e.g. canines and rodent) for proof of concept studies. Before proceeding to clinical trials in humans, surgical techniques, dosing and the efficacy of AAV vectors to transduce different retinal neurons may be thoroughly examined in NHPs[100]. Furthermore, another advantage of the use of NHPs for ocular gene therapy is the availability of ocular phenotyping tools which provide remarkable insight into the retinal condition in

living NHPs. For instance, spectral-domain optical coherence tomography (SD-OCT) is routinely used as it is a technique that provides transversal optical imaging of the retina, enabling the assessment of tolerability/safety of AAV-mediated retinal gene therapies[50,52,100].

In order to enhance the success of clinical trials, safety of AAV-mediated retinal gene therapy is crucial. In the last few years, pre-clinical studies on NHPs showed that innate and adaptive immune responses to AAV-mediated retinal gene therapy occur in a dose-dependent manner[15]. Intravitreal injections of high AAV vector loads produced inflammation and infiltration of immune cells in the retina of NHPs in two different studies carried out by this group[50,52]. Apart from this, many other phenotypic characteristics of ongoing immune responses are also found in the retina of NHPs after delivery of AAV vectors, such as RPE cell degeneration, persistent choroidal inflammation[101], cell infiltration in the vitreous and aqueous humor chambers[102] and loss of retinal thickness[15,103].

The absence of specialized models that adequately reproduce most human conditions, particularly for retinal disorders, is a current drawback of NHPs. As a result, researchers are already investigating well-defined NHP models of IRDs[104] that will serve as a therapeutic testing ground for the treatment of disorders such as achromatopsia using AAV-retinal gene therapy.

1.5. Aim of the project

The general aim of this thesis is to help fill in in the knowledge gaps regarding the innate immune responses to AAV vector- and AAV production system-dependent factors that modulate vector immunogenicity. This is done by investigating the participation of several lots of the same AAV vector from different production systems and manufacturers combined with the use of relevant research models.

Thus, the specific aims of the thesis include the study of:

- potential differences in the innate immune response to experimental HEK293- and *Sf9*-produced AAV vector lots using different immunocompetent cell models.
- immune responses to different PRR ligands and immunogenic AAV vector lots in different retinal cell models.

- hyper-reflective foci in the NHP retina as a potential marker for immune responses to clinical grade AAV vector.

In order to achieve these aims, fundamental-research techniques involving basic biochemistry, molecular biology, microscopy, cell culture work and organotypic culturing methodologies have been employed as well as clinical-research analysis and interpretation of SD-OCT and fundus autofluorescence images.

2. Materials and Methods

2.1. AAV vectors and titration assays

The experimental recombinant AAV vectors used in this thesis consisted of eight AAV8 and four AAV2 vector lots. All of them contained exactly the same transgene expression cassette sequence: cytomegalovirus promoter (CMV) and the gene that encodes for the enhanced green fluorescence protein (eGFP). Likewise, the AAV vectors were created from two different production systems: transient transfection of human HEK293 cells and live baculoviral infection of *Sf9* insect cells. They were produced from three different manufacturers: Virovek (CA, USA), Viral Vector Core Facility of the University of Iowa (Iowa, USA) and Vigene Biosciences (MD, USA); and purified using different methods: affinity chromatography, caesium chloride and iodixanol gradient. Exactly the same plasmid (pFB-CMV-GFP, 7122 bp) was used by both University of Iowa and Virovek to manufacture their AAV8 lots. A similar plasmid (pAV-CMV-eGFP, 5030 bp) was used by Vigene in order to produce AAV8.

Another three recombinant clinical grade AAV8 (cgAAV8) vector lots were used in this thesis. All of them contained a rhodopsin kinase (RK) promoter followed by the human *PDE6A* gene. Good manufacturing practice (GMP) was conducted for the production of the cgAAV8 vector lots. Detailed information about residual impurities or endotoxin levels contained in the final vector preparations was given by the manufacturer (**Table M.1.**).

Table M.1. List of clinical grade AAV8-RK-hPDE6A vector lots. BSA: bovine serum albumin; EU: endotoxin units; human Galectin-3-binding protein; LOQ: limit of quantification; vg: vector genomes

Lot number	*cgAAV8 lot 1*	*cgAAV8 lot 2*	*cgAAV8 lot 3*
Titre (vg/ml)	5.9 E+12	6.0 E+12	6.1 E+12
Endotoxin (EU/ml)	<0.015	<0.015	<0.015
Residual BSA protein (ng/ml)	<LOQ (0.25)	< LOQ (0.25)	<LOQ (0.25)
Residual HCP (hLG3BP) -HEK293 protein (ng/ml)	36.9	1433.7	582
Residual Benzonase (ng/ml)	<LOQ (0.2)	< LOQ (0.2)	<LOQ (0.2)
Residual cell DNA Albumin (ng/ml)	< LOQ (< 1.3)	< LOQ (2.5)	< LOQ (3.9)

2.1.2. Titration of AAV capsid particles

The number of capsid particles of the experimental AAV8 and AAV2 vector lots was determined by enzyme-linked immunosorbent assays (ELISA) using AAV8 titration ELISA kit or AAV2 titration ELISA kit (Progen Biotechnik GmbH, Heidelberg, Germany). First of all, the AAV vector lots were diluted with assay buffer so that they could be quantified within the ELISA range. Then, 100 µl of serial diluted standard and samples were transferred to the wells of the ELISA plate and incubated for 1 hour at 37˚C. After that, another 100 µl of the biotin conjugate was added to the wells and incubated at 37˚C for 1 hour, followed by 100 µl of streptavidin conjugate (1 hour, 37˚C) and 100 µl of substrate solution (15 minutes at room temperature). After adding 100 µl of stop solution (2N sulfuric acid), absorbance was quantified using M200 NanoQuant spectrophotometer (Tecan, Männedorf, Switzerland) at 450 nm (650 nm correction wavelength). Results were calculated using GraphPad Prism (version 8.0.0, GraphPad Software, San Diego, CA, USA) by applying a 4-parameter logistic (4PL) regression model.

2.1.3. Droplet digital PCR

To re-quantify the vector genome (vg) numbers of the purchased AAV vectors accurately, side-by-side measurements were carried out using droplet digital PCR (ddPCR). Using their given titres as reference, AAV vector lots were diluted in order to be quantified by the system (1:500,000 approximately). In order to ensure consistent results, two different master mixes were prepared with two pairs of primers and probes (CMV and eGFP assays). The mixes were assembled with 10 µl ddPCR Supermix (Bio-Rad, Hercules, CA, USA), 5 µl TaqMan primers and probes (Applied Biosystems, Foster, CA, USA) (final concentrations of 10 µM), and 5 µl template in a volume of 20 µl. The sequences of the primers/probe of the CMV assay were: Forward 5′- GCACCAAAATCAACGGGACT -3′; Reverse 5′- CTCCCACCGTACACGCCTAC -3′; and Probe 5′- 6FAM-AATGTCGTAACAACTCCG-MGB -3′. The sequences of the primers/probe of the eGFP assay were: Forward 5′- GGAGCGCACCATCTTCTTCA -3′; Reverse 5′- CAGGGTGTCGCCCTCGA -3; and Probe 5′- 6FAM- CTACAAGACCCGCGCCGAGGTG-MGB -3).

With the assistance of Luise Luib from the Department of Paediatrics (University Children's Hospital, Tübingen), the mixes were loaded into the wells of disposable cartridges (Bio-Rad). After adding the droplet generator oil (Bio-Rad), the cartridges with the samples were loaded into the droplet generator machine (Bio-Rad). Then, the droplets were transferred to a 96-well PCR plate, sealed, and amplified (95˚C for 10 minutes, followed by 40 cycles of 94˚C for 30 seconds, 56˚C for 1 minute, and 72˚C for 15 seconds followed by a final 98˚C heat treatment for 10 minutes). The plate was scanned by a QX100 droplet reader (Bio-Rad). Results were analysed with QuantaSoft software (Bio-Rad) and GraphPad Prism (GraphPad Software).

2.2. PRR ligands and antagonists

To evaluate the presence of the main PRRs in our cell models, several validated PRR ligands were purchased from Invivogen (San Diego, CA, USA). The following PRR were tested with: 1 μg/ml PAM3CSK4 for TLR2, 10 μg/ml Poly(I:C) for TLR3, 10 ng/ml lipopolysaccharide (LPS) for TLR4, 5 μg/ml imiquimod for TLR7, 100 μg/ml of a benzoazepine analog (TL8-506) for TLR8, 0.77 μM class A CpG oligonucleotide (ODN; ODN2216) and 5 μM class B CpG ODN (ODN2006) for TLR9, 1 μg/ml Poly(I:C)/LyoVec for RIG1/MDA5, 10 ng/ml LPS + 5 mM ATP for NLRP3 inflammasome and 500 ng/ml dsDNA for cGAS. To block TLR9 pathway, 50 μM phosphorothioate-stabilized of TLR9 antagonist ODN H154 was tested (5′-CCTCAAGCTTGAGGGG-3′; Biomers.net, Ulm, Germany).
For experiments using retinal organoids, PRR ligands were used at different concentrations than above: 10 ng/ml PAM3CSK4, 10 μg/ml LPS, and 10 μM ODN2216.

2.3. Cell lines and stimulation procedure

2.3.1. THP-1 cells and TLR2 KO THP-1 cells

THP-1 monocyte cell line was purchased from ATCC (Manassas, VA, USA) and TLR2 KO THP-1 cells were donated by Alexander Weber from the Immunology department (University of Tübingen, Tübingen). Cells were cultured in "THP-1 medium" consisting on RPMI 1640 (Sigma-Aldrich, San Luis, MO, USA)

supplemented with 10% heat-inactivated foetal bovine serum (hiFBS; Gibco, Thermo Fisher Scientific, MA, USA), 1% GlutaMAX (Gibco) and 1% penicillin/streptomycin (P/S; Gibco). Medium was replaced 2 times per week. Cells were maintained in the incubator at 5% CO2, 37°C.

Before stimulation experiments, cells were seeded at a density of $5x10^4$ cells/well in 96-well plates (Corning, New York, NY, USA) and differentiated with phorbol 12-myristate 13-acetate (PMA; Sigma-Aldrich, St. Louis, MO, USA) at a concentration of 100 nM in THP-1 medium. After 48 hours, medium was replaced by fresh THP-1 medium without PMA and cells were kept in the incubator for 24 hours. The following day, cells were checked to confirm adherence and used for further stimulation experiments with either PRR ligands/antagonists or AAV vectors.

For stimulation experiments using PRR ligands/antagonists, PMA-differentiated THP-1 cells were stimulated with the above mentioned PRR ligands. Supernatant was collected from the wells after 24 hours in order to analyse the release of inflammatory cytokines and chemokines.

For stimulation experiments using AAV vectors, PMA-differentiated THP-1 cells were stimulated with AAV8 vector lots 1-8 using a multiplicity of infection (MOI) of $1:1x10^6$ vg in THP-1 medium containing 10% human serum (HS; Sigma-Aldrich). Cells were incubated for 24 hours followed by eGFP fluorescence check using an Axioplan2 imaging fluorescent microscope (Zeiss, Oberkochen, Germany) and supernatant collection.

2.3.2. HEK293T cells

HEK293T cell line (CRL-3216™, ATCC) was donated by Sally Williamson from the Institute for Ophthalmic Research (University of Tübingen, Tübingen). Cells were cultured in DMEM GlutaMAX-I (Gibco) supplemented with 10% hiFBS and 1% P/S. Medium was replaced 2-3 times per week. Cells were maintained in the incubator at 5% CO2, 37°C.

HEK293T cells were used in experiments to analyse transduction efficiency of AAV vectors. A density of $2x10^4$ cells/well were seeded in 96-well plates and incubated 24 hours in the incubator. When the cells reached 70-80% confluence of the plate, they were stimulated with different lots of AAV8 (MOI: $1:1x10^4$ vg) or with AAV8 lots pre-treated with deoxyribonuclease I -DNase I- (100 µg/ml, 37°C,

30 minutes; Stemcell). eGFP expression was monitored at 24, 48 and 72 hours after transduction using the Axioplan2 imaging fluorescent microscope followed by the quantification of the transduction rate by flow cytometry (FACSCantoTM II, Becton Dickinson Bioscience, NJ, USA).

2.4. Isolation of human pDCs and stimulation procedure

Human pDCs were obtained from buffy coats of healthy young donors from the Centre for Clinical Transfusion Medicine (University of Tübingen, Tübingen) after approval by the local ethics board of the University Hospital Tübingen. Peripheral blood mononuclear cells (PBMCs) were isolated using Ficoll density gradient centrifugation (Ficoll-Paque; GE Healthcare, Uppsala, Sweden) for 35 minutes at 400xg. pDCs were purified from PBMCs by magnetic activated cell sorting (MACS) by negative selection using biotin-conjugated antibodies and anti-biotin microbeads (Miltenyi Biotec, Bergisch Gladbach, Germany). Flow cytometry was performed by Kirsten Bucher and Kristin Bieber (University of Tübingen, Tübingen) to assess the pDC purity of the protocol. Cells were stained using PE Mouse Anti-Human CD123 and BV421 Mouse Anti-Human BDCA-2 (CD303) antibodies (Becton Dickinson Bioscience). Measurement was performed on a FACSCantoTM II and data were evaluated with FlowJo software.

For each stimulation experiment, pDCs were required to be isolated from buffy coats following the above procedure of negative selection by MACS. Then, pDCs were seeded at $1.25x10^4$ cells/well on 384-well plates (Corning) in medium containing RPMI 1640 supplemented with 10% HS, 1% GlutaMAX, 1% MEM Non-Essential Amino Acids (NEAA; Gibco), 1% Sodium Pyruvate (Gibco) and 1% P/S. After seeding, cells were stimulated with PRR ligands/antagonists or AAV vector lots (MOI: $1:1x10^6$ vg) in side-by-side experiments and were incubated for 18 hours at 5% CO2, 37°C. Cell proliferation and eGFP expression were assessed using the Axioplan2 imaging fluorescent microscope after 18 hours. Supernatants were collected and kept at -80˚C until being used.

pDCs were also stimulated during 18 hours with AAV vectors that were either pre-treated with 100 µg/ml DNase (37°C, 30 minutes) to eliminate potential extra-viral DNA impurities or heat-treated (95°C, 10 minutes) in order to expose the intra-viral DNA to the cells.

2.5. hiPSC-derived retinal cell models and stimulation procedure

2.5.1. hiPSC-RPE

hiPSC-RPE cells were generated by Marius Ader's group from the Centre for Regenerative Therapies (Dresden).

For stimulation experiments, $2x10^5$ hiPSC-RPE cells were seeded into 96-well plates in DMEM-GlutaMAX supplemented with 20% KO serum replacement (Gibco), 1% NEAA, 1 mM L-Glutamine and 0.1 mM β-mercaptoethanol. The cells were incubated at 5% CO2, 37°C and the medium was changed every 2–3 days. After 14 days, when cells reached confluence, hiPSC-RPE cells were stimulated with different PRR ligands (Poly(I:C) and LPS) and AAV8 vector lot 1 (MOI: $1:2.5x10^5$ vg) in medium containing 10% HS instead of 20% KO serum replacement. Supernatants were collected at 3, 12 and 24 hours.

2.5.2. Retinal organoids

hiPSC-derived ROs were generated by Kevin Achberger's group from the Institute of Neuroanatomy (University of Tübingen, Tübingen).

For experiments using ROs, 200±30 days old ROs were transferred into 96-well plates (1 RO/well) and stimulated with different PRR ligands and AAV8 vector lots ($1x10^{12}$ vg/RO). Supernatants were collected at 18 hours, 3, 5 and 7 days after stimulation. Transduction efficiency was also checked under EVOS FL Auto Fluorescence Inverted Microscope (Life Technologies, Carlsbad, CA, USA) at these timepoints.

In order to generate a co-culture model of ROs with microglia cells (μROs), hiPSC-derived retinal microglia cells (expressing mCherry) were produced by Deborah Kronenberg-Versteeg from the Institute for Clinical Brain Research (University of Tübingen, Tübingen) and seeded on top of halved ROs. For stimulation experiments, the same stimulation procedure than above was followed including a new 6 hours timepoint.

To generate a model of retinal cell damage in ROs, different concentrations of ATP (10, 5 and 1 mM; Invivogen) were applied to the ROs. Medium change was performed every day with fresh ATP. Incubation with 2 μM of live cell fluorescent

dye Caspase3/7 (CellEvent™, Thermo Fisher Scientific) was applied to the ROs during 30 minutes in order to monitor apoptosis under EVOS FL Auto Fluorescence Inverted Microscope. ROs were collected for histological analysis after 4 days. This model of retinal cell damage was also stimulated with PRR ligands and AAV vectors following the same stimulation procedure than above and collecting supernatant at 6h, 18h and 3 days.

2.6. Analysis of innate immune responses

Secretion of inflammatory cytokines/chemokines related to the NF-κB pathway activation and type I interferons were measured using sandwich-ELISA kits of human IL-1β, TNF-α, IL-8, MIP-1α, MIP-1β, IL-6 and IFN α/β (R&D systems, MN, USA). Using half-area 96-well plates (Corning), wells were coated with capture anti-human polyclonal antibody against the corresponding cytokine/chemokine or type I IFN overnight at room temperature. The following day, plates were washed with wash buffer (PBS supplemented with 0.05% Tween 20 (Sigma-Aldrich)), and blocked for 1 hour in reagent diluent (PBS with 1% bovine serum albumin (BSA, Sigma-Aldrich)). After another washing steps, samples of interest and 2-fold serial diluted standard were added to the wells and incubated for 2 hours at room temperature. Biotin-conjugated detection antibody was added after washing the plate in order to attach to any detectable cytokine/chemokine or type I IFN captured by the first antibody. After 2 hours, wells were washed to remove unbound antibodies. Then, streptavidin-HRP was added and bound to the biotin-conjugated detection antibody for 20 minutes. After washing the plate, a substrate solution (TMB, Thermo Fisher Scientific) was added and incubated for 20 minutes. After that time, a coloured product was formed in proportion to the amount of cytokine/chemokine or type I IFN present in the samples. The colour reaction was stopped by adding 2N sulfuric acid. Absorbance was quantified using M200 NanoQuant spectrophotometer (Tecan) at 450 nm (570 nm correction wavelength). Results were calculated using GraphPad Prism by applying a 4PL regression model.

In order to simultaneously measure different cytokines/chemokines or type I IFNs, a Bio-Plex Pro Human Cytokine 17-Plex Panel (Bio-Rad), complemented by a Bio-Plex Pro Human Cytokine IP-10 (Bio-Rad) and Bio-Plex Pro Human Cytokine

IFN-a2 (Bio-Rad), was used in order to analyse 19 targets: IP-10, MIP-1β, TNF-α, IFN-α, IL-1β, IL-2, IL-4, IL-5, IL-6, IL-7, IL-8, IL-10, IL-12, IL-13, IL-17, G-CSF, GM-CSF, IFN-γ and MCP-1. These magnetic bead-based Multiplex assays were performed on a Luminex 200 system (Bio-Rad) with the support of Dorothea Siegel-Axel's group in accordance with the manufacturer's instructions. Standards were analysed in duplicates and each sample in triplicates. Washing was performed between each step using a HydroFlex microplate equipped with a magnetic plate carrier (Tecan). Analysis of the data was performed using Bio-Plex Manager (Bio-Rad).

2.7. AAV-mediated retinal gene therapy in non-human primates

2.7.1. Animals

This study used data from twelve cynomolgus monkeys (*Macaca fascicularis*) obtained in a formal toxicology assessment for an investigational new drug developed to treat patients with PDE6A related retinitis pigmentosa. The use of these data allowed us to reduce the number of animals needed in line with the principles of the 3Rs (Replace, Reduce, Refine).

2.7.2. Dosing and immunosuppressive treatment

Left eyes of all non-human primates (NHP) were treated with 170 µl of clinical grade AAV8-RK-hPDE6A (cgAAV8 lot 3) vector delivered by subretinal injection. Animals were divided in three groups depending on the received dose: low-dose group ($1x10^{11}$ vg, group 1), medium-dose group ($5x10^{11}$ vg, group 2) and high-dose group ($1x10^{12}$ vg, group 3). Right eyes received a sham injection of 170 µl buffered salt solution (BSS). All animals received systemic immunosuppression treatment with intramuscular injection of prednisolonacetat (1 mg/kg) for one week (from 2 days before the surgery until day 5 post-surgery). Animals also received local treatment during the first week consisting of prednisolonacetat (10 mg/ml) and eye drops of 0.5% moxifloxacin. All surgeries were performed by Dominik Fischer (University of Tübingen, Tübingen). Euthanasia was carried out under sedation followed by an intravenous injection of sodium pentobarbitone overdose after 90 days.

2.7.3. In vivo follow-up

Animals were evaluated with a complete ophthalmic examination before surgery and at days 30, 60 and 90 after surgery. Ophthalmological examinations consisted of infrared (IR), fundus autofluorescence (FAF), and SD-OCT imaging using Spectralis HRA + OCT (Heidelberg Engineering, Heidelberg, Germany).

2.8. *In silico* analysis of immune responses to AAV in NHPs

2.8.1. Counting and distribution of HRF

On SD-OCT, hyperreflective foci (HRF) were determined as discrete and well-circumscribed features with a reflectivity equal or greater than the RPE layer. Because the blebs were generated in the superior retinas after a retinotomy along the superior arcade, B-scans from inside the bleb areas and B-scans from the non-detached retinas were consistently identified. Using 9-mm SD-OCT volume scan pictures, HRF were counted in regions from both inside and outside the blebs and from right and left eyes from all animals at two different timepoints (30 and 90 days). To do so, HRF were manually counted using the FIJI software's cell counting plugin (ImageJ software, Bethesda, MD, USA) by three masked and independent assessors. The HRF were split into two sections based on the retinal layers: ONL and outer retina (from external limiting membrane to RPE, included). By identifying the position of each individual HRF from SD-OCT images, all HRF were plotted on IR and FAF images in order to create HRF distribution maps using Inkscape 1.0 (Software Freedom Conservancy, Brooklyn, NY, USA). Three colours were used per HRF in the distribution map depending on the number of assessors who observed the same HRF at the same location: green – HRF were identified by three assessors; yellow – by two; and red – by three assessors.

2.8.2. Outer nuclear layer thickness

The thickness of the ONL was assessed using 6-mm SD-OCT volume scan images at baseline, 30- and 90-days following treatment. The thickness measurements were taken in the bleb region 2 mm above the fovea using the Spectralis thickness maps tool and the 1-, 2- and 3-mm ETDRS grid (area= 7.065 mm^2) from HEYEX software (Heidelberg Engineering).

2.9. Immunohistochemistry

2.9.1. Retinal organoids

For cryostat sectioning, ROs were fixed with 4% paraformaldehyde (PFA; Polysciences, Warrington Pa., USA) during 20 minutes at room temperature and equilibrated in 30% sucrose solution overnight at 4°C. The following day, the organoids were embedded in a cryomatrix compound (Tissue-Tek O.C.T. Compound, Sakura, Netherlands) and were frozen at -80°C. Cryosections (14 µm) were produced using a Leica CM 3050s Cryocut (Leica, Germany), mounted on Superfrost glass slides (Thermo Fisher Scientific) for further immunohistochemical staining, and stored at 4°C.

Sections were rehydrated in PBS for 10 minutes at room temperature followed by a blocking step with PBS supplemented with 0.2% Triton-X (Carl Roth, Karlsruhe, Germany) and 10% normal donkey serum (Merck Millipore, USA) for 1 hour at room temperature. Primary antibodies (**Table M.2.**) were added to the blocking buffer and were kept at 4°C overnight. The following day, washing steps were performed in order to remove residual primary antibodies. The secondary antibodies (**Table M.3.**) were added and incubated 1 hour at room temperature. After another washing step, the sections were counterstained with HOECHST 33342 (1:2,000 dilution; Thermo Fisher Scientific) for 10 minutes at room temperature. A final washing step was performed before the antifade mounting reagent (Thermo Fisher Scientific) was added to the sections and covered with a coverslip (Thermo Fisher Scientific).

Table M.2. List of primary antibodies and stains

1° Antibody/Stain	Host	Dilution	Supplier
Anti-human Casp3	Rabbit	1:200	Calbiochem, AP1027
Anti-human Recoverin	Rabbit	1:2000	Millipore, AB5585
Anti-human DKK3	Rabbit	1:500	Thermo Fisher, PA5-21325
Anti-human Arrestin	Goat	1:100	Santa Cruz, sc13140
Anti-GFP	Rabbit	1:1000	Thermo Fisher, A-11122
Phalloidin 647	*Amanita phalloides*	1:100	Sigma Aldrich, P1951
Hoechst 33342	-	1:2000	Thermo Fisher, H3570
Anti-human CD20	Mouse	1:200	Dako, M0755

Anti-human CD3	Rabbit	1:100	Abcam, ab5690
Anti-human Iba-1	Rabbit	1:500	Wako, 019-19741
Anti-human CD68	Mouse	1:50	Dako, M0814
Anti-human RPE65	Rabbit	1:6000	Abcam, ab231782

Table M.3. List of secondary antibodies

2° Antibody	**Host**	**Dilution**	**Supplier**
Anti-mouse IgG Alexa Fluor 488	Donkey	1:500	Abcam, ab150105
Anti-mouse IgG Alexa Fluor 568	Donkey	1:500	Abcam, ab175472
Anti-mouse IgG Alexa Fluor 647	Donkey	1:500	Abcam, ab150107
Anti-rabbit IgG Alexa Fluor 488	Donkey	1:500	Abcam, ab150073
Anti-rabbit IgG Alexa Fluor 568	Donkey	1:500	Abcam, ab175470
Anti-rabbit IgG Alexa Fluor 647	Donkey	1:500	Abcam, ab150075
Anti-chicken IgG Alexa Fluor 647	Donkey	1:500	Abcam, ab150171
Anti-goat IgG Alexa Fluor 647	Donkey	1:500	Abcam, ab150131

2.9.2. Eye sections

Eyes from NHP were fixed in 4% PFA and kept at 4°C overnight. Eye-cups were then dehydrated in ethanol-xylol gradients and embedded in paraffin for sectioning by Labcorp Drug Development (formerly Covance).

For immunofluorescence staining, sections were deparaffinized in different concentrations of xylol-ethanol (2x 100% xylol, and 2x 100%, 80%, 70%, 50% ethanol for 5 minutes each) and heated in a pressure cooker with a citrate-based antigen unmasking solution (Vector Laboratories, Burlingame, CA, USA) for 2 minutes. After washing with PBS, the slides were blocked with PBS supplemented with 0.05% Tween 20 and 10% normal donkey serum for 1 hour at room temperature. Then, primary antibodies (**Table M.2.**) were added for 1 hour at room temperature and washed. Secondary antibodies (**Table M.3.**) were incubated for 2 hours at room temperature in the dark. After another washing step, sections were mounted with antifade mounting medium with DAPI (Vector Laboratories) and covered with coverslip.

For immunohistochemical permanent staining of RPE65, deparaffinized eye sections were incubated for 10 minutes with the BIOXAL blocking solution (Vector Laboratories) and washed with tris-HCl buffered saline (TBS). In order to observe the staining in the RPE layer, lipofuscin pigment from the RPE was removed. To

do so, samples were incubated with a 3% H2O2 solution for 40 minutes at room temperature and washed with 1% acetic acid. Next, a solution of 2.5% horse serum was added to the sections for 20 minutes followed by the incubation with the RPE65 primary antibody for 30 minutes. After washing with TBS, sections were incubated with the secondary antibody (ImmPRESS – AP reagent horse anti-rabbit IgG; Vector Laboratories) for 30 minutes. Then, ImmPACT Vector Red (Vector Laboratories) was added to the sections and they were incubated in the dark for 30 minutes followed by another washing step and the incubation with haematoxylin (Vector Laboratories) for 25 seconds. Then, sections were washed with water and dehydrated with ethanol-xylol gradients and covered with antifade mounting media and coverslip.

2.10. Statistical analysis

Prior to performing data analysis, normal distribution of the data was assessed. Unless otherwise specified, data were provided as means ± SD (standard deviation). GraphPad Prism (GraphPad Software, San Diego, CA, USA), Excel 2016 (Microsoft Office, Redmond, WA, USA) and JMP 16.0 (SAS Institute Inc, Cary, NC, USA) were used for statistical analysis. To determine significance the appropriate sample tests were used and p values were provided as indicated in their respective Results section.

3. Results

3.1. CHAPTER 1**.** Evaluation of potential differences in the immune response to HEK293- and *Sf9*-produced AAV vector lots using different immunocompetent cell models.

Rationale. According to recent research, HEK293 cell-derived and *Sf9* cell-derived AAV vectors vary in terms of PTMs of the capsid and impurities in the viral suspension[45]. In this chapter, we hypothesize that these differences between production systems could result in differences in the immunogenicity of HEK293 cell-derived and *Sf9* cell-derived vector lots. To test this hypothesis, several AAV vectors from different production systems were tested in a range of immunocompetent cell models.

3.1.1 Titration of AAV vectors by ddPCR

A total of eight AAV8-CMV-eGFP lots (5 HEK293- and 3 *Sf9* cell-derived lots) and four AAV2-CMV-eGFP lots (2 HEK293- and 2 *Sf9* cell-derived lots) from three different manufacturers were analysed (**Table R.1.**). As AAV titres were originally quantified by the three different manufacturers using different protocols, a ddPCR re-titration of the experimental AAV8 and AAV2 vector lots was performed using two different targets: one within the CMV promoter and the other within the eGFP transgene of the vector. The results obtained by the quantification of the CMV target were used in the next experiments to titrate the AAV vector lots (**Table R.1.**).

Table R.1. List of experimental AAV8-CMV-eGFP and AAV2-CMV-eGFP vector lots. ddPCR report is included.

AAV	Lot number	CMV target (vg/ml)	eGFP target (vg/ml)	Production platform	Purification method	Manufacturer
AAV8-CMV-eGFP	AAV8 lot 1	6.53 E+12	6.69 E+13	HEK293 cells	Affinity chromatography	University of Iowa
	AAV8 lot 2	4.61 E+12	4.57 E+12	HEK293 cells	Affinity chromatography	University of Iowa
	AAV8 lot 3	5.88 E+12	5.97 E+12	HEK293 cells	Affinity chromatography	University of Iowa
	AAV8 lot 4	4.45 E+13	5.09 E+13	*Sf9* cells	Affinity chromatography	University of Iowa
	AAV8 lot 5	1.15 E+14	1.31 E+14	*Sf9* cells	Affinity chromatography	University of Iowa
	AAV8 lot 6	5.24 E+12	5.83 E+12	HEK293 cells	Caesium chloride	Virovek

	AAV8 lot 7	2.50 E+13	2.84 E+13	*Sf9* cells	Caesium chloride	Virovek
	AAV8 lot 8	3.63 E+13	3.69 E+13	HEK293 cells	Iodixanol gradient	Vigene
AAV2-CMV-eGFP	AAV2 lot 1	2.47 E+13	2,74E+13	*Sf9* cells	Caesium chloride	Virovek
	AAV2 lot 2	1.96 E+13	2,06E+13	*Sf9* cells	Caesium chloride	Virovek
	AAV2 lot 3	9.59 E+12	1,23E+13	HEK293 cells	Iodixanol gradient	Vigene
	AAV2 lot 4	9.73 E+12	1,12E+13	HEK293 cells	Iodixanol gradient	Vigene

3.1.2 Establishment of THP-1 cells as immunocompetent cell model

Human THP-1 monocyte cells are minimally sensitive to PRR ligands when undifferentiated. However, they become more responsive following differentiation into macrophages[105]. Therefore, THP-1 monocytes cells were differentiated into macrophages by incubation with 100nM PMA. Differentiation was evident after 48 hours when cells became adherent, proliferation stopped and they phenotypically resembled macrophages (**Figure R.1.**).

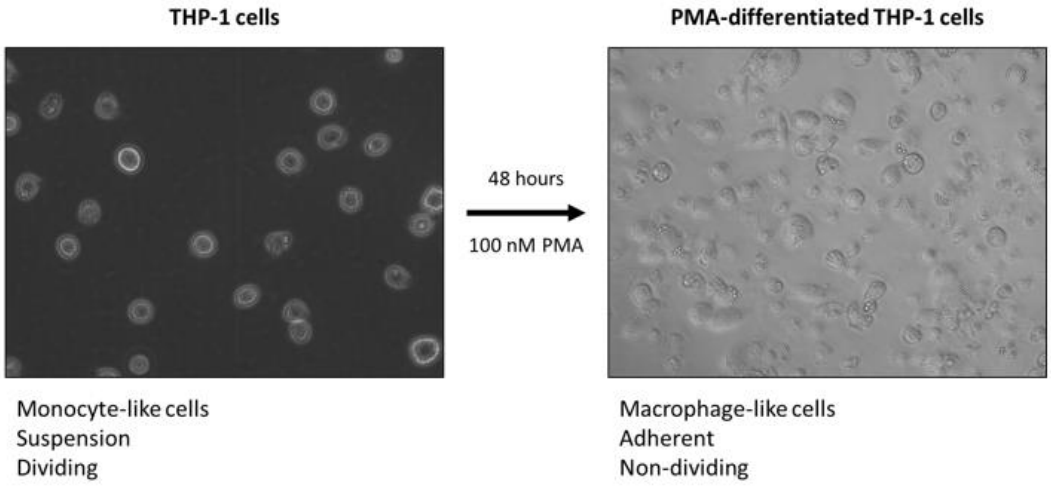

Figure R.1. THP-1 monocyte differentiation into macrophages. THP-1 cells were incubated 48 hours in the presence of 100 nM PMA and then in THP-1 medium during 24 h. PMA: phorbol 12-myristate 13-acetate.

It is known that AAV vectors can be sensed by the TLR2 (viral capsid) and TLR9 (viral DNA)[64,65]. Hence, PMA-differentiated THP-1 cells were stimulated with not only the ligands for these two receptors but with all major PRR ligands in order to assess the immune receptors that were present in the cell model. After 24 hours,

the PRR ligands induced the release of proinflammatory cytokines/chemokines (IL-1β, IL-8, MIP-1α, TNF-α) and type I IFNs (IFN-α, IFN-β) (**Figure R.2.**), confirming the presence of PRRs in this model. It is noteworthy that there was a release of proinflammatory cytokines/chemokines after stimulation with PAM3CSK4 indicating the presence of TLR2 and its NF-κB downstream pathway. In addition, the TLR9 pathway was also assessed with the release of IFN-β after stimulation with ODN2006.

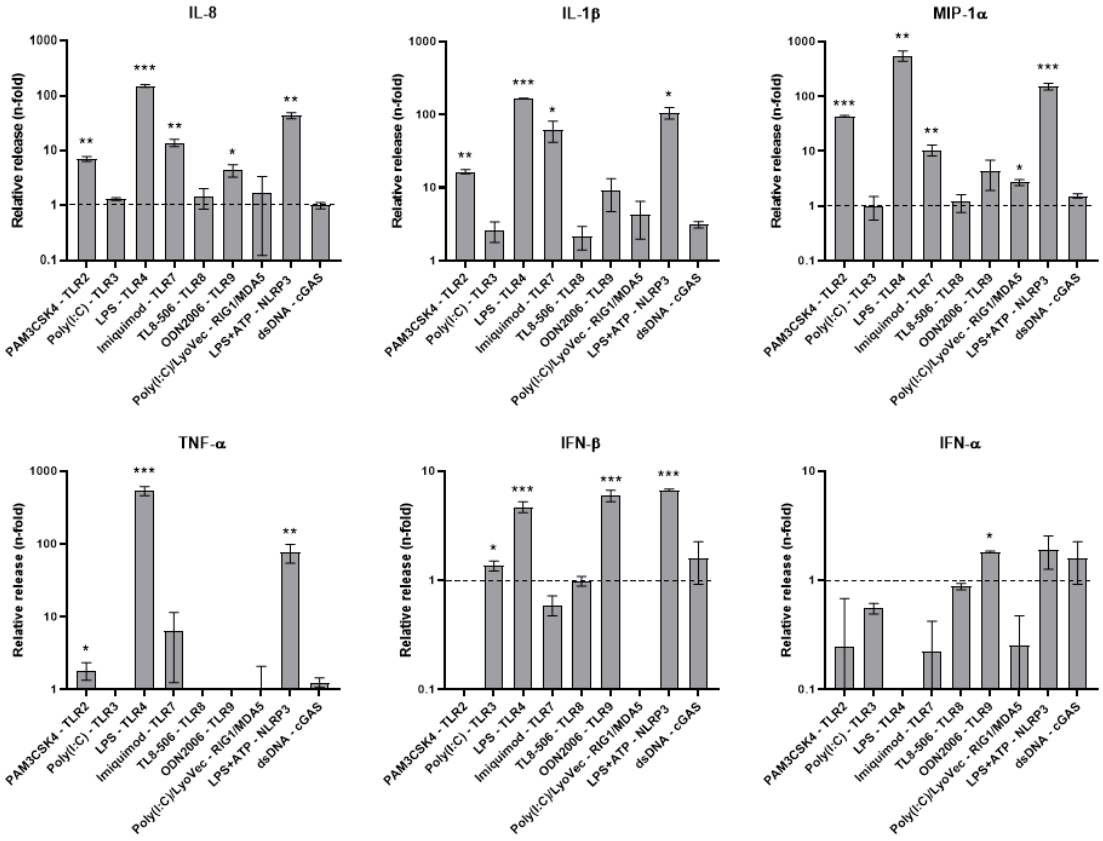

Figure R.2. Release of proinflammatory cytokines/chemokines and type I IFNs by PMA-differentiated THP1 cells in response to all major PRR ligands. Fold increase of cytokine release of IL-8, IL-1β, MIP-1α, TNF-α, IFN-β and IFN-α by PMA-differentiated THP-1 cells at 24 hours after stimulation with 1 µg/ml PAM3CSK4, 10 µg/ml poly(I:C), 10 ng/ml LPS, 5 µg/ml imiquimod, 100 µg/ml of TL8-506, 5µM ODN2006, 1 µg/ml Poly(I:C)/LyoVec, 10 ng/ml LPS + 5mM ATP and 500 ng/ml dsDNA. Error bars indicate the standard deviations between replicate assays. Statistical significance was determined using unpaired Student t-test. P-values: ≤0.05: *; ≤0.01: **; ≤0.001: ***.

Additionally, PMA-differentiated TLR2 KO THP-1 cells were tested to confirm its inability to generate an innate immune response upon stimulation with the TLR2 ligand, PAM3CSK4. After 24 hours, stimulation with PAM3CSK4 in PMA-

differentiated TLR2 KO THP-1 did not induce any detectable innate immune response. LPS was also used as stimulatory control and IL-1β, IL-8 and TNF-α were detected in the media. There was no release of type I IFNs. Therefore, as these cells were TLR2 KO cells, they were not able to respond to TLR2 ligand but they were still responsive to other stimuli such as LPS.

3.1.3 Stimulation of THP-1 cells with AAV8 vector lots

After establishing PMA-differentiated THP-1 cells as immunocompetent cell model, stimulatory experiments with AAVs were performed in order to investigate potential differences between HEK293- and *Sf9*- produced vectors. Cells were stimulated with all AAV8-CMV-eGFP vector lots (lots 1-8) for 24 hours. Incubation with AAV8 vector lots resulted in different transduction rates between HEK293- and *Sf9*-produced vectors. HEK293-vectors showed a significantly higher transduction rate than *Sf9*-vectors (7.1 ± 1.5% vs 0.65 ± 0.3%; P<0.001) (**Figure R.3.a-b.**). However, stimulation with AAV8 vector lots did not result in any detectable innate immune response in the supernatant (**Figure R.3.c**). For that reason, TLR2 KO THP-1 cells were not further used.

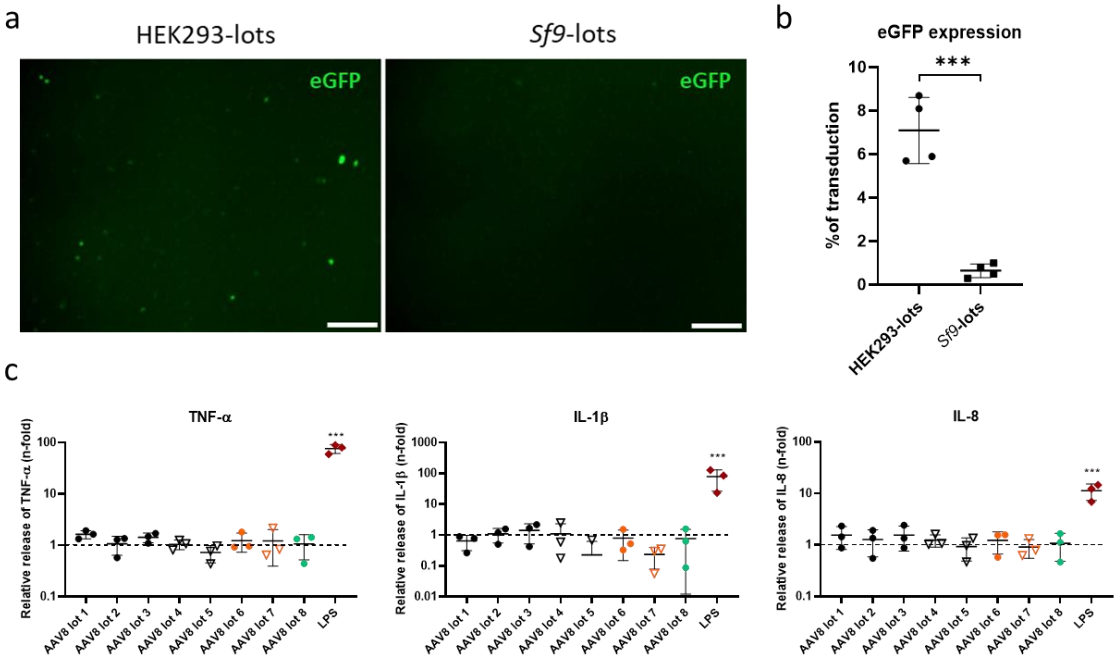

Figure R.3. Evaluation of transduction and immune responses after AAV stimulation of PMA-differentiated THP-1 cells. Cells were stimulated with AAV8 vector lots 1-8 for 24 hours (MOI: 1:1x10^6 vg). (a) Representative green fluorescence images of PMA-differentiated THP-1

cells after stimulation with HEK293- and *Sf9*-derived AAV8 lots. Scale bar is 100 µm. (b) Transduction efficiency of all HEK293- and *Sf9*-derived AAV8 vector lots. (c) Fold increase of cytokine release of TNF-α, IL-1β and IL-8 by AAV-stimulated PMA-differentiated THP-1 cells.10 ng/ml LPS (red diamonds) served as stimulation control. Circle: HEK293-derived vector lot; triangle: *Sf9*-derived vector lot; black: vector lot from Viral Vector Core Facility of the University of Iowa; orange: vector lot from Virovek; green: vector lot from Vigene Biosciences. Representative plots of one of three independent experiments. Error bars indicate the standard deviations between replicate assays. Statistical significance was determined using unpaired Student t-test. P-values: ≤0.001: ***.

3.1.4. Establishment of pDCs as immunocompetent cell model for TLR9

Although PMA-differentiated THP-1 cells were established as an immunocompetent cell model, a more sensitive cell model was required to detect AAV vectors. Human pDCs were chosen as it is known that these cells are specialized viral sensors that massively produce proinflammatory cytokines and type I IFNs upon viral infection[78], including AAV vectors via TLR9 recognition[65]. After isolation from buffy coats using MACS, purity of isolated pDCs was confirmed via flow cytometry analysis (90% purity, **Figure R.4.a-c.**). pDCs were seeded and stimulated with the TLR9 ligand, ODN2216. After 18 hours, ODN2216 induced reactive cell proliferation in the stimulated pDCs (**Figure R.4.d.**). In addition, a significant release of proinflammatory cytokines (IP-10, MIP-1β, TNF-α) and type I IFN (IFN-α) was detected compared to vehicle control using a multiplex assay, indicating the presence of TLR9 in these cells (**Figure R.4.e.**). No significant changes in the release of the rest of the measured cytokines included in the multiplex assay were detected (IL-1β, IL-2, IL-4, IL-5, IL-6, IL-7, IL-8, IL-10, IL-12, IL-13, IL-17, G-CSF, GM-CSF, IFN-γ, MCP-1).

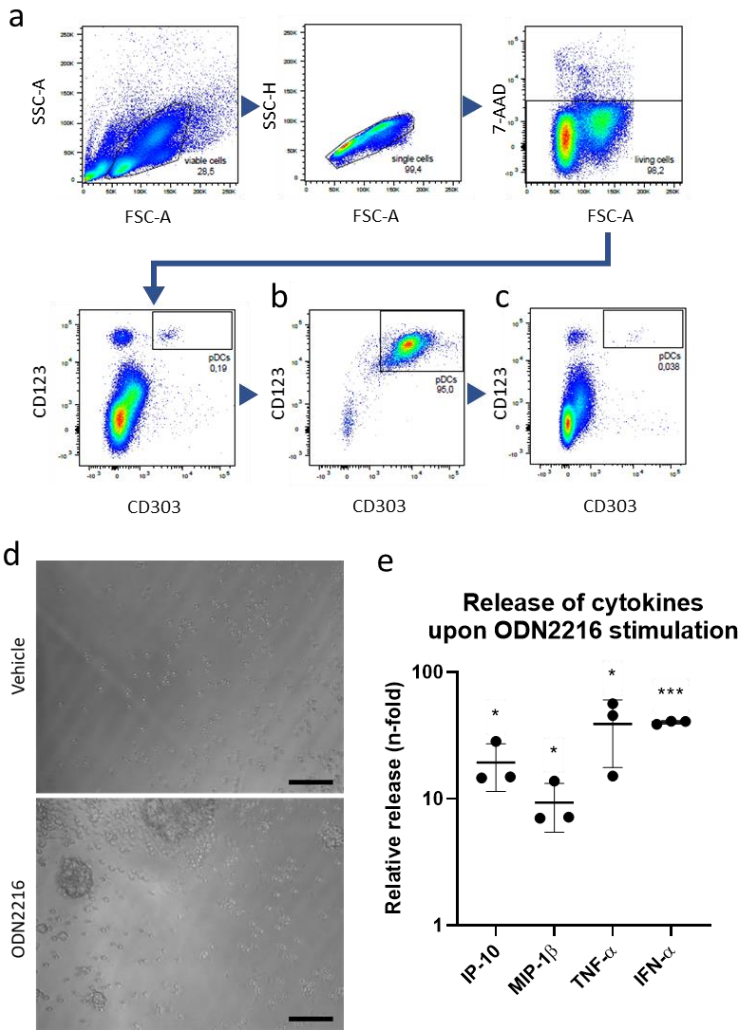

Figure R.4. Purification and ODN-stimulation of pDCs. (a-c) pDCs were stained with fluorescent antibodies and analysed by flow cytometry. pDCs were gated as single, 7-AAD negative living cells that were positive for CD123 and CD303. (a) Gating strategy for pDCs shown by the example of the complete PBMC fraction before MACS enrichment (total PBMCs). (b) Percentage of pDCs after MACS (pDCs). Enriched living pDCs had a purity of over 90%. (c) Percentage of pDCs in the remaining PBMC fraction after removal of pDCs by MACS (PBMC-pDCs). (d-e) Purified pDCs were stimulated with 0.77 µM ODN2216 for 18 hours. (d) Representative bright field images of pDCs stimulated with vehicle control (*upper image*) or ODN2216 (*lower image*). Scale bar is 100 µm. (e) Fold increase of cytokine release of IP-10, MIP-1β, TNF-α and IFN-α2 by ODN2216-stimulated pDCs. Error bars indicate the standard deviations between replicate assays. Statistical significance was determined using unpaired Student t-test. P-values: ≤0.05: *; ≤0.001: ***.

3.1.5 Stimulation of pDCs with AAV vector lots

Isolated and purified human pDCs were then stimulated with AAV8-CVM-eGFP vector lots (AAV8 lots 1-8) and AAV2-CMV-eGFP vector lots (AAV2 lots 1-4) for 18 hours. Transgene expression was not detectable after incubation with AAV8 and AAV2 vector lots. However, reactive cell proliferation was present in pDCs stimulated with four of the eight AAV8 lots (lots 1-4) and two of the four AAV2 lots (lots 1-2) (**Figure R.5.a.**). Furthermore, there was a significant release of IP-10, MIP-1β, TNF-α and IFN-α indicating the immunogenicity of these AAV8 and AAV2 vector lots, from now on named immunogenic AAV vector lots. In contrast, neither cell proliferation nor cytokine release was induced by the remining AAV8 vector lots (lots 5-8) and AAV2 vector lots (lots 3-4) (**Figure R.5.b.**), from now on named non-immunogenic AAV vector lots. The cytokine concentrations of these experiments were statistically analysed using linear mixed effect model and *post hoc* Dunnett's test (Q=2.6) by comparing the least-square means of the different AAV vector lots with the vehicle control. This demonstrated statistical differences between immunogenic (AAV8 lots 1-4 and AAV2 lots 1-2) and non-immunogenic (AAV8 lots 5-8 and AAV2 lots 3-4) AAV vector lots (p values from *post hoc* analysis ranged between 0.0015 and <0.0001). No other significant changes in the release of the rest of the measured cytokines were detected with neither immunogenic nor non-immunogenic AAV vector lots.

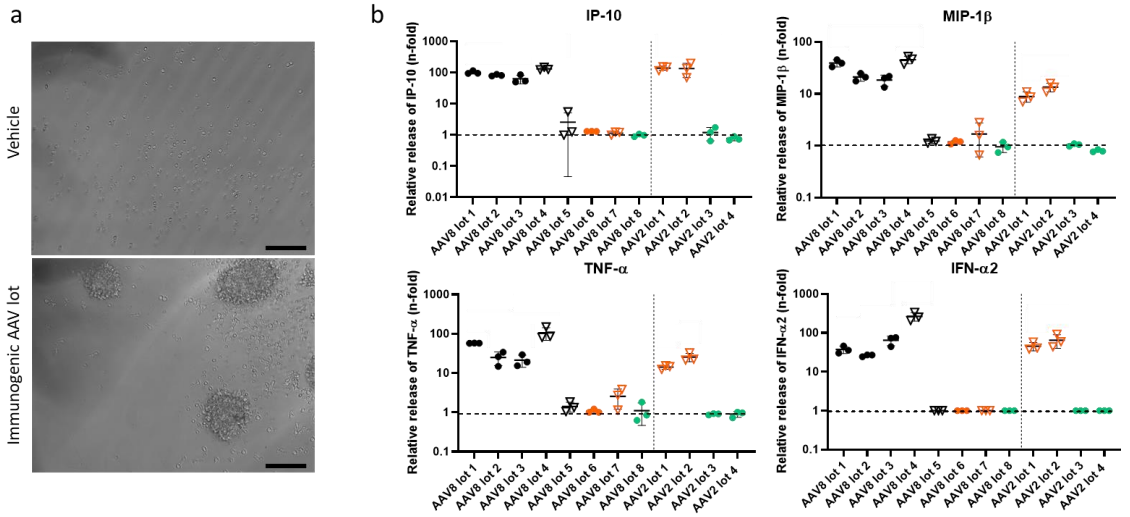

Figure R.5. Induction of AAV vector lot-specific immune responses in human pDCs. Human pDCs were stimulated with different lots of AAV8-CMV-eGFP and AAV2-CMV-eGFP (MOI: 1:1x10^6 vg) for 18h. (a) Representative bright field images of pDCs stimulated with vehicle control (*upper image*) or an immunogenic AAV vector lot (*lower image*). Scale bar is 100 µm. (b) Fold

increase of cytokine release of IP-10, MIP-1β, TNF-α and IFN-α2 by AAV-stimulated pDCs. Representative plots of one of three independent experiments. Error bars indicate the standard deviations between replicate assays. Vertical dashed lines separate AAV8 lots from AAV2 lots. Circle: HEK293-derived vector lot; triangle: *Sf9*-derived vector lot; black: vector lot from Viral Vector Core Facility of the University of Iowa; orange: vector lot from Virovek; green: vector lot from Vigene Biosciences.

To investigate whether a higher dose of a non-immunogenic AAV8 vector lot was able to trigger an immune response, pDCs were stimulated with the technically maximum applicable MOI (1:4.61x10^6 vg/well). However, neither reactive cell proliferation nor cytokine release were detected upon stimulation with this increased titre.

Therefore, contrary to our initial hypothesis, these results demonstrated that innate immune responses to AAV in pDCs were lot-specific and not related to a specific production system, manufacturer or even serotype.

3.1.6 Evaluation of the relation between capsid/vg ratios and immune responses

Preclinical studies have shown that differences in the numbers of full and empty vector particles in AAV vector suspensions can influence the immune response[106]. To investigate if variations in immunogenicity across AAV vector lots were attributable to differences in the ratio of full and empty vector particles, the titre of vector capsids in all AAV lots was measured using AAV titration ELISA and the capsid/vg ratios were calculated in combination to the ddPCR results. Interestingly, great differences in the capsid/vg ratio were found among all AAV lots. Approximately two times more capsids than vg (2:1) were found in AAV8-CMV-eGFP lots 1, 3, 5 and AAV2-CMV-eGFP lot 1; and four times more (4:1) in AAV8 lot 4. A 1:1 ratio was observed in the rest of the lots. However, no significant differences between capsid/vg ratios of immunogenic and non-immunogenic AAV vector lots were found in AAV8 (P= 0.27) nor in AAV2 (P= 0.37) vector lots (**Figure R.6.**). This implies that variations in the immunogenicity of the AAV vector lots were not related to changes in the ratio of full and empty vector particles.

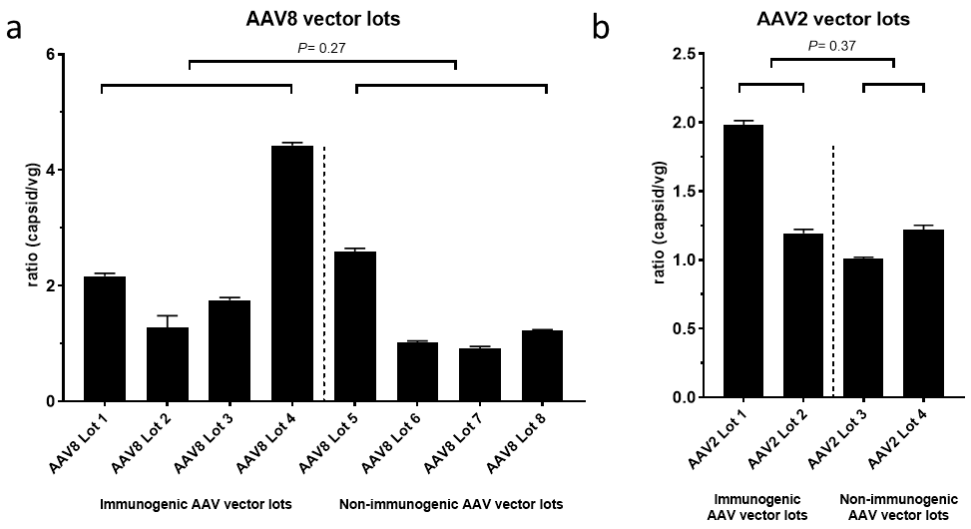

Figure R.6. Comparison of capsid/vg ratios of twelve different AAV8-CMV-eGFP and AAV2-CMV-eGFP vector lots. The capsid/vg ratios derive from absorbance measurements (ELISA) and ddPCR results of (a) 8 AAV8 vector lots and (b) 4 AAV2 vector lots. Dashed lines separate immunogenic from non-immunogenic AAV vector lots. Error bars indicate the standard deviations between replicate assays. Statistical significance was determined using unpaired Student t-test.

3.1.7 Establishment of the TLR pathway involved in the recognition of immunogenic AAV8 vector lots in pDCs

It has been shown that the innate immune recognition of AAV by murine and human pDCs is mediated by DNA sensing TLR9[65]. Accordingly, we evaluated whether TLR9 was also involved in the recognition of our immunogenic AAV8 vector lots. To do so, pDCs were seeded and cultured with the TLR9 antagonist, H154, followed by stimulation with the immunogenic AAV8 vector lots 1-4. After 18 hours, no evidence of cell proliferation was observed and a significant reduction in the release of IP-10, MIP-1β, TNF-α and IFN-α, was measured (**Figure R.7.**). This implies that immune responses to immunogenic AAV8 vector lots in human pDCs were mediated by the TLR9 signalling.

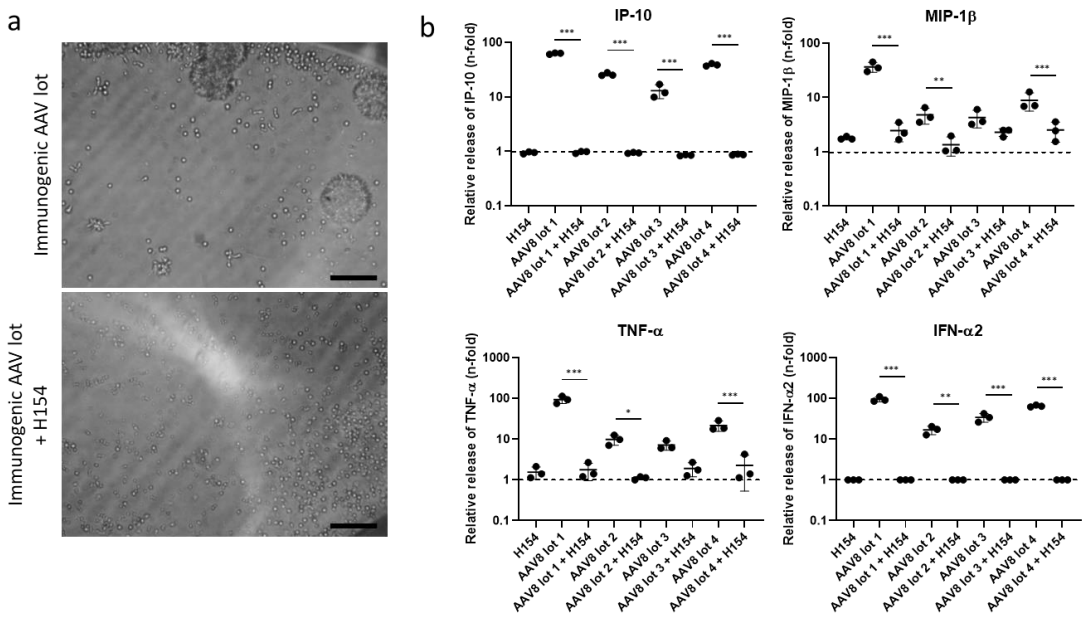

Figure R.7. TLR9-dependent recognition of immunogenic AAV8-CMV-eGFP vector lots by pDCs. Human pDCs were treated with the TLR9 antagonist H154 (50μM) followed by stimulation with immunogenic AAV8 vector lots (MOI: 1:1x10^6 vg) for 18h. (a) Representative bright field images of purified pDCs treated with immunogenic AAV vector lots (*upper image*) or immunogenic AAV vector lots and H154 (*lower image*). Scale bar is 100 μm. (b) Fold increase of cytokine release of IP-10, MIP-1β, TNF-α and IFN-α2 by stimulated pDCs. Error bars indicate the standard deviations between replicate assays. Statistical significance was determined using one-way ANOVA and Holm-Sidak's post hoc analysis. P-values: ≤0.05: *; ≤0.01: **; ≤0.001: ***.

3.1.8. Modulation of the innate immune response to immunogenic AAV vector lots by DNase

We have shown that immunogenic AAV8 vector lots are sensed by the DNA receptor TLR9 in human pDC. However, the non-immunogenic AAV8 vector lots were not able to trigger a TLR9-dependent immune response in human pDCs. We previously proved via ddPCR that all AAV vector lots used in this study had intraviral DNA, thus, we hypothesised that potential external residual DNA in the viral suspension rather than the intraviral DNA could be the reason of the observed immune responses to immunogenic AAV vector lots. Hence, if external residual DNA was present in the viral suspension of the immunogenic AAV8 vector lots, the innate immune response should be attenuated in the presence of DNase. To test this hypothesis, immunogenic AAV8 vector lots were pre-treated with DNase I prior to AAV stimulation. Then, pDCs were seeded and stimulated

with the DNase pre-treated immunogenic AAV8 vector lots. pDCs which were treated with DNase only or sham-treated served as controls. Interestingly, a significant reduction in the innate immune response was found after DNase treatment (**Figure R.8.**). The induction of reactive cell proliferation and the release of IP-10, MIP-1β, TNF-α and IFN-α were abolished from the wells of the AAV8 lots 2 and 4 treated with DNase. On the other hand, a still present but significantly reduced proliferation and release of IP-10, MIP-1β, TNF-α and IFN-α was observed after stimulation with the DNase-treated AAV8 lots 1 and 3.

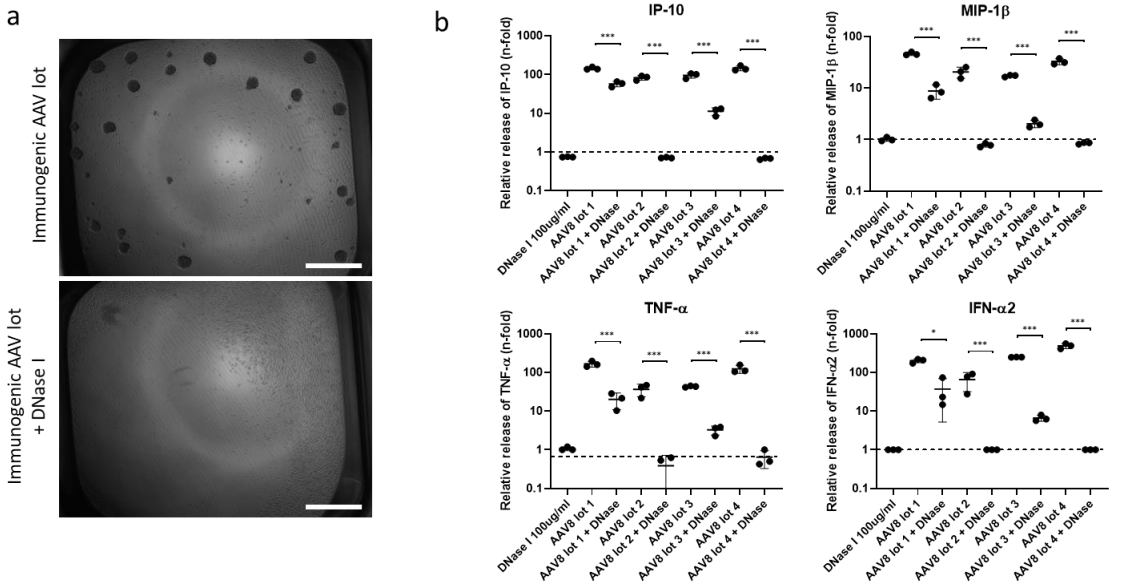

Figure R.8. DNase pre-treatment reduces immune responses induced by immunogenic AAV8-CMV-eGFP vector lots. Human pDCs were stimulated with DNase-treated immunogenic AAV8 vector lots for 18h (MOI: 1:1x10^6 vg). (a) Representative bright field images of purified pDCs stimulated with immunogenic AAV vector lots (*upper image*) and immunogenic AAV vector lots pre-treated with 100 µg/ml of DNase I (*lower image*). Scale bar is 500 µm. (b) Fold increase of cytokine release of IP-10, MIP-1β, TNF-α and IFN-α2 by stimulated pDCs. Error bars indicate the standard deviations between replicate assays. Statistical significance was determined using one-way ANOVA and Holm-Sidak's post hoc analysis. P-values: ≤0.05: *; ≤0.001: ***.

In addition, to test whether the immunogenicity of AAV vectors increased after the release of the intra-viral DNA, the viral capsids of AAV8 lot 1 were deliberately opened by heat-treatment. Heat-treated AAV vector lot 1 was then used to stimulate pDCs. Although there were no differences in the reactive cell proliferation upon AAV8 lot 1 stimulation with and without heat-treatment, there was a significant increase in the release of IP-10, MIP-1β, TNF-α and IFN-α in the heat-treated condition, indicating that the release of intra-viral DNA into the

vector suspension could contribute to the induction of immune responses (**Figure R.9.**).

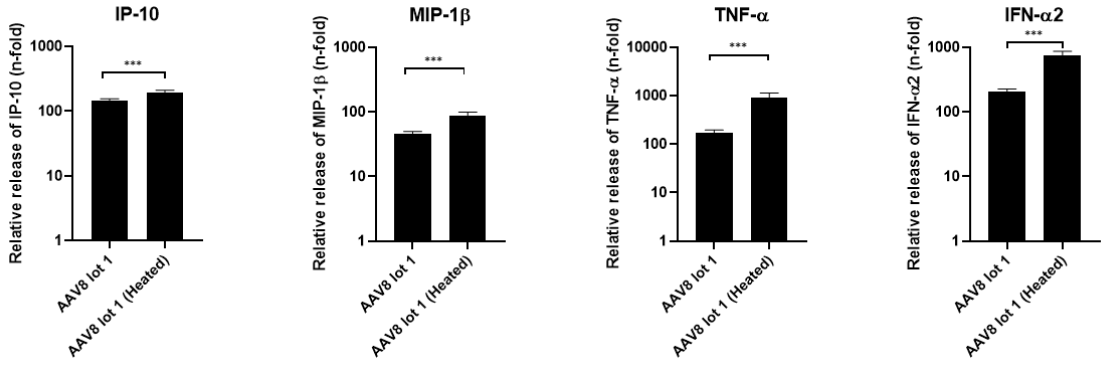

Figure R.9. Release of intra-viral DNA by heat-treatment of vectors increases the immunogenicity of AAV. Fold increase of cytokine release of IP-10, MIP-1β, TNF-α and IFN-α2 by pDCs 18h after stimulation with heat-treated AAV8 (MOI: $1:1x10^6$ vg). Error bars indicate the standard deviations between replicate assays. Statistical significance was determined by using Student t-test. P-value: ≤0.001: ***.

Together, DNase treatment decreased or impaired pDC proliferative responses to immunogenic vector lots, as well as the production of proinflammatory cytokines. Heat-treatment, on the other hand, increased the immunological response to AAV by releasing intra-viral DNA into the vector solution. This suggests that extra-viral DNA causes innate immune responses to AAV8 vector lots in human pDCs.

3.1.9. Assessment of viral transduction in HEK293T cells

HEK293T cells are a well-known cell model to analyse transduction efficiency upon AAV infection[107]. To evaluate the impact of residual DNA impurities on viral transduction, we stimulated HEK293T cells with all eight AAV8 in the presence or absence of DNase. The transduction efficiency was evaluated by fluorescence microscopy (**Figure R.10.a.**) and after 3 days, the transduction rate was determined by flow cytometry (**Figure R.10.b-c.**). Similar to our transduction results obtained in PMA-differentiated THP-1 cells, HEK293-derived AAV8 vector lots showed a significantly higher potency than the *Sf9*-derived ones (P= 0.001) (**Figure R.10.c.**). Furthermore, pre-treatment with DNase significantly increased the transduction efficiency (c. 50%) in the HEK293-derived AAV8 vector lots (P=

0.01). A non-significant increase was also measured in *Sf9*-derived AAV8 vector lots (P= 0.09) (**Figure R.10.c.**). To evaluate whether the immunogenicity, as determined in pDCs, influenced the transduction efficiency in HEK293T cells, we also compared the HEK293T cell transduction rates of immunogenic and non-immunogenic vector lots with and without DNase pre-treatment. Interestingly, we found that the assessed immunogenicity of the AAV8 vector lots had no influence on their transduction potency in HEK293T cells (**Figure R.10.d.**).

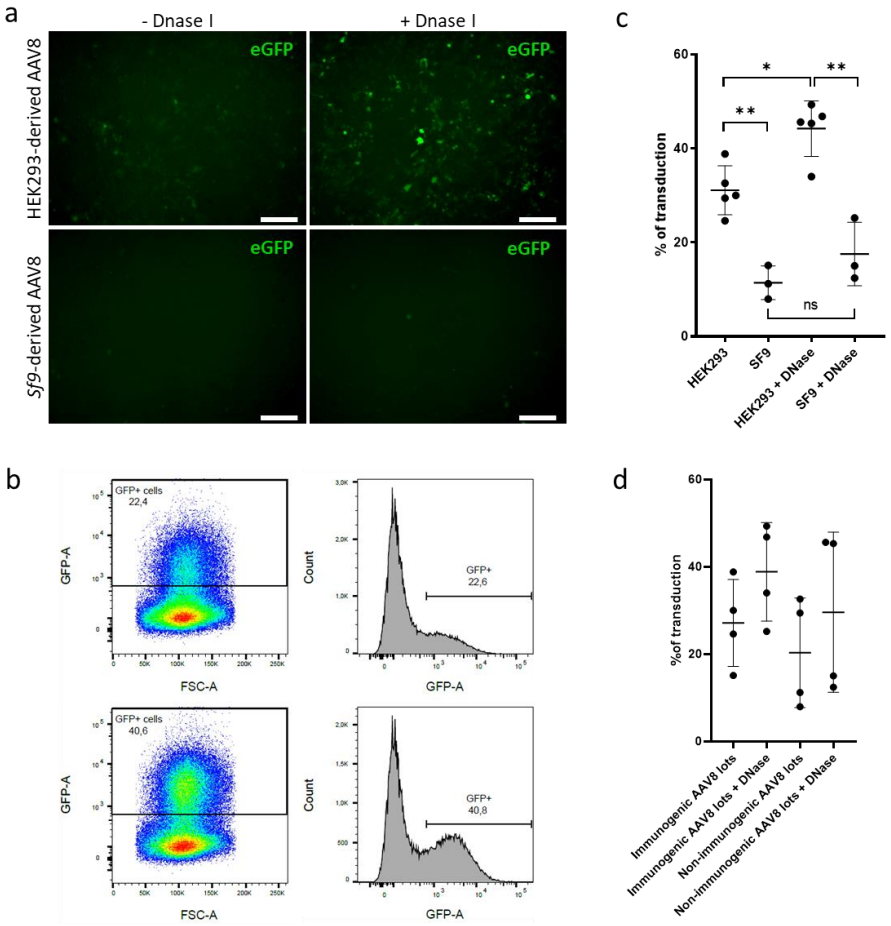

Figure R.10. DNase pre-treatment increases transduction efficiency of AAV8-CMV-eGFP vector lots in HEK293T cells. HEK293T cells were stimulated with DNase-treated AAV8 vector lots for 3 days (MOI: 1:8x10^4 vg). (a) Representative green fluorescence images of HEK293T cells after stimulation with DNase-treated or untreated HEK293- and Sf9-derived AAV8 lots. Scale bar is 100 µm. (b) Gating strategy for eGFP detection in HEK293T cells after AAV8 stimulation in the absence (*upper graphs*) or presence (*lower graphs*) of 100 µg/ml of DNase I. (c) Transduction efficiency of HEK293- and *Sf9*-derived AAV8 lots with and without DNase treatment. (d) Transduction efficiency of AAV8 lots grouped by their immunogenicity with and without DNase treatment. Error bars indicate the standard deviations between replicate assays. Statistical significance was determined using unpaired Student t-test. P-values: ≤0.05: *; ≤0.01: **; ns: not significant.

Collectively, these data indicate that AAV vector preparations may contain extra-viral DNA impurities that can trigger lot-specific TLR9-dependent immune responses in pDCs and reduce the transduction potency in HEK293T cells.

3.1.10. Stimulation with clinical grade AAV8 vector lots

Apart from extra-viral DNA impurities in the vector suspensions, host cell protein impurities could also influence the immunogenicity of the AAV vector lots. To study this, two different lots of clinical grade AAV8-RK-hPDE6A vector (cgAAV8 vector lots 1-2) containing different amounts of host cell proteins (36.9 ng/ml in cgAAV8 vector lot 1 and 1433.7 ng/ml in cgAAV8 vector lot 2) were used.
Human pDCs were seeded and stimulated with cgAAV8 lots 1-2 for 18 hours. Incubation with these two cgAAV8 lots carrying different host cell protein contents did not result in any detectable immune response in pDCs (**Figure R.11.a.**). In addition, the vector with the highest host cell protein content, cgAAV lot 2, was tested in PMA-differentiated THP-1 cells in parallel to LPS as control for 24 hours. However, no immune response was detected upon stimulation with the vector in comparison to vehicle control (**Figure R.11.b.**).

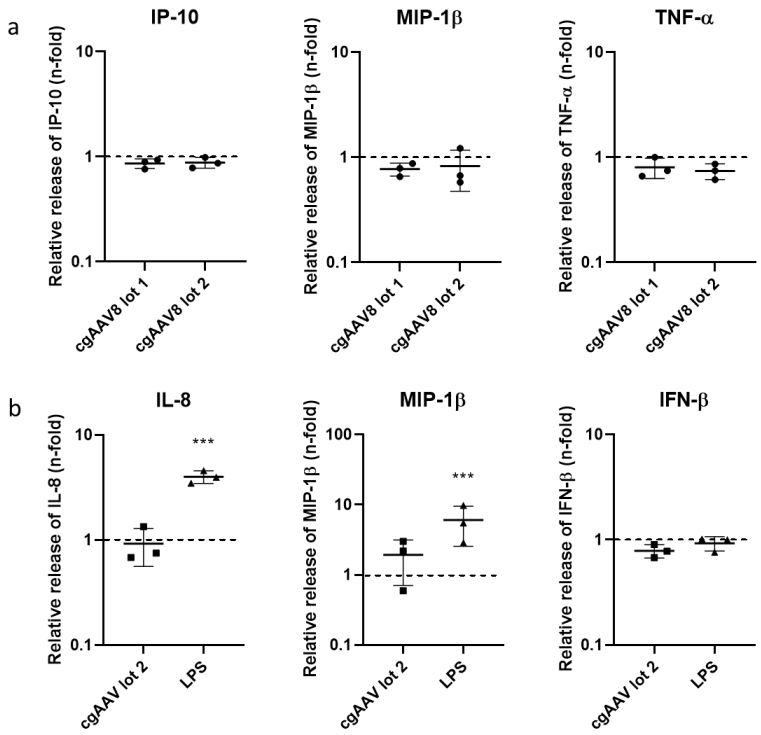

Figure R.11. Evaluation of immune responses to cgAAV8 lots containing different HCP contents in pDCs and PMA-differentiated THP-1 cells. Fold increase of cytokine release of IP-10, MIP-1β, TNF-α, IL-8 and IFN-β after stimulation of (a) pDCs and (b) PMA-differentiated THP-1 cells with cgAAV8-RK-hPDE6A vector lots (MOI: $1{:}1x10^6$ vg) carrying different HCP contents (36.9 ng/ml in cgAAV8 vector lot 1 and 1433.7 ng/ml in cgAAV8 vector lot 2). LPS served as stimulation control in experiments with PMA-differentiated THP-1 cells. Error bars indicate the standard deviations between replicate assays. Statistical significance was determined using unpaired Student t-test. P-values: ≤0.001: ***.

3.2. CHAPTER 2**.** Assessment of immune responses to different PRR ligands and immunogenic AAV vector lots in different retinal cell models.

Rationale. In this chapter, we evaluate whether retinal cells are able to sense our AAV vectors and elicit innate immune responses. We first used RPE cells obtained from human induced pluripotent stem cells (hiPSC) derived from a healthy donor. In the retina, RPE cells are key players in the first-line of defence against invading organisms such as viruses and bacteria[108]. We also used hiPSC-ROs as they are known to largely recapitulate key features of an *in vivo* neural retina which also express innate immune receptors[91,109].

3.2.1. Evaluation of immune responses in hiPSC-RPE cells

hiPSC-RPE cells were seeded and stimulated with the ligands for TLR3 and TLR4 (Poly(I:C) and LPS, respectively) and with our immunogenic AAV8 lot 1. Poly(I:C) induced a significant release of IFN-β at all timepoints (3h, 12h and 24h). LPS also induced an innate immune response with the release of IL-8 at all timepoints. However, hiPSC-RPE cells were not able to detect AAV8 lot 1 as neither proinflammatory cytokines nor type I IFNs were detected in the supernatants at any timepoint (**Figure R.12**). Any significant changes in the release of the rest of the measured cytokines were detected (IL-1β, IL-6, TNF-α, MIP-1α and IFN-α).

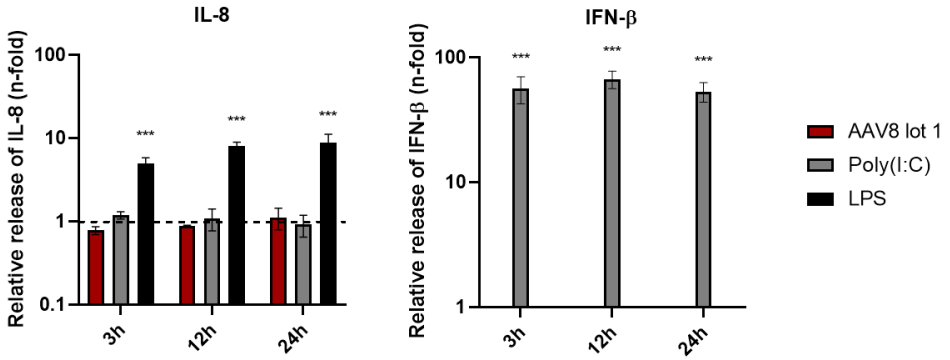

Figure R.12. Evaluation of immune responses to PRR ligands and immunogenic AAV8 lot in hiPSC-RPE cells. Fold increase of cytokine release of IL-8 and IFN-β hiPSC-RPE cells stimulated with 10 ng/ml LPS, 10 µg/ml Poly(I:C) and immunogenic AAV8 lot 1 (MOI: $1:2.5x10^5$ vg). Error bars indicate the standard deviations between replicate assays. Statistical significance was determined using unpaired Student t-test. P-values: ≤0.001: ***.

3.2.2. Evaluation of immune responses in retinal organoids co-cultured with microglia

Another and more complex human model of retinal cells was required to study the innate immune response of the neural retina. ROs consist of photoreceptors (rods and cones), bipolar cells, Müller glia, amacrine cells, horizontal cells and astrocytes, but are absent of ganglion cells, microglia, and RPE cells. In order to improve their immunocompetency, ROs were co-cultured with hiPSC-microglia cells (µROs) as they are known to be key immune-competent cells in the retina[4]. µROs were stimulated with PAM3CSK4, LPS and ODN, ligands for TLR2, TLR4 and TLR9, respectively. Also, immunogenic AAV8 vector lot 4 was used to stimulate the µROs. At early timepoints (6 and 18 hours) after stimulation with PRR ligands and AAV8 vectors, the relative fluorescence of mCherry expressing-µROs was non-significantly increased suggesting a potential response by the microglia cells (**Figure R.13.a.**). Expression of eGFP was detected in AAV8-stimulated µROs from day 3 until the end of the experiment (**Figure R.13.b.**).

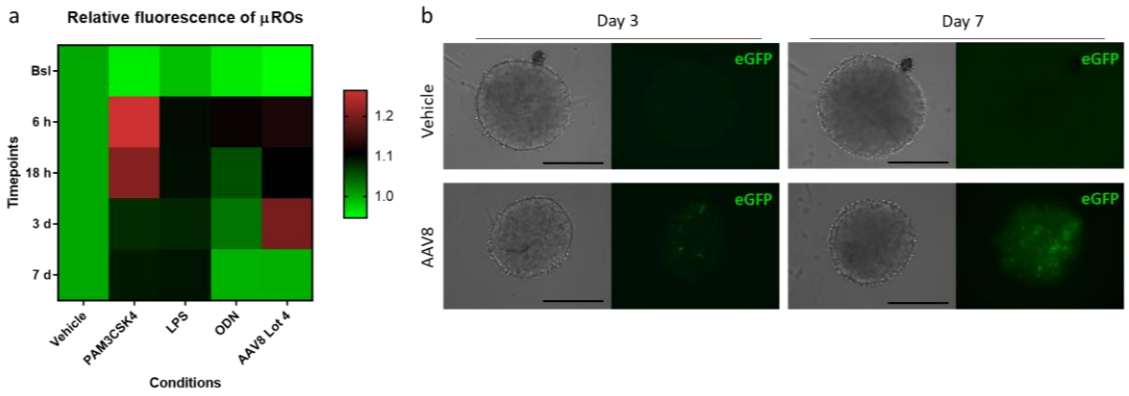

Figure R.13. Fluorescence assessment of µROs upon stimulation with PRR ligands and AAV. µROs were stimulated with 10ng/ml PAM3CSK4, 10µg/ml LPS, 10µM ODN2216 and $1x10^{12}$ vg/ml of AAV8-CMV-eGFP vector (AAV8 lot 4). (a) Heatmap of relative fluorescence of mCherry expressing-microglia cells from µROs at baseline (Bsl) and different timepoints (6h, 18h, 3 days and 7 days) after stimulation. (b) Representative bright field and green fluorescence images of µROs after 3 days (left panel) and 7 days (right panel) of stimulation with immunogenic AAV8 lot 4. Scale bar: 400µm.

In order to assess whether microglia cells improved the immunocompetency of the µRO model, ROs without microglia were also stimulated with PRR ligands and AAV8 vector (no data was collected from ROs without microglia at 6 hours). In general, elicited immune responses were higher at earlier timepoints and

decreased over time. After 6 hours, the release of IFN-γ, IP-10 and MCP-1 was significantly increased in the supernatant of PAM3CSK4-stimulated µROs compared to vehicle (**Figure R.14.a.**). The release of IFN-γ, IP-10, MCP-1 and MIP-1 β was non-significantly increased in LPS-stimulated µROs compared to vehicle at 6 and 18 hours (**Figure R.14.b.**). ODN2216 only induced a significant increase of G-CSF at 6 hours, 18 hours and 3 days (**Figure R.14.c.**). The release of any proinflammatory cytokine was increased after stimulation with AAV8 vector (**Figure R.14.d.**). Although the induction of proinflammatory cytokines upon stimulation with these PRR ligands suggested the presence of TLR2, 4 and 9 in µROs, there was no indication that microglia cells enhanced the immunocompetency of the µROs after comparison with ROs without microglia (**Figure R.14.**).

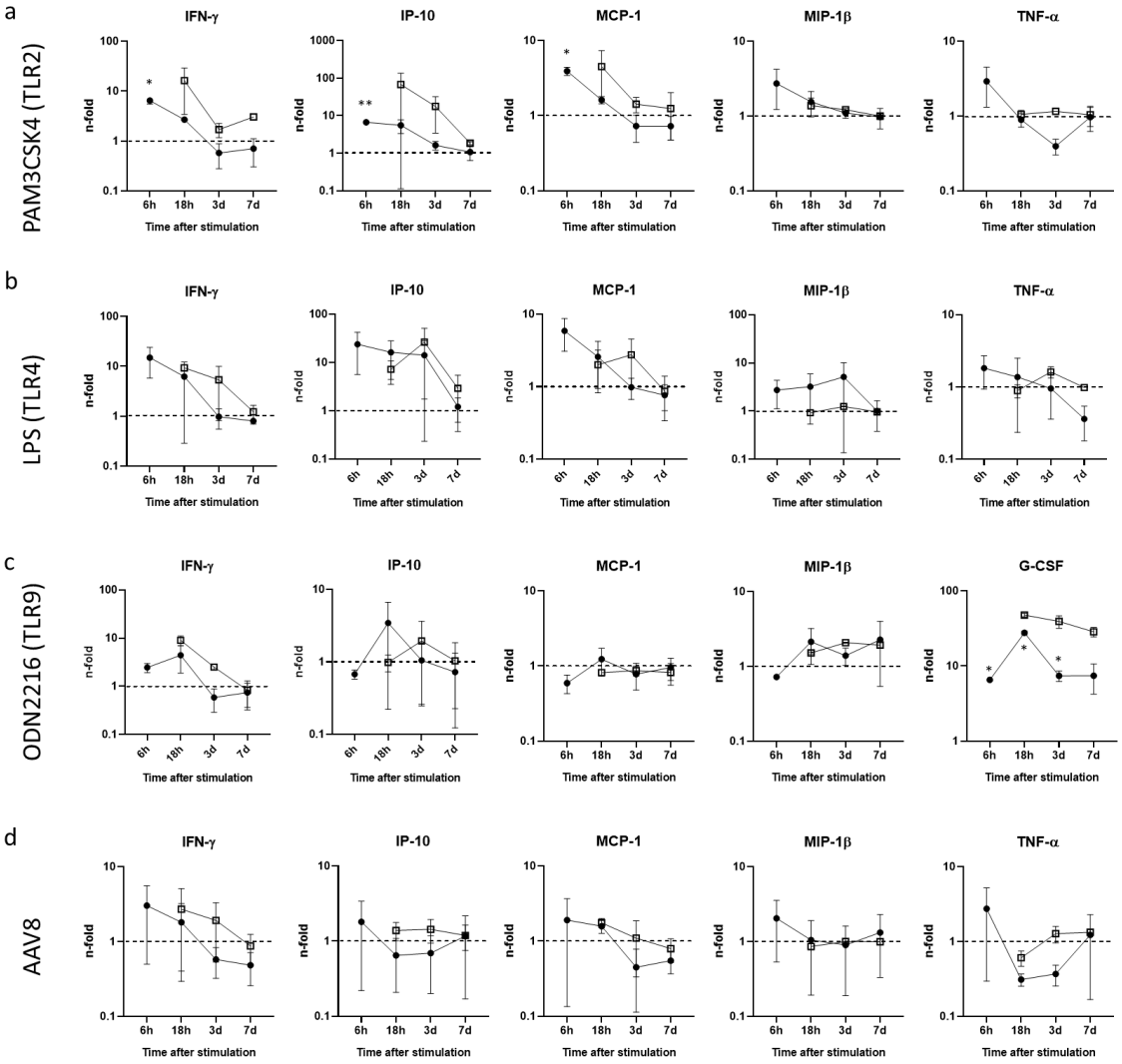

Figure R.14 Innate immune responses induced by µROs following PRR ligands and immunogenic AAV8 vector stimulation. µROs and ROs without microglia cells were stimulated

with (a) 10ng/ml PAM3CSK4, (b) 10µg/ml LPS, (c) 10µM ODN2216 and (d) $1x10^{12}$ vg/ml of AAV8-CMV-eGFP vector (AAV8 lot 4). Supernatants were collected at 6h (except for ROs without microglia), 18h, 3 days and 7 days after stimulation. Fold increase of cytokine release of IFN-γ, IP-10, MCP-1, MIP-1β and TNF-α or G-CSF by stimulated µROs. Error bars indicate the standard deviations between replicate assays. Statistical significance was determined using one-way ANOVA and Holm-Sidak's post hoc analysis. P-values: ≤0.05: *; ≤0.01: **. Black circles: immune responses from µROs; white squares: immune responses from ROs without microglia cells.

3.2.3. Establishment and stimulation of ATP-induced retinal damaged organoids

Because microglia cells were not able to enhance the ability of ROs to generate immune responses, another approach was required. A RO model of ATP-induced retinal damage (ATP-RO) was created in order to mimic the inflammatory state of the retina in a patient with ongoing retinal degeneration undergoing subretinal gene therapy injections *in vivo*. It is known that extracellular inflammatory DAMPs, such as ATP, can induce a distinct activation state in the cells favouring the recognition of other PRR ligands or AAV vectors and generate a synergistic immune response[110].

To establish the ATP-RO model, ROs were incubated with different concentrations of ATP. Using the live cell fluorescent dye Caspase3/7, apoptosis was monitored during several days in order to obtain a suitable ATP concentration to create retinal damage in ROs (**Figure R.15.**). After 2 days, high concentration of ATP (10 mM) induced some cell death in the ROs and caused major changes its morphology. No effect was detected using the medium (5 mM) and low concentrations (1 mM) of ATP at day 2. After 4 days, 10 mM ATP induced massive cell death in ROs and drastic changes in its morphology. At this timepoint, ROs incubated with 5mM ATP also showed cell death (lower than using high concentration) and its morphology suffered mild changes. No differences were found in ROs incubated with 1 mM ATP.

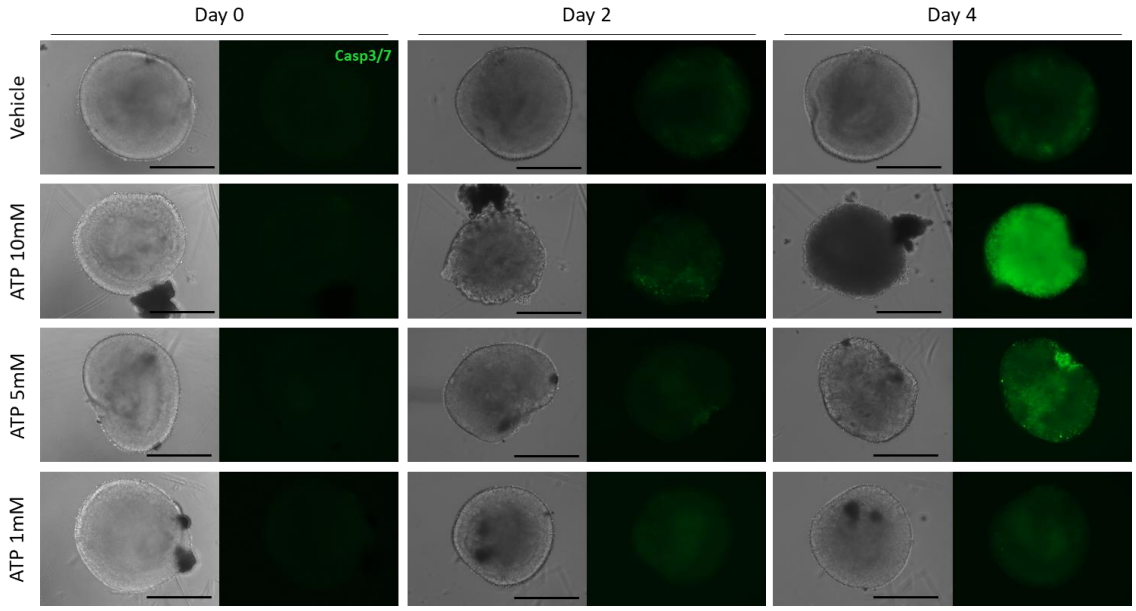

Figure R.15. Retinal organoids treated with ATP for 4 days to induce apoptosis. ROs were incubated with 10-, 5- and 1-mM ATP. Apoptosis was evaluated with the live cell fluorescent dye Caspase3/7. Left panel shows ROs at day 0 (baseline), middle panel at day 2 and right panel at day 4. Cells were imaged using the bright field channel (left images from each panel) and the green fluorescence channel (right images from each panel). Scale bar: 400µm.

Immunostaining analysis was performed in 5 mM ATP-ROs after 4 days in order to further characterize the model (**Figure R.16.**). Nuclei staining (Hoechst) confirmed that ATP was able to induce morphological changes in ROs as observed by the partially disorganized ONL and the loss of F-actin positive structures (Phalloidin). Arrestin and recoverin staining showed the presence and distribution of the photoreceptors in the RO with minor alterations in its polarization. Dickkopf 3 (DKK3) revealed the activity of the Müller glia cells. The intensity of this marker was elevated in ATP-ROs indicating the response of the Müller glia cells against photoreceptor cell death. Also, staining for caspase-3 (Casp3) showed higher cell death in the ONL of ATP-ROs than in vehicle condition.

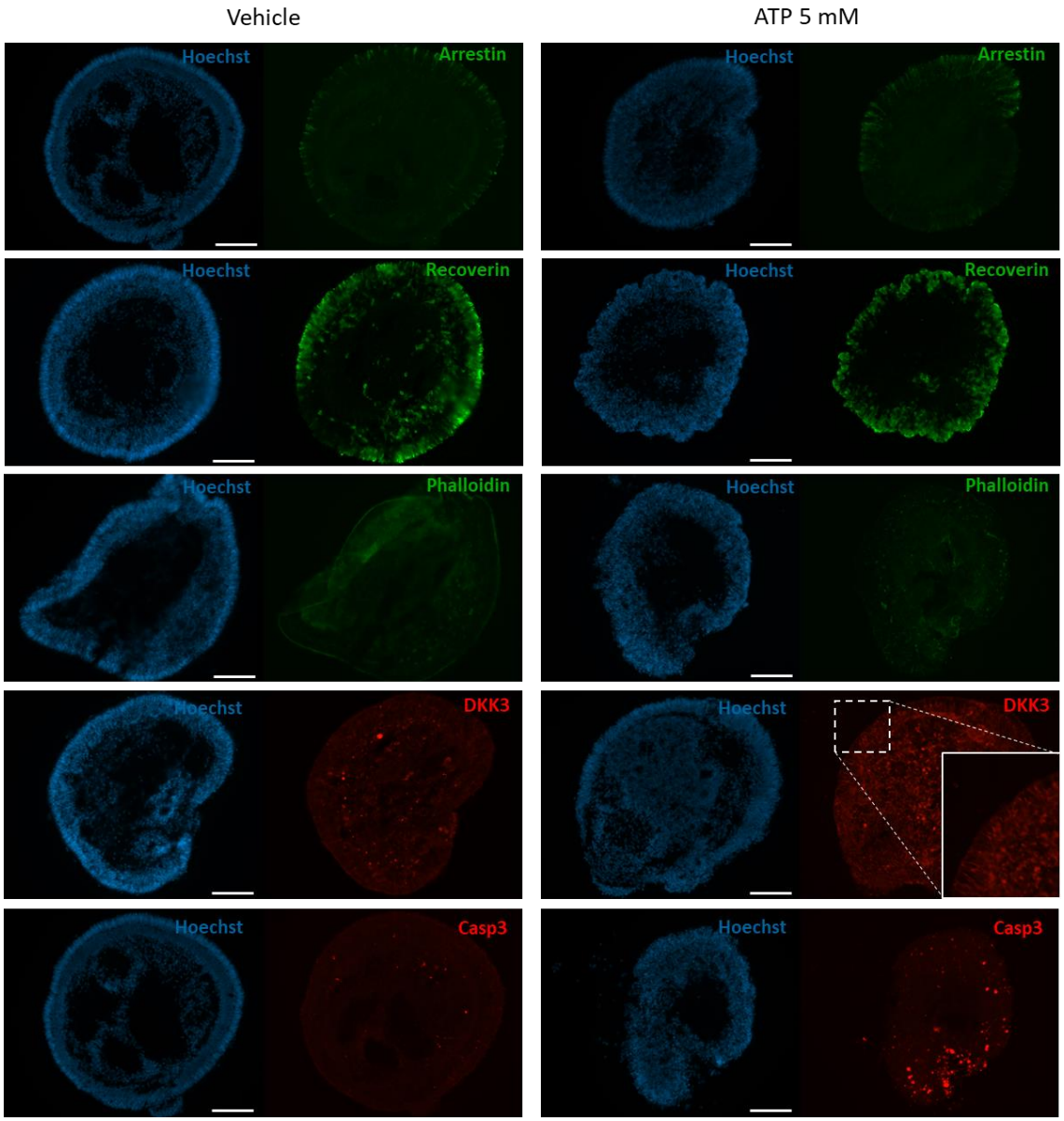

Figure R.16. Immunohistochemical analysis of the ATP-RO model. ROs were incubated with 5 mM ATP or vehicle (control) during 4 days. Sections through retinal organoids using antibodies against: Arrestin (green), Recoverin (green), Phalloidin (green), DKK3 (red) and Casp3 (red) along with the nuclear stain Hoechst 33342 (blue). Magnified image in DKK3 staining shows Müller cell extensions within the outer nuclear layer. Left panel shows sections from ROs without ATP. Right panel shows sections from ATP-ROs. Scale bar: 100 μm.

To evaluate whether ATP-induced retinal cell damage improved the immunocompetency of the ROs, ATP-ROs were stimulated with PRR ligands (PAM3CSK4, LPS and ODN2216) and AAV8 lot 4 and further compared against the previously obtained data from non-damaged ROs. In general, elicited immune responses were higher at 18 hours. The release of IP-10 and MCP-1 was non-

significantly increased in PAM3CSK4- and LPS-stimulated ATP-ROs compared to vehicle at all timepoints (**Figure R.17.a-b.**). The release of MIP-1 β was significantly increased at all timepoints in the supernatant of ODN2216-stimulated ATP-ROs compared to vehicle (**Figure R.17.c.**). No proinflammatory cytokines were increased after stimulation with AAV8 vector (**Figure R.17.d.**). Similar to results from µROs experiments, the induction of proinflammatory cytokines upon stimulation with PRR ligands suggested the presence of TLR2, 4 and 9 in ATP-ROs. However, there was no indication that ATP-induced retinal cell damage enhanced the immunocompetency of the ATP-ROs after comparison with non-damaged ROs (**Figure R.17.**).

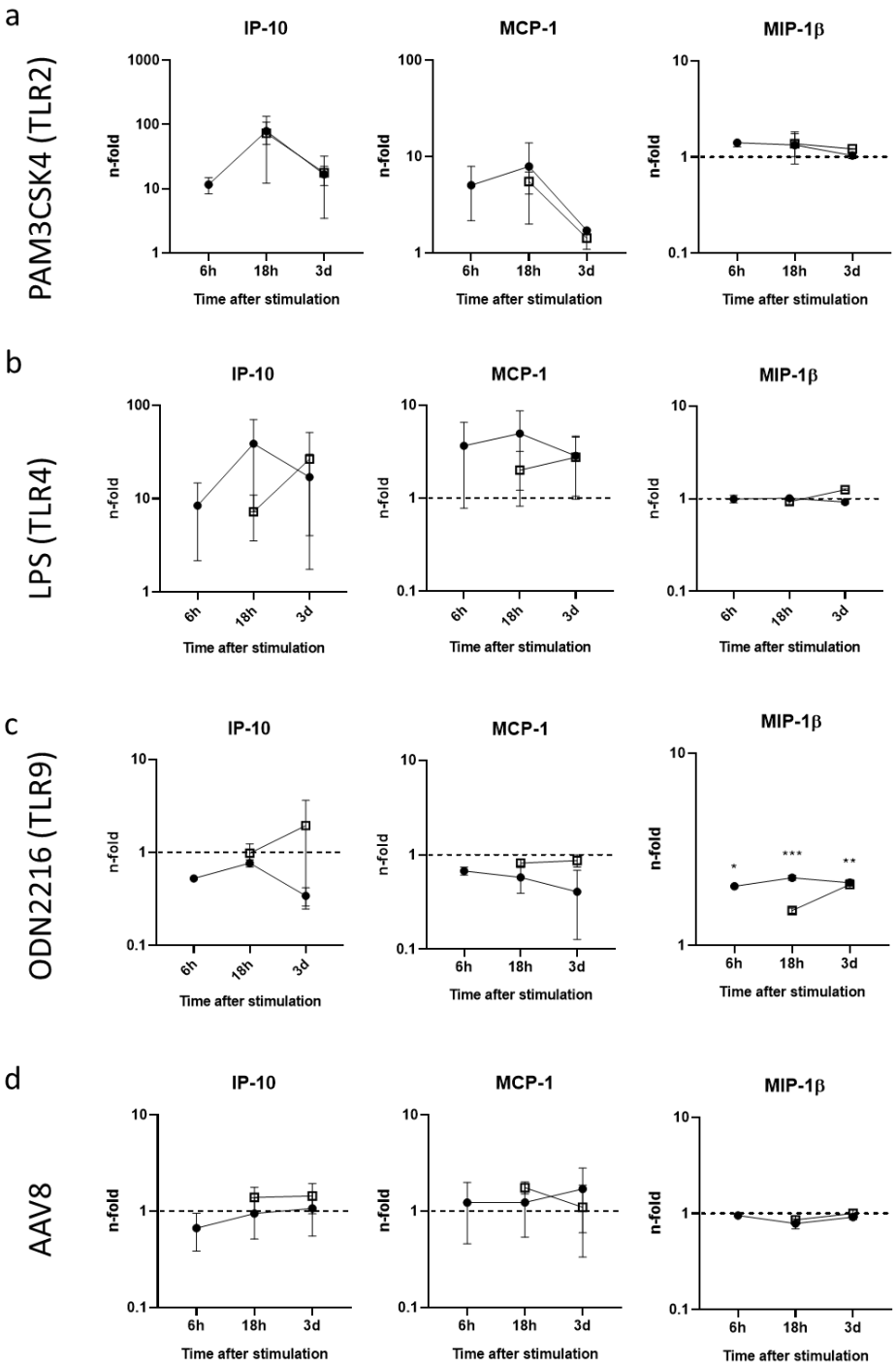

Figure R.17. Innate immune responses induced by ATP-ROs following PRR ligands and immunogenic AAV8 vector stimulation. ATP-ROs and non-damaged ROs were stimulated with (a) 10ng/ml PAM3CSK4, (b) 10µg/ml LPS, (c) 10µM ODN2216 and (d) $1x10^{12}$ vg/ml of AAV8-CMV-eGFP vector (AAV8 lot 4). Supernatants were collected at 6h (except for non-damaged ROs), 18h, and 3 days after stimulation. Fold increase of cytokine release of IFN-γ, IP-10, MCP-1, MIP-1β and TNF-α or G-CSF by stimulated ATP-ROs. Error bars indicate the standard deviations between replicate assays. Statistical significance was determined using one-way ANOVA and Holm-Sidak's post hoc analysis. P-values: ≤0.05: *; ≤0.01: **; ≤0.001: ***. Black circles: immune responses from ATP-ROs; white squares: immune responses from ROs.

To evaluate whether the immunogenicity, as determined in pDCs, influenced the transduction efficiency in the ATP-RO model, we also compared the relative fluorescence of the immunogenic *Sf9*-derived AAV8 lot 4 with and without DNase pre-treatment. We found that just as in HEK293T cells, pre-treatment with DNase increased the transduction efficiency in the AAV8 vector lot, but in a non-significant manner in this model (P= 0.28) (**Figure R.18.**).

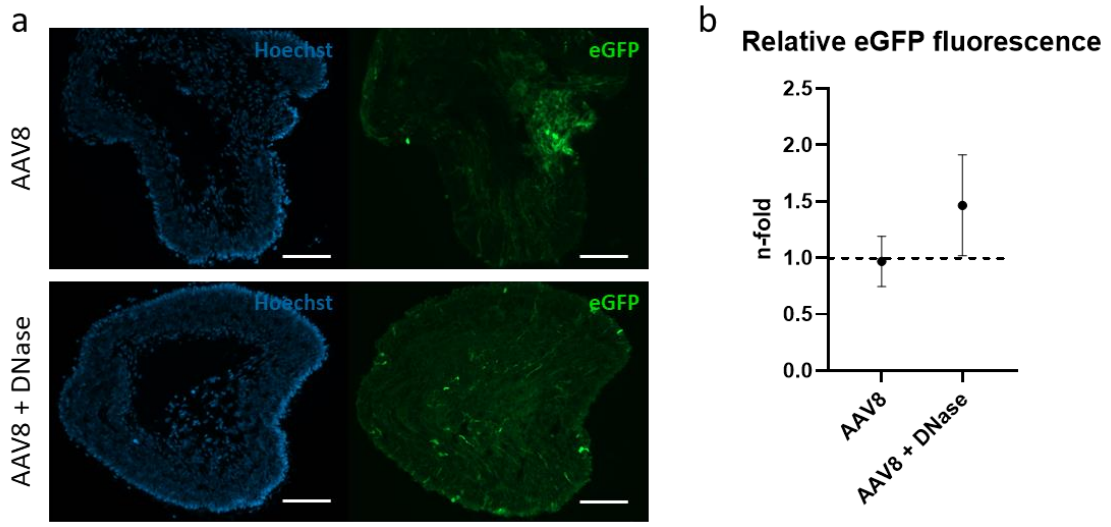

Figure R.18. eGFP fluorescence of ATP-ROs incubated with DNase-treated AAV8-CMV-eGFP vector lot 4. ATP-ROs were stimulated with $1x10^{12}$ vg/ml DNase-treated AAV8 vector lot 4 for 7 days. (a) Sections of ATP-ROs using antibody against eGFP (green) along with the nuclear stain Hoechst 33342 (blue). Scale bar is 100 µm. (b) Relative fluorescence of transduced cells expressing eGFP from ATP-ROs with and without DNase treatment after 7 days. Error bars indicate the standard deviations between replicate assays. Statistical significance was determined using unpaired Student t-test.

3.3. CHAPTER 3. Assessment of hyper-reflective foci in the NHP retina as a potential marker for immune responses to AAV

Rationale. Factors related to AAV-mediated retinal gene therapy such as dose, route of administration, AAV capsid and transgene expression may induce the appearance of discrete hyperreflective elements or HRF in SD-OCT scans. Despite the fact that the appearance of HRF after gene therapy is poorly understood, the presence of HRF in the outer retinal layers is generally considered to be an indicator of immune responses in the form of cellular activation/infiltration by immune-competent cells in retinal disease[111]. In the context of subretinal AAV gene therapy, HRFs may be associated with the surgical procedure, the AAV treatment, or a combination of both. In this chapter, we evaluate whether clinical grade AAV8-RK-hPDE6A (cgAAV8 lot 3, **Table M.1.**) leads to increased appearance of HRF in the retina of NHPs following subretinal gene therapy injection. In order to reduce the number of animals used in studies and in line with the principle of the 3Rs[112] we utilized data (tissue and images) collected for formal toxicology assessment of a gene therapy drug developed for the treatment of patients with PDE6A related retinitis pigmentosa.

3.3.1. Presence and distribution of HRF

Animals were treated with different doses of clinical grade AAV8-RK-hPDE6A (left eyes) and sham-injections (right eyes). In order to look for HRF, a total of 24 eyes from 12 healthy NHPs were assessed. After evaluating ca. 3,600 SD-OCT scans, HRF were observed in 12 of 12 (100%) sham-treated eyes, as well as in 12 of 12 (100%) AAV8-treated eyes after 30 and 90 days (**Figure R.19.**). In this study, there was a significant degree of interexaminer interclass correlation coefficient (ICC) among the three assessors (81%) on the number of HRF in the ONL. However, quantification of HRFs among the hyperreflective structures of the outer limiting membrane, ellipsoid zone, RPE and Bruch's membrane was difficult leading to a high degree of discrepancy among the assessors (inter-rater correlation below 40%). We thus decided to not rely on the quantification of HRF beyond the ONL.

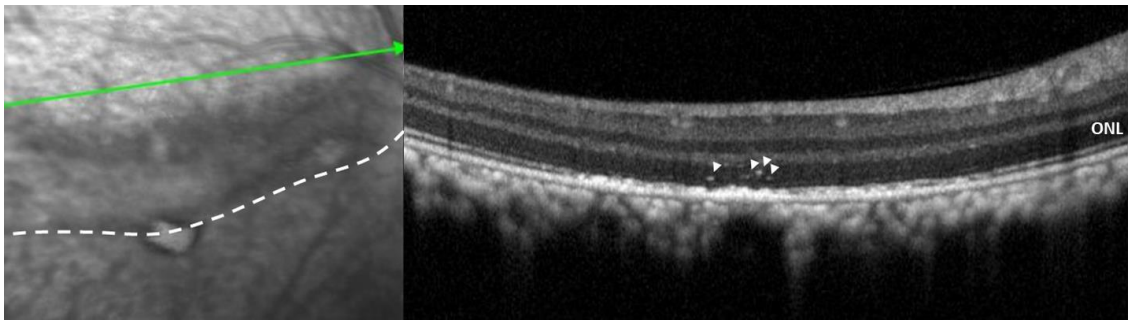

Figure R.19. SD-OCT image of HRF in a sham-treated eye of NHP. The 30˚ fundus IR image with overlying position of B-Scan (left panel, green line) and cross-sectional SD-OCT B-scan (right panel) demonstrate the appearance of HRF in the ONL (arrow heads) within the bleb area (white dashed line) 30 days after subretinal injection. HRF: hyperreflective foci; IR: infrared; NHP: non-human primate; ONL: outer nuclear layer; SD-OCT: spectral-domain optical coherence tomography. Adapted from Rodríguez-Bocanegra et al (2021)[52].

To understand how HRF were distributed across the retina of the animals, HRF distribution maps were generated. According to the HRF distribution maps, HRF were primarily found at the retinotomy site and also in transition zones between the bleb border and non-detached retina (**Figure R.20.**). In general, the observed numbers of HRF from both right and left eyes of low- and medium-dose groups (groups 1 and 2) were higher when measured at 30 days than at 90 days. The same trend was observed in sham-treated eyes from high-dose group (group 3). In contrast, the number of HRF in AAV8-treated eyes from the high-dose group (group 3) increased from day 30 to day 90. Statistical analysis was performed in order to evaluate these observations in the HRF distribution maps.

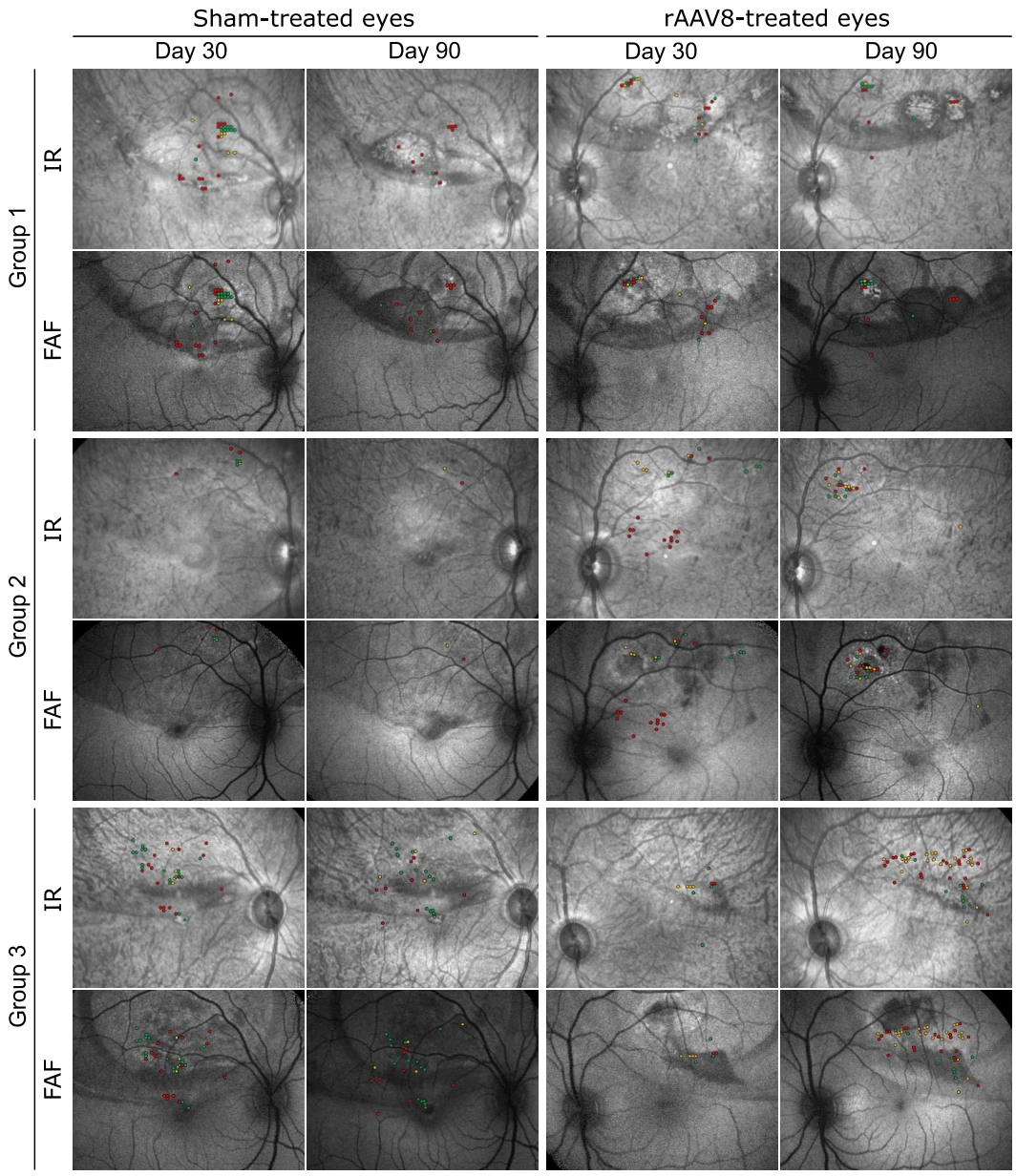

Figure R.20. Representative distribution maps of HRF in the retina of NHPs 30- and 90-days after subretinal injection of BSS (sham) or different doses of AAV8. HRF are plotted on IR and FAF images in different colours. Green dots: HRF were identified by three observers; yellow dots: HRF were identified by two observers; red dots: HRF were identified by one observer. FAF: fundus autofluorescence; Group 1: low-dose group ($1x10^{11}$ vg); Group 2: medium-dose group ($5x10^{11}$ vg); Group 3: high-dose group ($1x10^{12}$ vg); HRF: hyperreflective foci; IR: infrared; NHP: non-human primate. Obtained from Rodríguez-Bocanegra, et al (2021)[52].

The mean number of all HRF in sham- vs AAV8-treated eyes at 30- and 90-days post-treatment were calculated and summarized in **Table R.2**. In groups 1 and 2, there were no significant changes in the number of HRF between sham- and AAV8-treated eyes at 30 days or 90 days after treatment. However, in group 3,

there was a significant difference in the number of HRF at 90 days between sham- and AAV8-treated eyes, with the AAV8-treated eyes having a higher number of HRF. These results confirmed the differences observed in the representative HRF distribution maps.

Table R.2. Mean number of HRF in sham- vs AAV8-treated eyes per dose group after 30- and 90-days post treatment. Statistical analysis was performed by using two-way ANOVA and Sidak's correction *post hoc* analysis. P-values: ≤0.05: *.

			30 days after treatment			90 days after treatment		
Dose group	**Dose (vg)**	***n***	**Right eye (Sham)**	**Left eye (AAV8)**	***P***	**Right eye (Sham)**	**Left eye (AAV8)**	***P***
1 (Low)	$1x10^{11}$	4	20.7 ± 23.4	11.4 ± 17.2	0.60	10.4 ± 8.7	16.4 ± 20.5	0.91
2 (Medium)	$5x10^{11}$	4	28.2 ± 27.4	18.8 ± 14.8	0.59	7.2 ± 9.2	13.4 ± 12.5	0.90
3 (High)	$1x10^{12}$	4	21.3 ± 24.8	5.9 ± 4.6	0.19	14.4 ± 16.0	43.2 ± 51.8	0.02 (*)

The number of HRF was also compared between the dose-groups (**Table R.3.**). There were significant differences in the number of HRF at 90 days between eyes treated with low and high dose (16.4 ± 20.5 vs 43.2 ± 51.8, $P = 0.03$) and between medium and high dose AAV8 (13.4 ± 12.5 vs 43.2 ± 51.8, $P = 0.01$).

Table R.3. Multiple comparisons of mean difference in the number of HRF in sham- and AAV8-treated eyes among the three dose-groups. Statistical analysis was performed by using multiple comparisons and Tukey's HSD *post hoc* analysis. P-values: ≤0.05: *.

					95% CI of the diff.		
Eye	**Timepoint**	**Groups (J)**	**Groups (K)**	**Mean diff. (J-K)**	**Lower**	**Upper**	***P***
Sham-	30 days	Group 1	Group 2	-7.50	-26.79	11.79	0.62
			Group 3	-0.67	-19.96	18.63	0.99
		Group 2	Group 3	6.83	-12.46	26.13	0.67
	90 days	Group 1	Group 2	3.25	-16.04	22.54	0.91
			Group 3	-4.00	-23.29	15.29	0.87
		Group 2	Group 3	-7.25	-26.54	12.04	0.64
AAV8-	30 days	Group 1	Group 2	-7.33	-31.97	17.30	0.76
			Group 3	5.50	-19.14	30.14	0.85
		Group 2	Group 3	12.83	-11.80	37.47	0.43

	90 days	Group 1	Group 2	3.00	-21.64	27.64	0.95
			Group 3	-26.75	-51.39	-2.11	0.03 (*)
		Group 2	Group 3	-29.75	-54.39	-5.11	0.01 (*)

3.3.2. Kinetics of HRF over time

The number of HRF was compared between timepoints, i.e. 30 vs. 90 days, to assess its kinetics (**Table R.4.**). There were two instances when substantial changes between timepoints were observed. The first was found in sham-treated eyes of group 2, where the number of HRF was substantially greater at day 30 than at day 90 (28.2 ± 27.4 vs 7.2 ± 9.2, P = 0.003, **Figure R.21.a.**). Furthermore, a non-significant trend in the decrease of the number of HRF was detected in the sham-treated eyes of the three dosage groups. AAV8-treated eyes from group 3, on the other hand, showed an increase in HRF over time, with considerably higher numbers at day 90 compared to day 30 (43.2 ± 51.8 vs 5.9 ± 4.6, *P* = 0.001, **Figure R.21.b.**). **Figure R.21.c.** shows the changes in the numbers of HRF, normalized for 30-days measurements, in the sham- and AAV8-treated eyes per group. There was a drop in the number of HRF in sham-treated eyes from groups 1, 2, and 3, equivalent to a mean loss of 49%, 74%, and 32%, respectively. In parallel, in AAV8-treated eyes, there was a decrease in the number of HRF, equivalent to a mean loss of 28%, whereas groups 1 and 3 exhibited an increase in the number of HRF, corresponding to a mean gain of 30% and 86%, respectively.

Table R.4. Multiple comparisons of mean difference in the number of HRF in sham- and rAAV8-treated eyes between the two different timepoints. Statistical analysis was performed by using multiple comparisons and Sidak's correction *post hoc* analysis. P-values: ≤0.01: **.

					95% CI of the diff.		
Eye	**Groups**	**Timepoint (J)**	**Timepoint (K)**	**Mean diff. (J-K)**	**Lower**	**Upper**	***P***
Sham-	Group 1	30 days	90 days	10.25	-4.59	25.09	0.25
	Group 2			21.00	6.16	35.84	0.003 (**)
	Group 3			6.92	-7.92	21.75	0.58
AAV8-	Group 1	30 days	90 days	-5.00	-28.52	18.52	0.93
	Group 2			-5.33	-18.18	28.85	0.92
	Group 3			-37.25	-60.77	-13.73	0.001 (**)

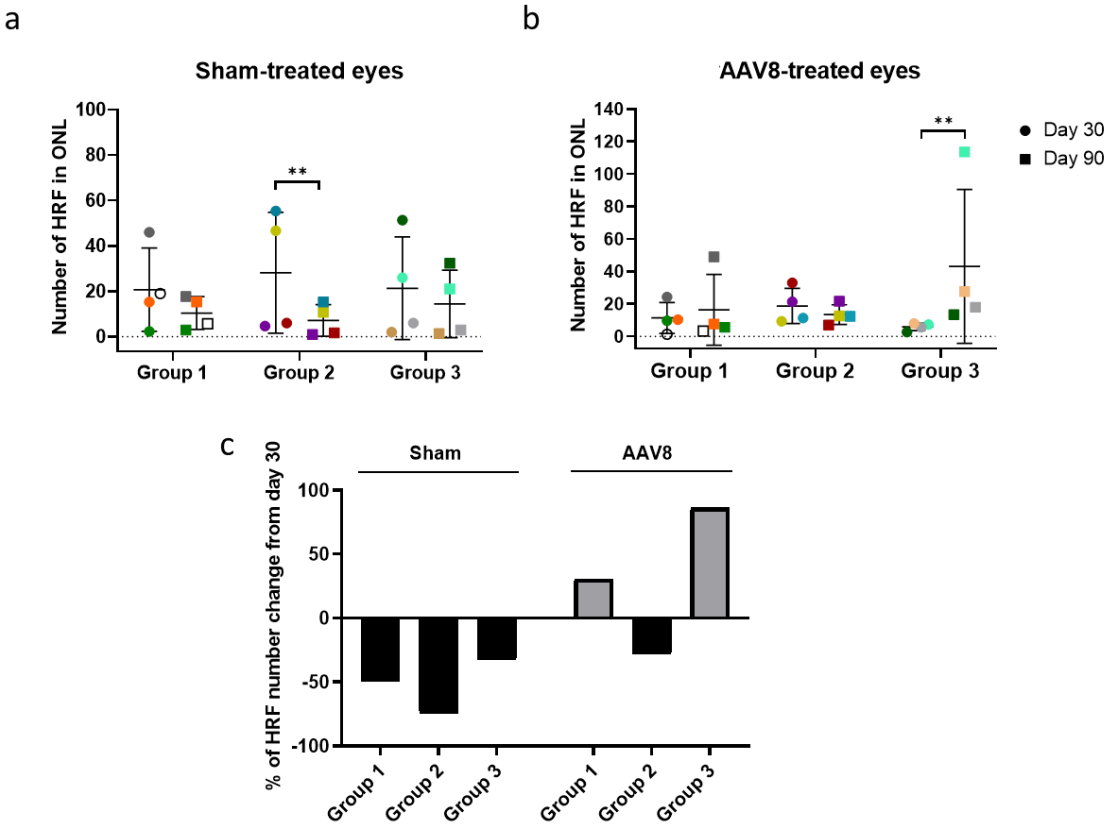

Figure R.21. Kinetics of HRF of over time. Graphic representation of the number of HRF in ONL in (a) sham- and (b) AAV8- treated eyes for the three groups at days 30 and 90 post-subretinal injection. Each coloured symbol represents one animal (4 per group). Statistical analysis was performed by using multiple comparisons and Sidak's correction *post hoc* analysis. P-values: ≤0.01: **. c) Graphic representation of the percentage of mean change in the number of HRF normalized to 30-days measurements. Values below 0 indicate a decrease in the % of the number of HRF from day 30 to day 90; and values above 0 indicate an increase of HRF. Group 1: low-dose group; Group 2: medium-dose group; Group 3: high-dose group; HRF: hyperreflective foci; ONL: outer nuclear layer. Adapted from Rodríguez-Bocanegra, et al (2021)[52].

3.3.3. Assessment of variations in the outer nuclear layer

It is known that the damage that is produced in the tissue upon subretinal injection can also induce morphological changes in the retina, such as thinning of the ONL due to the loss of the photoreceptors[69]. Therefore, the thickness of the ONL was also measured. We found that it was significantly decreased in the sham-treated eyes of all dose groups 30 days after subretinal injection (P = 0.015, 0.013, and 0.0003, for groups 1, 2 and 3, respectively; **Table R.5.** and **Figure R.22.a**).

Groups 1 and 3 exhibited no variations in ONL thickness after 90 days compared to day 30 (P = 0.23 and 0.68, respectively), whereas group 2 was significantly reduced (P = 0.0001). In contrast, the thickness of the ONL in the AAV8-treated eyes did not alter after the first 30 days (P = 0.96, 0.07 and 0.29, for groups 1, 2 and 3, respectively; **Table R.5.** and **Figure R.22.b.**). At day 90, the thickness of the ONL was significantly reduced in group 2 (P = <0.0001) but not in the other two groups (P = 0.27 and 0.36, for groups 1 and 3, respectively).

Table R.5. Multiple comparisons of mean difference in the thickness of ONL (µm) in sham- and rAAV8-treated eyes among the three different timepoints using Tukey's HSD *post hoc* analysis. P-values: ≤0.05: *; ≤0.001: ***.

					95% CI of the diff.		
Eye	**Groups**	**Timepoint (J)**	**Timepoint (K)**	**Mean diff. (J-K)**	**Lower**	**Upper**	***P***
Sham-	Group 1	BSL	30 days	3.27	0.56	5.89	0.015 (*)
		30 days	90 days	-1.68	-4.14	0.78	0.23
	Group 2	BSL	30 days	1.47	0.29	2.65	0.013 (*)
		30 days	90 days	2.60	1.60	3.60	<0.0001 (***)
	Group 3	BSL	30 days	12.17	5.31	19.03	0.0003 (***)
		30 days	90 days	-1.31	-5.11	2.48	0.68
AAV8-	Group 1	BSL	30 days	-0.23	-2.26	1.81	0.96
		30 days	90 days	-1.32	-3.40	0.74	0.27
	Group 2	BSL	30 days	-1.28	-2.64	0.09	0.07
		30 days	90 days	3.85	2.54	5.17	<0.0001 (***)
	Group 3	BSL	30 days	-2.294	-5.95	1.37	0.29
		30 days	90 days	2.18	-1.67	6.04	0.36

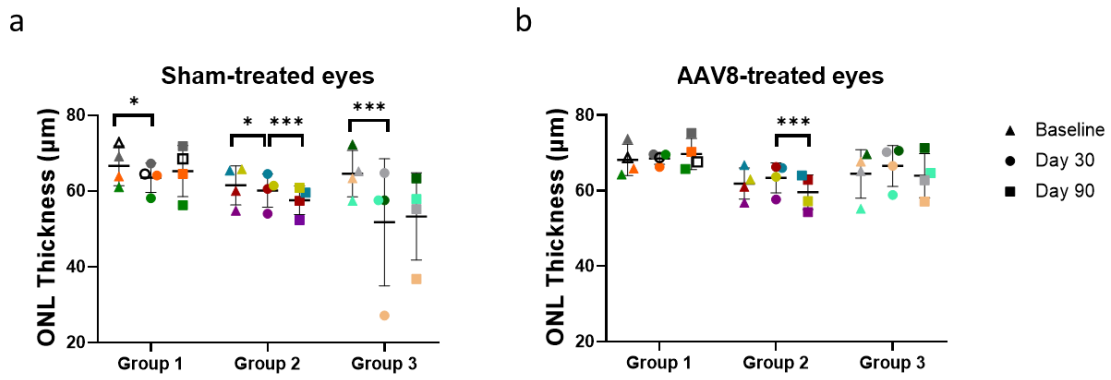

Figure R.22. Thickness of ONL over time. Graphic representation of the ONL thickness in a) sham- b) and AAV8-treated eyes for the three groups of animals at baseline and days 30 and 90

post-subretinal injection. Each coloured symbol represents one animal (4 per group). Statistical analysis was performed by using multiple comparisons and Tukey's HSD *post hoc* analysis. P-values: ≤0.05: *; ≤0.001: ***. Group 1: low-dose group; Group 2: medium-dose group; Group 3: high-dose group; ONL: outer nuclear layer. Adapted from Rodríguez-Bocanegra, et al (2021)[52].

3.3.4. Evaluation of immune cell infiltrates in retinal sections

Immunohistochemistry was conducted on NHP retinas to investigate a possible histological counterpart of the HRF observed in SD-OCT images. Due to their separate spatial orientations and probable artefacts in the processing of eye cups, a reliable correlation between horizontal SD-OCT scans and vertical retinal sections was not achievable. To do a semiquantitative comparison, the sections were labelled with the macrophage marker CD68, the B-cell marker CD20, and the T-cell marker CD3. Microglia activation was labelled with Iba-1 and RPE cells with RPE65.

Staining with the immune cell markers CD20, CD3, and CD68 in sham-treated eyes was negative in all groups, including in regions close the retinotomy (**Figure R.23.a-l.**). H&E staining revealed no tissue abnormalities, indicating that these eyes did not have any specific signs of inflammatory cell infiltration in the retina (despite the frequency of HRF evident from the SD-OCT data). However, both sham- and AAV8-treated eyes had positive Iba-1 staining in the bleb region, but Iba-1 staining was negative in non-treated parts of the same retinas. Iba-1 staining was considerably more visible in regions surrounding the retinotomy site in AAV8-treated eyes than in sham-treated eyes (**Figure R.23.m-x.**). B- and T-cells were found in the retinas of four out of twelve animals: one from group 1 and three from group 3, but none in animals from group 2. Using the RPE65 specific antibody, no RPE cell migration was observed.

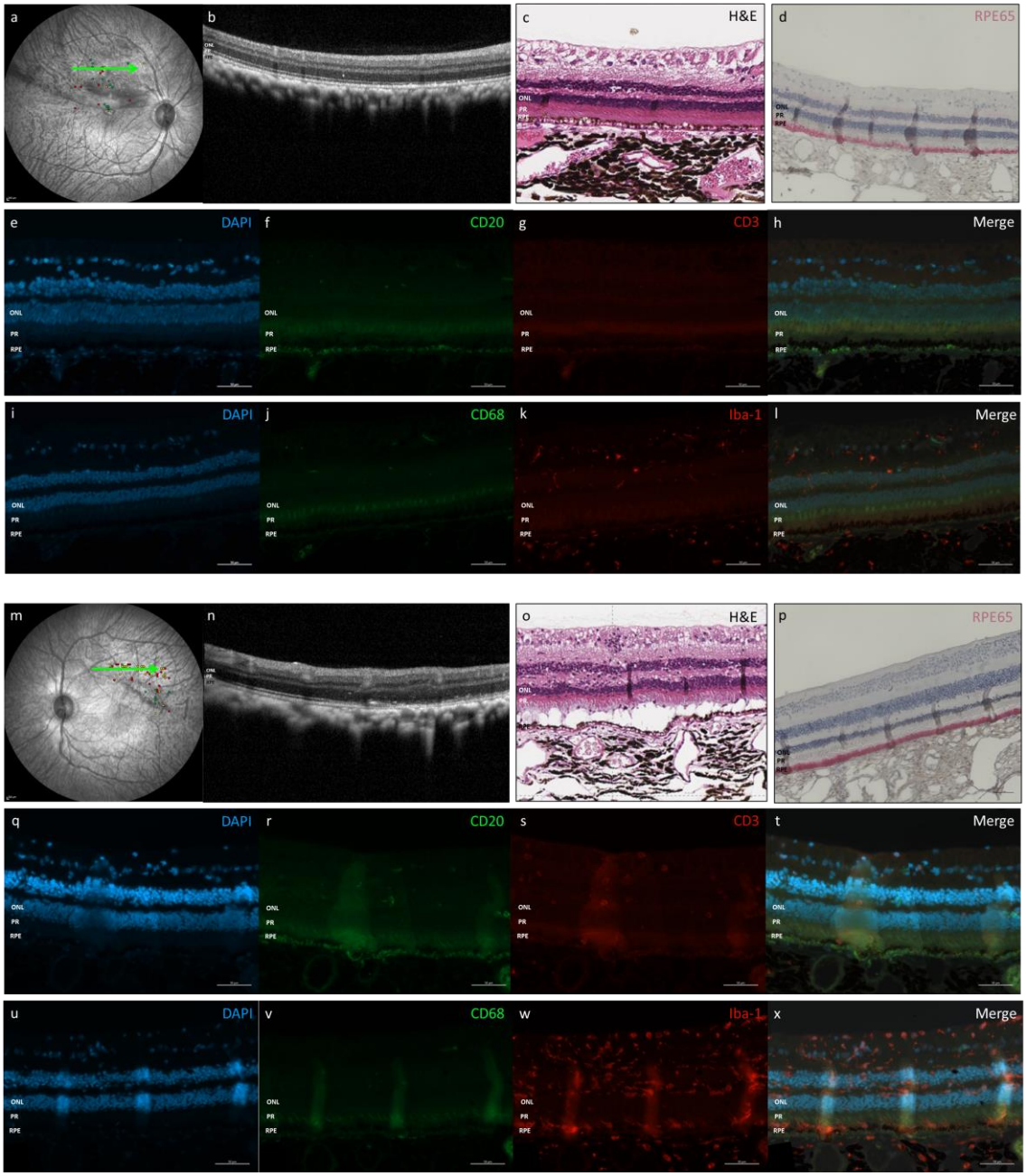

Figure R.23. Immunohistochemical analysis of retinas from high dose group. Analysis was performed in sham- (a-l) and AAV8- (m-x) treated eyes from group 3 animals. The 60˚ fundus IR image showing the representative HRF distribution maps (a and m) with overlying position of B-Scan (green line) and cross-sectional SD-OCT B-scans (b and n) demonstrate the appearance of HRF within the treated area 90 days after subretinal injection. Normal H&E staining of an area close to the SD-OCT scan (c and o). Immunohistochemical permanent staining of RPE65 shows the integrity of the RPE layer (d and p). B- and T- cells ($CD20^+$ and $CD3^+$ cells, respectively) were not detected in the sham treated eyes (e-h) but they were found in the AAV8 treated eyes (q-t). The macrophage marker CD68 was not detected neither in sham- (j) nor in AAV8- (v) treated eyes. However, microglia cells were more active in AAV8-treated eyes (w) than in sham-treated eyes (k). Scale bar: 50 µm. HRF: hyperreflective foci; H&E: haematoxylin and eosin; IR: infrared; ONL: outer nuclear layer; PR: photoreceptors; RPE: retinal pigment epithelium; SD-OCT:

spectral-domain optical coherence tomography. Obtained from Rodríguez-Bocanegra, et al (2021)[52].

The presence of cell infiltrates in the retina was observed first in H&E staining of two AAV8-injected eyes from groups 1 and 3. Perivascular infiltrates developed around retinal blood vessels in both animals (**Figure R.24.a-j.**); there was also evidence of a subretinal cell infiltration (**Figure R.24.k-t.**) in the area where the retinotomy was performed in one animal from group 1. Such infiltrates were discovered around some retinotomy sites. The bulk of infiltrating cells tested positive for immune cell markers. In both perivascular and subretinal infiltrates, B- and T- cells, and activated microglia cells were dominating. Except for the area where the subretinal infiltration was evident, the integrity of the RPE layer was normal in all animals from all groups.

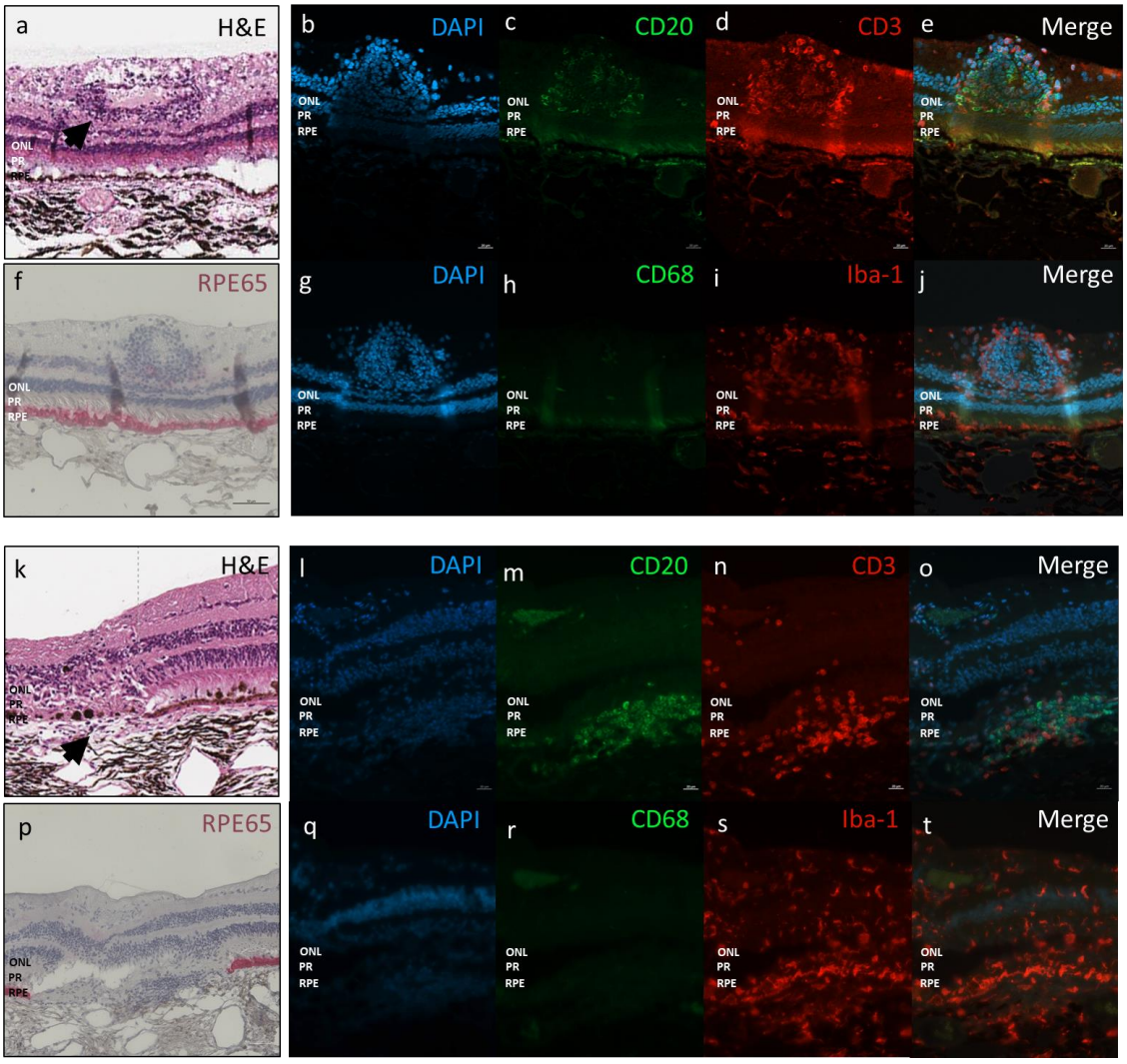

Figure R.24. Immune retinal infiltrates in the retina of NHP primates. Infiltrates were found in perivascular (a-j) and subretinal (k-t) areas of animals from group 3 and group 1, respectively,

treated with AAV8. H&E staining shows the appearance of leukocytic cells infiltration in the perivascular area of a retinal blood vessel (a, black arrow) and between the neural retina and the choroid (k, black arrow). RPE65 staining shows the state of the RPE layer (f and p) being completely absent in the area where the subretinal infiltrate is present (p). $CD20^+$ and $CD3^+$ cells (b-e and l-o) together with microglia activation (i and s) were found in both types of infiltrates. The macrophage marker CD68 was only detected in the perivascular infiltrate (h). Scale bar: 30 µm. H&E: haematoxylin and eosin; ONL: outer nuclear layer; PR: photoreceptors; RPE: retinal pigment epithelium. Obtained from Rodríguez-Bocanegra, et al (2021)[52].

4. Discussion

Retinal gene therapy using AAV vectors has been an innovative force with an approved drug (*voretigene neparvovec*) leading the charge. However, it is still hampered by a number of challenges that must be addressed in order to enhance the safety and efficacy of these therapies. In light of this, it is becoming increasingly critical to have a better knowledge of the mechanisms underlying immunological responses to AAV vectors. In this PhD project, we focused on the innate immune responses to AAV vector- and AAV production system-dependent factors that modulate vector immunogenicity in different *in vitro* models and its impact on AAV-mediated retinal gene therapy. Indeed, our immunocompetent cell model, based on human pDCs, was able to respond to AAV vectors in a lot-dependent manner. To understand this phenomenon, we developed several strategies to find out which factor was modulating the AAV lots-specific immunogenicity and the innate immune pathway involved in its recognition. This process allowed us identify extra-viral DNA as the main cause of the different immunogenicity amongst the vectors and to distinguish between immunogenic and non-immunogenic AAV vector lots. We also performed further studies with more specialized and complex retinal *in vitro* cell models to test the immunogenicity of AAV vectors as they were known to have proper innate immune mechanisms to sense the vectors. However, these retinal models did not show significant reactions to the AAV stimulus. It is currently unclear, whether this is due to fundamental limitations of the respective models based on iPSCs of

one individual donor or due to a limited immunogenicity of AAV in more complex tissue settings. Interestingly, additional studies following application of clinical grade vectors in NHPs suggested again that AAV can induce a relevant immune response in the retina as evidenced by the appearance of HRF as indicators of immune cell infiltration.

4.1. Elucidating what lies behind the AAV lot-specific innate immune responses

In a recent publication, a comparative study of AAV vectors produced in HEK293 and *Sf9* cells was conducted[45]. The authors showed that PTMs and residual HCP impurities varied between HEK293- and *Sf9*-derived vectors across all AAV serotypes and manufacturers that were tested. Furthermore, they also suggested that immunogenicity of AAV vectors might differ depending on the production system. In this project, we analysed the potential immunogenicity differences between these two main production systems using various lots of the same AAV construct from different suppliers and two distinct serotypes in different *in vitro* models.

The use of immunocompetent cell models has allowed researchers to more precisely examine the involvement of PRR pathways in AAV-induced innate immune responses[64,65]. For that reason, both human pDCs and PMA-differentiated THP-1 cells were chosen as immunocompetent cell models in our project as it has been previously described that they are able to sense AAV vectors[65,73]. Interestingly, the immunogenicity identified in our human pDC *in vitro* model to AAV was lot-specific rather than related to a specific production system, manufacturer, serotype or the full-to-empty capsid ratio.

Previous pre-clinical and clinical investigations of AAV-mediated retinal gene therapy have found that variations in capsid/vg ratios[106] or differences in AAV vector dose[15] might have an impact on immunological responses to AAV vectors, such as ocular inflammation or immune cell infiltration. Nonetheless, our findings revealed that high capsid/vg ratios were found in both immunogenic and non-immunogenic AAV vector lots, indicating that a high number of capsids in the viral suspension was not the reason of the immunogenicity variations between the

lots. In addition, we also observed that raising the dose of non-immunogenic AAV vectors was insufficient to elicit innate immune responses in human pDCs.

To explore the mechanism involved in the identification of the immunogenic AAV vector lots in order to understand the source of the variations in immunogenicity, we analysed the PRR pathway by which pDCs were known as antiviral sensors: the TLR9[65,78]. Similar to experiments from Zhu et al.[65], we employed one of the most specific TLR9 antagonists, H154, in order to block this signalling pathway in our human pDC model[65,113–116]. With this, we indirectly observed that immunogenic AAV2 and AAV8 lots elicited TLR9-dependent innate immune responses in human pDCs.

As TLR9 is a DNA receptor[117], the immunological responses to immunogenic AAV vector lots were likely elicited by DNA components. We first evaluated whether the viral DNA was the responsible of these differences in immunogenicity among the AAV vector lots. However, our ddPCR measurements confirmed that viral DNA was present in both immunogenic and non-immunogenic vector lots. In addition, we also showed that when the DNA contained in the viral capsids of the AAV vectors was exposed to the cells by heat-treatment, the immune response increased. Nevertheless, as it is known that impurities such as DNA from plasmids or host cells used in vector production systems, can also be packaged during assembly of AAV vectors[118,119], it is unclear if this increased immunogenicity after opening the viral capsids was caused by the viral DNA or by non-vector DNA sequences.

Collectively, this showed that the immunological response to immunogenic AAV vector lots in pDCs was triggered by extra-viral DNA components found in viral suspensions rather than the AAV particle themselves. In order to determine the source of the extra-viral DNA, further experiments such as next-generation sequencing[120] or super-resolution microscopy could be performed. However, it must be noted that the fact that DNase treatment decreased or eliminated the immunogenicity of the immunogenic AAV vector lots supports this hypothesis.

4.2. Relevance of residual impurities in clinical grade vector preparations.

As previously discussed, through the use of human pDCs, we detected that extra-viral DNA impurities caused half of our experimental AAV vectors lots to show

higher immunogenicity. Additionally, presence of HCP impurities are also known to be a potential source of immunogenicity in AAV vector preparations[45,121] and in other biotherapeutics[122]. For safety reasons, cgAAV vectors produced in accordance with current GMP guidelines are frequently inspected for impurities (as opposed to experimental AAV vectors which are subject to less stringent standards). For instance, in the first authorised gene-therapy treatment by the European Medicines Agency (EMA), an inspection revealed excessive levels of impurities, including residual host cell impurities, in lots of cgAAV vector for alipogene tiparvovec (Glybera) gene therapy, leading to the deauthorisation of those lots[123].

In the manufacturer's detailed information of our cgAAV8 vector lots, there was no indication of known extra-viral DNA impurities in the viral suspensions. It was specified that human Galectin-3-binding protein (hLG3BP) was the only HCP impurity (from HEK293 cells) found in different amounts in our three lots of cgAAV vector. Therefore, we applied the cgAAV lot with the highest HCP content (cgAAV8 lot 2, 1433.7 ng/ml) to human pDCs in order to measure potential innate immune responses to HCP impurities. However, we showed that no pro-inflammatory cytokines were released after stimulation the vectors.

It is known that hLG3BP is a protein that has a strong interaction with AAV6 vectors reducing their potency, but poorly interact with AAV8[124,125]. That means that hLG3BP is co-purified with the AAV8 particles, but not bound to the capsids. In addition, it has been shown that hLG3BP could act as a ligand for TLR4[126]. Then, we used our cgAAV8 lot 2 in PMA-differentiated THP-1 cells as it was considered a model that secretes inflammatory cytokines and chemokines upon TLR4 stimulation[127]. However, the stimulation did not elicit any immune response. Therefore, this might imply that either the quantity of HCP content in our cgAAV vector lots was insufficient to elicit immunological responses in our *in vitro* models, or that HCP impurities were less immunogenic than extra-viral DNA impurities.

In turn, AAV-mediated subretinal gene therapy of AAV8-RK-hPDE6A (cgAAV8 lot 3) carrying 582 ng/ml HCP content (approximately half as much as cgAAV8 lot 2) induced immune responses in NHPs from the high dose group ($1x10^{12}$ vg). Therefore, although the mechanism by which this cgAAV8 vector induced an

immune response *in vivo* is not known, it can be assumed that it was mediated by the AAV particles rather than extra-viral impurities (DNA or HCP).
Therefore, although there are no universally agreed-upon standards for what levels of impurities are appropriate in cgAAV vector lots[15], improving their manufacturing process is key to avoid the presence of residual impurities in the viral suspensions and thus, reduce their potential immunogenicity.

4.3. Discrepancies between strong immune responses *in vivo* and weak immune responses in our *in vitro* retinal models

Innate immune response in the retina is a crucial response of the host to retinal insults. As mentioned in section 1.4.2., the RPE cells and ROs have the capability to detect pathogens through the use of numerous TLR molecules and generation of immune mediators. In addition, it is known that AAV vectors can induce innate and adaptive immune responses in the retina such as inflammation or B and T cell infiltration[15], something we also observed in the analysis of our NHP samples. Therefore, we used these models to investigate the retinal cell types that could recognize the AAV vectors.
Apart from expressing TLRs, the RPE also forms the BRB between the neural retina and the choriocapillaris *in vivo,* which makes it a good candidate for the recognition of the AAV vectors, especially when applied subretinally. Xiong et al. suggested that the AAV8 vectors (containing broadly active promoters such as CMV) are sensed by the RPE cells in mice[69]. However, the stimulation of hiPSC-RPE with our AAV8-CMV-eGFP vectors did not elicit any immune response, perhaps due to the artificial nature of this model that lacks the natural interaction with the underlying choroid through the Bruch's membrane and the neuroretinal tissue leading to the vitreous cavity and anterior segment of the eye.
Microglia cells, considered the retina's main resident immune cell, are able to detect viruses and produce immune mediators in response to them[128]. In a recent study where AAV vectors were intravitreally injected in mice eyes, the authors showed that AAV8 vectors carrying the same promoter and transgene that we used in this study, induced the activation of microglia cells so, they suggested that these cells might be involved in vector recognition[69]. However, our μROs

(ROs co-cultured with hiPSC-microglia cells) were not able to detect the AAV vectors using the same dose that is applied in clinical settings ($1x10^{12}$ vg). A potential explanation is that there could be transcriptomic deficiencies related to culture environment. Studies have demonstrated that cultured microglia cells suffer significant changes in their gene expression compared to resident microglia[129], and thus, this could be a critical drawback for the immunocompetency of the cells. It is also important to note that microglia cells can interact with blood vessels and infiltrating peripheral immune cells in the tissue[130]. However, in μROs this kind of interactions are missing, which could explain the lack of immune responses to AAV vectors *in vitro*.

Another possibility we raised is that a co-stimulus could trigger an enhanced innate immune response. It is known that the disease that makes gene therapy indicated and the surgical procedure of subretinal injections cause retinal damage *in vivo*[131]. When retinal detachment is induced (as in the subretinal injection), ATP is released to the extracellular space and may interact with the surrounding cells acting as inflammatory DAMPs[110]. This may lead to the induction of a different activation state in the cells that favors the recognition of another potential co-stimulus such as AAV vectors. Here, we tried to mimic the inflammatory state of the retina right after subretinal gene therapy injections *in vivo* by incubating ROs with ATP. ATP induced mild morphological changes and caspase-3 activation in ROs which is associated with apoptotic cell death. These phenomena have also been observed in experiments *in vivo*. Zacks et al. showed a disruption of the normal organization of the photoreceptors and the activation of caspase-3 in experimental models of retinal detachment[132]. However, our results showed no differences in terms of pro-inflammatory cytokines release upon PRR ligands and AAV stimulation between ROs and ROs suffering ATP-induced retinal damage.

The fact that none of our retinal models were able to detect AAV vectors leads us to speculate that either the retinal models do not adequately reflect the situation *in vivo* and further complexity (matrix, co-culture of RPE-ROs or vasculature) is required to measure an immune response to AAV, or that retinal cells might not be playing a relevant role in vector recognition and that other cells of the immune system (e.g. circulating pDCs) are responsible for doing so *in vivo*.

4.4. Influence of residual impurities on vector potency.

Aside from looking at the immunogenicity of different AAV vector lots in human pDCs, it was also important to see if residual DNA contaminants had an impact in viral transduction. Because AAV vectors did not transduce pDCs, another cell type was needed to investigate the effect of remaining DNA contaminants on viral transduction. We utilized HEK293T cells in our investigation because they have previously been used to test the transduction efficiency of AAV vectors[45,107,133]. Confirming previous findings[45], we observed that the efficacy of HEK293-derived vectors was higher than that of *Sf9*-derived ones. More notably, we also found that by removing extra-viral DNA from viral suspension significantly increased the transduction efficiency in HEK293-derived AAV8 vector lots. A non-significant rise in *Sf9*-derived AAV8 vector lots was also observed. Furthermore, we found that the immunogenicity of a given AAV8 lot, as assessed in pDCs, was not predictive of reduced vector potency.

This implies that AAV preparations generated from both HEK293 and *Sf9* production systems can contain a variety of extra-viral DNA components: some of them are only found in certain lots and elicit lot-specific inflammatory immune responses, while others reduce transduction efficacy across all lots. Although the mechanism by which extra-viral DNA impurities decrease AAV transduction efficiency is unclear, it can be assumed that the effects of extra-viral DNA are not immune-mediated as HEK293T cells have minimal expression of TLR and cytosolic DNA sensors[134,135]. Therefore, optimizing the manufacturing process is critical to avoiding the existence of residual contaminants in viral suspensions and, as a result, increasing potency while decreasing immunogenicity.

4.5. What HRF can tell us about the immune status of the retina after AAV-mediated subretinal injection

Many ocular diseases, including AMD, Stargardt's disease, retinitis pigmentosa, diabetic macular oedema, and uveitis, can manifest retinal HRF[136–140]. However, the development of HRF in eyes following AAV-mediated subretinal injection is poorly understood. To date, only three distinct clinical trials that used AAV have documented the presence of HRF[50,141,142]. In our study, the addition of clinical

grade AAV8-RK-hPDE6a vector to the surgical trauma of subretinal injection and its potential influence on the appearance of HRF as an indicator of immune cell activation/infiltration after subretinal injection in NHPs, was investigated.

We showed that the presence of HRF in sham-treated eyes was most likely attributable to the surgical damage associated with the subretinal injection, given the absence of viral particles in those eyes. In contrast, while the number of HRF dropped in the sham group over time, there was a significant increase of the number of HRF in the AAV8-treated eyes from the high dose group. This dynamic has also been observed in experimental studies where intravitreal injections of AAV2 resulted in a significant increase in the number of HRF in rodent retinas[70]. Previous research has also provided plausible explanations for the nature of HRF in the outer retinal layers in various retinal disorders, such as microglia activation[143] or immune cell infiltration[50,144]. In this study, although the virtual cross-sections of the SD-OCT B-scans could not be perfectly aligned with the fixed eyecup sections, we attempted to confirm whether HRF could be grossly correlated (in terms of appearance, location and frequency in sham- and AAV8-treated eyes) with microglia activation or infiltrating immune cells.

Once activated, microglia cells can quickly proliferate and move to the boundaries of the neural retina and RPE, where they release cytokines and chemokines[145]. We found that microglia cells were active around the retinotomy (where HRF were detected and the bleb originates) but inactive outside the bleb (no trauma, no AAV, and no HRF). In addition, the activation of microglia was more pronounced in the AAV8-treated eyes from the high dose group (where the HRF number increased) than in eyes without AAV vectors indicating the potential role of these cells in the recognition of the AAV vectors. Recently, Chandler et al. also suggested that retinal microglia cells were capable of detecting AAV vectors through activation of TLR9 and cGAS pathways, and recruitment of infiltrating immune cells and that; and that would be consistent with the increase of the microglia activation marker Iba-1 observed in the retina after delivery of AAV vectors[68]. Unfortunately, we found it difficult to identify HRF in layers other than the ONL (such as the outer retina, for example, where we obtained an ICC of <40%) which might simply be owing to increased reflectivity in other layers compared to the relatively ‘dark’ appearance of the ONL on SD-OCT, which provides significant contrast to HRF. However, this might imply that microglia

cells were present in the photoreceptor or RPE layers but were not identified as HRF on SD-OCT scans due to their reflectivity, as indicated by our histology results, and also in other inner retinal layers.

It is known that retinal microglia cells are able to recruit immune cells[146]. Interestingly, B and T cells were detectable in most of the AAV8-treated eyes from the high dose group but practically non-existent in the two other groups. Previous investigations have shown perivascular and subretinal infiltrates of B and T cells after AAV treatment[50,101,147], but their role in the tissue is unknown. In our study, the immune infiltrates were mostly found in NHPs whose HRF numbers did not diminish over time (high dose), indicating an ongoing adaptive immune response to AAV8.

As a whole, a dose-dependent immunological response to AAV8 can be assumed, and the HRF shown on SD-OCT might indicate migration of activated microglia into the retinal layers. Thus, increased or consistently high HRF on SD-OCT may indicate an ongoing immune response to AAV-mediated subretinal injection.

4.6. Strategies to prevent or treat immune responses to AAV vector preparations

AAV manufacturing is non-trivial. AAV vector preparations can include several production system-related impurities and most of them have unknown safety limits. To remove extra-viral DNA from the viral suspension, DNAse or Benzonase are routinely applied during the AAV-production process[148,149]. However, our human pDC model still sensed DNA impurities in this study, so that the incubation time with the nucleases could be optimized during production processes. In addition, non-viral DNA impurities have also been shown to be present in AAV vector particles[150]. This is made possible through a mechanism termed reverse packaging[151] which leads to infrequent (< 1%) packaging of plasmid DNA not intended to be in the vector. Once non-viral DNA is encapsidated in the capsid of the AAV vector, it is not possible to be extracted by conventional purification techniques as it is protected against nuclease treatment. Also, these encapsidated non-viral DNA impurities are not easy to remove since they closely resemble to viral DNA. Today, this remains a critical challenge to

enhance the purity of vector preparations and to prevent unwanted immune responses.

Recently, Chan et al. were able to engineer AAV vectors to evade innate immunity[115]. The reason of why these vectors are less immunogenic resides in their viral DNA. They incorporate a short DNA oligonucleotide that acts as antagonist for TLR9, the receptor that detects foreign DNA. Chan et al. also tested these vectors in mice and showed reduced innate immune responses and improved gene expression. However, while these AAV vectors delayed the immune response when they were tested in NHPs, it did not prevent it completely. This strategy, although still under development, could be the basis of preventing innate immune responses to both the viral DNA and the DNA impurities contained in either the vector suspension or encapsidated in the viral capsid.

Apart from trying to prevent the induction of immune responses to AAV vectors, immunosuppressive treatment options (e.g. steroids and other immunomodulatory drugs) are also a useful approach to counteract immune responses once the vectors have been recognised by the immune system. As discussed earlier, HRF could be used as marker of increased or sustained inflammation in the retina. It is known that the dynamic component of HRF can be modulated by immunosuppressive treatment. Nowadays, patients usually receive steroids before and after AAV-mediated gene therapy for some weeks followed by a tapering similar to the treatment regimen used in patients with uveitis[50,141,142]. However, there are cases in which HRF still appear. In previous investigations, appearance of HRF in the retina of patients following subretinal AAV injection was directly related to the gene therapy treatment[50,141,142] and led to transient regression of retinal function[142]. Nevertheless, additional treatment with oral steroids was enough to resolve HRF in all cases.

However, further investigations are required to understand a recently observed phenomenon in patients injected with *voretigene neparvovec* (Luxturna, AAV2-hRPE65v2). Gange et al. described a progressive perifoveal chorioretinal atrophy in 80% of the patients after gene therapy treatment[152]. Although the mechanism of this phenomenon is still unknown, the authors discussed several potential factors that might be involved, such as surgical delivery, ocular parameters or vector-related factors including direct toxicity and immune responses to the AAV vector.

4.7. Conclusions

- We have found that extra-viral DNA impurities can affect the immunogenicity and efficacy of AAV vector lots. This finding may thus have implications not only for the study of innate immune mechanisms involved in AAV vector recognition, but it will also open the door a better understanding of immune responses to AAV-mediated gene therapies and how to tailor the vector production process to generate more effective and safer AAV vectors.

- We showed that retinal models were able to sense PRR-ligands and induce a transient immune response. This indicates the presence of PRRs in both RPE and ROs. However, experimental AAV vectors were not able to elicit an immune response in those models.

- Moreover, we found that AAV-mediated subretinal injection induces sustained immunogenicity when applied at high dose. This was consistent with the increase of the number of HRF observed on SD-OCT images and the presence of activated microglia and B and T cells in the retinal sections of animals injected with a high dose of AAV8. This finding may help to improve the detection of immune responses after AAV-mediated subretinal gene therapy and improve patient recovery after treatment.

5. Summary

AAV vectors are one of the most promising tools in retinal gene therapy. However, accumulating evidence points to the relevance of AAV's immunogenicity in the clinical setting. In light of this, it is critical to have a better knowledge of the mechanisms underlying immunological responses to AAV vectors. In this PhD project we focused on the innate immune responses to AAV vector- and AAV production system-dependent factors that modulate vector immunogenicity in different *in vitro* models and its impact on AAV-mediated retinal gene therapy. In order to do that, a wide range of basic-research techniques, including biochemistry, molecular biology, microscopy, cell culture and organotypic culturing methodologies as well as preclinical-research analyses and interpretation of SD-OCT and FAF were performed. The main results achieved in this dissertation may be summarised as follows:

1. Experimental AAV8 and AAV2 vectors induced lot-specific innate immune responses in human pDCs which were neither specific to the capsid/vg ratio nor the production platform nor the manufacturer. Also, innate immune responses in pDCs were dependent on TLR9 signalling pathway, which could be reduced by pre-treatment with DNase. Furthermore, DNase treatment increased the transduction rate across all AAV8 vector lots in HEK293T cells. This suggests that both HEK293- and *Sf9*-cell derived preparations of experimental AAV vectors may contain a variety of extra-viral DNA impurities. Some of them cause lot-specific innate immune responses in human pDCs and impair transduction in HEK293T cells.

2. cgAAV lots without any known extra-viral DNA impurities but carrying different amounts of HCP were not able to elicit any innate immune response in neither pDCs nor in PMA-differentiated THP-1 cells. This may suggest that either the amount of HCP content found in our cgAAV vectors lots may not be high enough to induce immune responses in our *in vitro* models, or that HCP impurities are less immunogenic than extra-viral DNA impurities.

3. PRR ligands induced innate immune responses in ROs at early timepoints suggesting the presence of at least TLR2, 4 and 9. On the other hand, immunogenic AAV vectors that were sensed by pDCs were not able to elicit

innate immune responses in retinal models. However, AAV vectors were able to transduce ROs.

4. SD-OCT analysis of NHPs after clinical grade AAV-mediated subretinal gene therapy revealed that, although the surgical procedure by itself induced the appearance of HRF in the ONL, the number of HRF increased over time in the high dose AAV-treated eyes. In addition, immune cell infiltration was detected in retinal sections from AAV treated eyes. Interestingly, the cgAAV lot used in this preclinical study contained lower HCP levels than the cgAAV lots used in THP-1 and pDCs in which no immune response was detected. This implies that an immune response to AAV and not to extra-viral impurities, appears to be the most plausible explanation for the group of animals injected with the high dose, and the HRF observed on SD-OCT could represent activated microglia activation into outer retinal layers.

Finally, we showed that extra-viral DNA contaminants can affect the immunogenicity and potency of AAV vector lots. This has significant implications for the study of innate immune mechanisms involved in AAV vector recognition (basic research), the safety and efficacy of AAV-mediated gene therapy in animal models or human patients (translational and clinical research), and it also provides new information on how to adapt the AAV production process to generate safer and more effective gene therapy vectors (vector production methods).

6. German summary

AAV-Vektoren sind eines der vielversprechendsten Instrumente für die retinale Gentherapie. Allerdings häufen sich die Hinweise auf die Bedeutung der Immunogenität von AAV in der klinischen Praxis. Vor diesem Hintergrund ist es von entscheidender Bedeutung, die Mechanismen besser zu verstehen, die den immunologischen Reaktionen auf AAV-Vektoren zugrunde liegen. In diesem Promotionsprojekt konzentrierten wir uns auf die angeborenen Immunreaktionen auf AAV-Vektoren und vom AAV-Produktionssystem abhängige Faktoren, die die Immunogenität des Vektors in verschiedenen In-vitro-Modellen modulieren, sowie auf deren Auswirkungen auf die AAV-vermittelte retinale Gentherapie. Zu diesem Zweck wurde eine breite Palette von Techniken der Grundlagenforschung eingesetzt, darunter biochemische Verfahren, Techniken aus der Molekularbiologie, Mikroskopie, Zellkultur und organotypische Kultivierungsmethoden, sowie präklinische Forschungsanalysen in der Analyse und Interpretation von SD-OCT und FAF. Die wichtigsten Ergebnisse dieser Dissertation lassen sich wie folgt zusammenfassen:

1. Experimentelle AAV8- und AAV2-Vektoren induzierten chargenspezifische angeborene Immunantworten in humanen pDCs, die weder spezifisch für das Kapsid/vg-Verhältnis noch für die Produktionsplattform oder den Hersteller waren. Außerdem waren die angeborenen Immunreaktionen in pDCs vom TLR9-Signalweg abhängig. Diese Immunreaktion konnte durch eine Vorbehandlung mit DNase reduziert werden. Darüber hinaus erhöhte die DNase-Behandlung die Transduktionsrate bei allen AAV8-Vektorchargen in HEK293T-Zellen. Dies deutet darauf hin, dass sowohl aus HEK293- als auch aus Sf9-Zellen gewonnene Präparationen experimenteller AAV-Vektoren extravirale DNA enthalten, welche chargenspezifische angeborene Immunreaktionen in menschlichen pDCs verursachen und die Transduktion in HEK293T-Zellen beeinträchtigen können.

2. cgAAV-Chargen ohne bekannte extravirale DNA-Verunreinigungen, aber mit unterschiedlichen Mengen an HCP konnten weder in pDCs noch in PMA-differenzierten THP-1-Zellen eine angeborene Immunantwort auslösen. Dies könnte darauf hindeuten, dass entweder der HCP-Gehalt in unseren cgAAV-Vektoren nicht hoch genug ist, um in unseren In-vitro-Modellen eine

Immunantwort auszulösen, oder dass HCP-Verunreinigungen weniger immunogen sind als extra-virale DNA-Verunreinigungen.

3. PRR-Liganden induzierten zu frühen Zeitpunkten angeborene Immunreaktionen in ROs, was auf das Vorhandensein von zumindest TLR2, 4 und 9 hindeutet. Andererseits waren immunogene AAV-Vektoren, die von pDCs erkannt wurden, nicht in der Lage, angeborene Immunantworten in Netzhautmodellen auszulösen. AAV-Vektoren waren jedoch in der Lage, ROs zu transduzieren.

4. SD-OCT-Analysen von NHPs nach AAV-vermittelter subretinaler Gentherapie ergaben, dass, obwohl der chirurgische Eingriff an sich das Auftreten von HRF in der ONL induzierte, die Anzahl der HRF in den mit hoher AAV-Dosis behandelten Augen im Laufe der Zeit zunahm. Darüber hinaus wurde in Netzhautschnitten von AAV-behandelten Augen eine Infiltration von Immunzellen festgestellt. Interessanterweise enthielt die in dieser präklinischen Studie verwendete cgAAV-Charge niedrigere HCP-Werte als die in THP-1 und pDCs verwendeten cgAAV-Chargen, bei denen keine Immunreaktion festgestellt wurde. Dies bedeutet, dass eine Immunreaktion auf AAV und nicht auf extravirale Verunreinigungen die plausibelste Erklärung für die Gruppe der mit der hohen Dosis injizierten Tiere zu sein scheint, und die auf dem SD-OCT beobachtete HRF könnte eine Aktivierung der Mikroglia in den äußeren Netzhautschichten darstellen.

Schließlich konnten wir zeigen, dass extravirale DNA-Verunreinigungen die Immunogenität und Wirksamkeit von AAV-Vektorchargen beeinflussen können. Dies hat erhebliche Auswirkungen auf die Untersuchung der Mechanismen des angeborenen Immunsystems, die an der Erkennung von AAV-Vektoren beteiligt sind (Grundlagenforschung), auf die Sicherheit und Wirksamkeit der AAV-vermittelten Gentherapie in Tiermodellen oder bei menschlichen Patienten (translationale und klinische Forschung), und es liefert auch neue Informationen darüber, wie der AAV-Produktionsprozess angepasst werden kann, um sicherere und wirksamere Gentherapievektoren zu erzeugen (Vektorproduktions-methoden).

7. References

1. London, A., Benhar, I., and Schwartz, M. (2013). The retina as a window to the brain - From eye research to CNS disorders. Nat. Rev. Neurol. *9*, 44–53.
2. Gollisch, T., and Meister, M. (2010). Eye Smarter than Scientists Believed: Neural Computations in Circuits of the Retina. Neuron *65*, 150–164.
3. Wallace, V.A. (2011). Concise Review: Making a Retina—From the Building Blocks to Clinical Applications. Stem Cells *29*, 412–417.
4. Okunuki, Y., Mukai, R., Nakao, T., Tabor, S.J., Butovsky, O., Dana, R., Ksander, B.R., and Connor, K.M. (2019). Retinal microglia initiate neuroinflammation in ocular autoimmunity. Proc. Natl. Acad. Sci. *116*, 9989–9998.
5. Wilkinson, C., Hinton, D., Sadda, S., and Wiedemann, P. (2012). Retina E-Book: 3 Volume Set.
6. Purves, D., Augustine, G.J., Fitzpatrick, D., Katz, L.C., LaMantia, A.-S., McNamara, J.O., and Williams, S.M. (2001). Phototransduction.
7. McBee, J.K., Palczewski, K., Baehr, W., and Pepperberg, D.R. (2001). Confronting Complexity: the Interlink of Phototransduction and Retinoid Metabolism in the Vertebrate Retina. Prog. Retin. Eye Res. *20*, 469–529.
8. Strauss, O. (2005). The Retinal Pigment Epithelium in Visual Function. https://doi.org/10.1152/physrev.00021.2004 *85*, 845–881.
9. Huang, S.H., Pittler, S.J., Huang, X., Oliveira, L., Berson, E.L., and Dryja, T.P. (1995). Autosomal recessive retinitis pigmentosa caused by mutations in the α subunit of rod cGMP phosphodiesterase. Nat. Genet. *11*, 468–471.
10. den Hollander, A.I., Roepman, R., Koenekoop, R.K., and Cremers, F.P.M. (2008). Leber congenital amaurosis: Genes, proteins and disease mechanisms. Prog. Retin. Eye Res. *27*, 391–419.
11. Blacharski, P.A. (1988). Fundus flavimaculatus. Retin. dystrophies Degener., 135–159.
12. Sundaram, V., Moore, A.T., Ali, R.R., and Bainbridge, J.W. (2011). Retinal dystrophies and gene therapy. Eur. J. Pediatr. 2011 1715 *171*, 757–765.
13. Talib, M., and Boon, C.J.F. (2020). Retinal dystrophies and the road to treatment: Clinical requirements and considerations. Asia-Pacific J. Ophthalmol. *9*, 159–179.
14. McClements, M.E., and MacLaren, R.E. (2013). Gene therapy for retinal disease. Transl. Res. *161*, 241–254.
15. Bucher, K., Rodríguez-Bocanegra, E., Dauletbekov, D., and Fischer, M.D. (2020). Immune responses to retinal gene therapy using adeno-associated viral vectors – Implications for treatment success and safety. Prog. Retin. Eye Res., 100915.
16. Fuller-Carter, P.I., Basiri, H., Harvey, A.R., and Carvalho, L.S. (2020). Focused Update on AAV-Based Gene Therapy Clinical Trials for Inherited Retinal Degeneration. BioDrugs 2020 346 *34*, 763–781.
17. Utz, V.M., Coussa, R.G., Antaki, F., and Traboulsi, E.I. (2018). Gene therapy for RPE65-related retinal disease. https://doi.org/10.1080/13816810.2018.1533027 *39*, 671–677.

18. Atchison, R.W., Casto, B.C., and Hammon, W.M. (1965). Adenovirus-Associated Defective Virus Particles. Science (80-.). *149*, 754–755.
19. Cotmore, S.F., Agbandje-McKenna, M., Canuti, M., Chiorini, J.A., Eis-Hubinger, A.M., Hughes, J., Mietzsch, M., Modha, S., Ogliastro, M., Pénzes, J.J., et al. (2019). ICTV virus taxonomy profile: Parvoviridae. J. Gen. Virol. *100*, 367–368.
20. Kerr, J., Cotmore, S., and Bloom, M. (2005). Parvoviruses 1st ed. (Oxford University Press Inc).
21. Cataldi, M.P., and McCarty, D.M. (2013). Hairpin-end conformation of adeno-associated virus genome determines interactions with DNA-repair pathways. Gene Ther. *20*, 686–693.
22. Xiao, X., Xiao, W., Li, J., and Samulski, R.J. (1997). A novel 165-base-pair terminal repeat sequence is the sole cis requirement for the adeno-associated virus life cycle. J. Virol. *71*, 941–948.
23. Buller, R.M., and Rose, J.A. (1978). Characterization of adenovirus-associated virus-induced polypeptides in KB cells. J. Virol. *25*, 331–338.
24. Snijder, J., Waterbeemd, M. van de, Damoc, E., Denisov, E., Grinfeld, D., Bennett, A., Agbandje-McKenna, M., Makarov, A., and Heck, A.J.R. (2014). Defining the Stoichiometry and Cargo Load of Viral and Bacterial Nanoparticles by Orbitrap Mass Spectrometry. J. Am. Chem. Soc. *136*, 7295–7299.
25. Opie, S.R., Warrington, K.H., Agbandje-McKenna, M., Zolotukhin, S., and Muzyczka, N. (2003). Identification of Amino Acid Residues in the Capsid Proteins of Adeno-Associated Virus Type 2 That Contribute to Heparan Sulfate Proteoglycan Binding. J. Virol. *77*, 6995–7006.
26. Gurda, B.L., DiMattia, M.A., Miller, E.B., Bennett, A., McKenna, R., Weichert, W.S., Nelson, C.D., Chen, W. -j., Muzyczka, N., Olson, N.H., et al. (2013). Capsid Antibodies to Different Adeno-Associated Virus Serotypes Bind Common Regions. J. Virol. *87*, 9111–9124.
27. Akache, B., Grimm, D., Pandey, K., Yant, S.R., Xu, H., and Kay, M.A. (2006). The 37/67-Kilodalton Laminin Receptor Is a Receptor for Adeno-Associated Virus Serotypes 8, 2, 3, and 9. J. Virol. *80*, 9831–9836.
28. Summerford, C., and Samulski, R.J. (1998). Membrane-Associated Heparan Sulfate Proteoglycan Is a Receptor for Adeno-Associated Virus Type 2 Virions. J. Virol. *72*, 1438–1445.
29. Asokan, A., Hamra, J.B., Govindasamy, L., Agbandje-McKenna, M., and Samulski, R.J. (2006). Adeno-Associated Virus Type 2 Contains an Integrin 5 1 Binding Domain Essential for Viral Cell Entry. J. Virol. *80*, 8961–8969.
30. Kashiwakura, Y., Tamayose, K., Iwabuchi, K., Hirai, Y., Shimada, T., Matsumoto, K., Nakamura, T., Watanabe, M., Oshimi, K., and Daida, H. (2005). Hepatocyte Growth Factor Receptor Is a Coreceptor for Adeno-Associated Virus Type 2 Infection. J. Virol. *79*, 609–614.
31. Sonntag, F., Bleker, S., Leuchs, B., Fischer, R., and Kleinschmidt, J.A. (2006). Adeno-Associated Virus Type 2 Capsids with Externalized VP1/VP2 Trafficking Domains Are Generated prior to Passage through the Cytoplasm and Are Maintained until Uncoating Occurs in the Nucleus. J. Virol. *80*, 11040–11054.
32. Nicolson, S.C., and Samulski, R.J. (2014). Recombinant Adeno-Associated Virus Utilizes Host Cell Nuclear Import Machinery To Enter

the Nucleus. J. Virol. *88*, 4132–4144.
33. Kotin, R.M., Siniscalco, M., Samulski, R.J., Zhu, X.D., Hunter, L., Laughlin, C.A., McLaughlin, S., Muzyczka, N., Rocchi, M., and Berns, K.I. (1990). Site-specific integration by adeno-associated virus. Proc. Natl. Acad. Sci. *87*.
34. Pereira, D.J., McCarty, D.M., and Muzyczka, N. (1997). The adeno-associated virus (AAV) Rep protein acts as both a repressor and an activator to regulate AAV transcription during a productive infection. J. Virol. *71*, 1079–1088.
35. Sonntag, F., Schmidt, K., and Kleinschmidt, J.A. (2010). A viral assembly factor promotes AAV2 capsid formation in the nucleolus. Proc. Natl. Acad. Sci. *107*, 10220–10225.
36. Chang, L.S., Shi, Y., and Shenk, T. (1989). Adeno-associated virus P5 promoter contains an adenovirus E1A-inducible element and a binding site for the major late transcription factor. J. Virol. *63*, 3479–3488.
37. Timpe, J., Bevington, J., Casper, J., Dignam, J., and Trempe, J. (2005). Mechanisms of Adeno-Associated Virus Genome Encapsidation. Curr. Gene Ther. *5*, 273–284.
38. Lipinski, D.M., Thake, M., and MacLaren, R.E. (2013). Clinical applications of retinal gene therapy. Prog. Retin. Eye Res. *32*, 22–47.
39. Rabinowitz, J.E., Rolling, F., Li, C., Conrath, H., Xiao, W., Xiao, X., and Samulski, R.J. (2002). Cross-Packaging of a Single Adeno-Associated Virus (AAV) Type 2 Vector Genome into Multiple AAV Serotypes Enables Transduction with Broad Specificity. J. Virol. *76*, 791–801.
40. Wright, J.F. (2008). Manufacturing and characterizing AAV-based vectors for use in clinical studies. Gene Ther. *15*, 840–848.
41. Zolotukhin, S., Byrne, B.J., Mason, E., Zolotukhin, I., Potter, M., Chesnut, K., Summerford, C., Samulski, R.J., and Muzyczka, N. (1999). Recombinant adeno-associated virus purification using novel methods improves infectious titer and yield. Gene Ther. *6*, 973–985.
42. Snyder, R., and Francis, J. (2005). Adeno-Associated Viral Vectors for Clinical Gene Transfer Studies. Curr. Gene Ther. *5*, 311–321.
43. Urabe, M., Ding, C., and Kotin, R.M. (2002). Insect cells as a factory to produce adeno-associated virus type 2 vectors. Hum. Gene Ther. *13*, 1935–1943.
44. Wright, J.F. (2014). Product-related impurities in clinical-grade recombinant AAV vectors: Characterization and risk assessment. Biomedicines *2*, 80–97.
45. Rumachik, N.G., Malaker, S.A., Poweleit, N., Maynard, L.H., Adams, C.M., Leib, R.D., Cirolia, G., Thomas, D., Stamnes, S., Holt, K., et al. (2020). Methods Matter: Standard Production Platforms for Recombinant AAV Produce Chemically and Functionally Distinct Vectors. Mol. Ther. - Methods Clin. Dev. *18*, 98–118.
46. Ohmori, T. (2018). Advances in gene therapy for hemophilia: basis, current status, and future perspectives. Int. J. Hematol. 2018 1111 *111*, 31–41.
47. Gaj, T., Epstein, B.E., and Schaffer, D. V. (2016). Genome engineering using Adeno-associated virus: Basic and clinical research applications. Mol. Ther. *24*, 458–464.
48. Garita-Hernandez, M., Routet, F., Guibbal, L., Khabou, H., Toualbi, L.,

Riancho, L., Reichman, S., Duebel, J., Sahel, J.A., Goureau, O., et al. (2020). AAV-mediated gene delivery to 3D retinal organoids derived from human induced pluripotent stem cells. Int. J. Mol. Sci. *21*.
49. Russell, S., Bennett, J., Wellman, J.A., Chung, D.C., Yu, Z.-F., Tillman, A., Wittes, J., Pappas, J., Elci, O., McCague, S., et al. (2017). Efficacy and safety of voretigene neparvovec (AAV2-hRPE65v2) in patients with RPE65 -mediated inherited retinal dystrophy: a randomised, controlled, open-label, phase 3 trial. Lancet *390*, 849–860.
50. Reichel, F.F., Dauletbekov, D.L., Klein, R., Peters, T., Ochakovski, G.A., Seitz, I.P., Wilhelm, B., Ueffing, M., Biel, M., Wissinger, B., et al. (2017). AAV8 Can Induce Innate and Adaptive Immune Response in the Primate Eye. Mol. Ther. *25*, 2648–2660.
51. Boyd, R.F., Boye, S.L., Conlon, T.J., Erger, K.E., Sledge, D.G., Langohr, I.M., Hauswirth, W.W., Komáromy, A.M., Boye, S.E., Petersen-Jones, S.M., et al. (2016). Reduced retinal transduction and enhanced transgene-directed immunogenicity with intravitreal delivery of rAAV following posterior vitrectomy in dogs. Gene Ther. *23*, 548–556.
52. Rodríguez-Bocanegra, E., Wozar, F., Seitz, I.P., Reichel, F.F.L., Ochakovski, A., Bucher, K., Wilhelm, B., Bartz-Schmidt, K.U., Peters, T., and Fischer, M.D. (2021). Longitudinal Evaluation of Hyper-Reflective Foci in the Retina Following Subretinal Delivery of Adeno-Associated Virus in Non-Human Primates. Transl. Vis. Sci. Technol. *10*, 15.
53. Trinchieri, G., and Sher, A. (2007). Cooperation of Toll-like receptor signals in innate immune defence. Nat. Rev. Immunol. 2007 73 *7*, 179–190.
54. Michallet, M.C., Rota, G., Maslowski, K., and Guarda, G. (2013). Innate receptors for adaptive immunity. Curr. Opin. Microbiol. *16*, 296–302.
55. Kumar, M.V., Nagineni, C.N., Chin, M.S., Hooks, J.J., and Detrick, B. (2004). Innate immunity in the retina: Toll-like receptor (TLR) signaling in human retinal pigment epithelial cells. J. Neuroimmunol. *153*, 7–15.
56. Delneste, Y., Beauvillain, C., and Jeannin, P. (2007). Immunité naturelle - Structure et fonction des Toll-like receptors. médecine/sciences *23*, 67–74.
57. Willermain, F., Rosenbaum, J.T., Bodaghi, B., Rosenzweig, H.L., Childers, S., Behrend, T., Wildner, G., and Dick, A.D. (2012). Interplay between innate and adaptive immunity in the development of non-infectious uveitis. Prog. Retin. Eye Res. *31*, 182–194.
58. Griffith, J.W., Sokol, C.L., and Luster, A.D. (2014). Chemokines and Chemokine Receptors: Positioning Cells for Host Defense and Immunity. http://dx.doi.org/10.1146/annurev-immunol-032713-120145 *32*, 659–702.
59. Huang, X., and Yang, Y. (2010). Targeting the TLR9–MyD88 pathway in the regulation of adaptive immune responses. http://dx.doi.org/10.1517/14728222.2010.501333 *14*, 787–796.
60. Turner, M.D., Nedjai, B., Hurst, T., and Pennington, D.J. (2014). Cytokines and chemokines: At the crossroads of cell signalling and inflammatory disease. Biochim. Biophys. Acta - Mol. Cell Res. *1843*, 2563–2582.
61. Li, S., Gong, M., Zhao, F., Shao, J., Xie, Y., Zhang, Y., and Chang, H. (2018). Type I Interferons: Distinct Biological Activities and Current Applications for Viral Infection. Cell. Physiol. Biochem. *51*, 2377–2396.

62. Gao, W., Xiong, Y., Li, Q., and Yang, H. (2017). Inhibition of Toll-Like Receptor Signaling as a Promising Therapy for Inflammatory Diseases: A Journey from Molecular to Nano Therapeutics. Front. Physiol. *0*, 508.
63. Singh, K., Kant, S., Singh, V.K., Agrawal, N.K., Gupta, S.K., and Singh, K. (2014). Toll-like receptor 4 polymorphisms and their haplotypes modulate the risk of developing diabetic retinopathy in type 2 diabetes patients. Mol. Vis. *20*, 704.
64. Hösel, M., Broxtermann, M., Janicki, H., Esser, K., Arzberger, S., Hartmann, P., Gillen, S., Kleeff, J., Stabenow, D., Odenthal, M., et al. (2012). Toll-like receptor 2-mediated innate immune response in human nonparenchymal liver cells toward adeno-associated viral vectors. Hepatology *55*, 287–297.
65. Zhu, J., Huang, X., and Yang, Y. (2009). The TLR9-MyD88 pathway is critical for adaptive immune responses to adenoassociated virus gene therapy vectors in mice. J. Clin. Invest.
66. Shao, W., Earley, L.F., Chai, Z., Chen, X., Sun, J., He, T., Deng, M., Hirsch, M.L., Ting, J., Samulski, R.J., et al. (2018). Double-stranded RNA innate immune response activation from long-term adeno-associated virus vector transduction. JCI Insight *3*.
67. Chandler, L.C., Barnard, A.R., Caddy, S.L., Patrício, M.I., McClements, M.E., Fu, H., Rada, C., MacLaren, R.E., and Xue, K. (2019). Enhancement of Adeno-Associated Virus-Mediated Gene Therapy Using Hydroxychloroquine in Murine and Human Tissues. Mol. Ther. - Methods Clin. Dev. *14*, 77–89.
68. Chandler, L.C., Yusuf, I.H., McClements, M.E., Barnard, A.R., MacLaren, R.E., and Xue, K. (2020). Immunomodulatory Effects of Hydroxychloroquine and Chloroquine in Viral Infections and Their Potential Application in Retinal Gene Therapy. Int. J. Mol. Sci. 2020, Vol. 21, Page 4972 *21*, 4972.
69. Xiong, W., Wu, D.M., Xue, Y., Wang, S.K., Chung, M.J., Ji, X., Rana, P., Zhao, S.R., Mai, S., and Cepko, C.L. (2019). AAV cis-regulatory sequences are correlated with ocular toxicity. Proc. Natl. Acad. Sci. U. S. A. *116*, 5785–5794.
70. Liu, Y.F., Huang, S., Ng, T.K., Liang, J.J., Xu, Y., Chen, S.L., Xu, C., Zhang, M., Pang, C.P., and Cen, L.P. (2020). Longitudinal evaluation of immediate inflammatory responses after intravitreal AAV2 injection in rats by optical coherence tomography. Exp. Eye Res. *193*.
71. Kumar, S.R.P., Hoffman, B.E., Terhorst, C., de Jong, Y.P., and Herzog, R.W. (2017). The Balance between CD8+ T Cell-Mediated Clearance of AAV-Encoded Antigen in the Liver and Tolerance Is Dependent on the Vector Dose. Mol. Ther. *25*, 880–891.
72. Mays, L.E., Wang, L., Tenney, R., Bell, P., Nam, H.-J., Lin, J., Gurda, B., Van Vliet, K., Mikals, K., Agbandje-McKenna, M., et al. (2013). Mapping the Structural Determinants Responsible for Enhanced T Cell Activation to the Immunogenic Adeno-Associated Virus Capsid from Isolate Rhesus 32.33. J. Virol. *87*, 9473–9485.
73. Zaiss, A.K., Cotter, M.J., White, L.R., Clark, S.A., Wong, N.C.W., Holers, V.M., Bartlett, J.S., and Muruve, D.A. (2008). Complement Is an Essential Component of the Immune Response to Adeno-Associated Virus Vectors. J. Virol. *82*, 2727–2740.

74. Wang, L., Calcedo, R., Bell, P., Lin, J., Grant, R.L., Siegel, D.L., and Wilson, J.M. (2011). Impact of Pre-Existing Immunity on Gene Transfer to Nonhuman Primate Liver with Adeno-Associated Virus 8 Vectors. https://home.liebertpub.com/hum *22*, 1389–1401.
75. Park, E.K., Jung, H.S., Yang, H.I., Yoo, M.C., Kim, C., and Kim, K.S. (2007). Optimized THP-1 differentiation is required for the detection of responses to weak stimuli. Inflamm. Res. 2007 561 *56*, 45–50.
76. Schwende, H., Fitzke, E., Ambs, P., and Dieter, P. (1996). Differences in the state of differentiation of THP-1 cells induced by phorbol ester and 1,25-dihydroxyvitamin D3. J. Leukoc. Biol. *59*, 555–561.
77. Li, Z.H., Si, Y., Xu, G., Chen, X.M., Xiong, H., Lai, L., Zheng, Y.Q., and Zhang, Z.G. (2017). High-dose PMA with RANKL and MCSF induces THP-1 cell differentiation into human functional osteoclasts in vitro. Mol. Med. Rep. *16*, 8380–8384.
78. Ye, Y., Gaugler, B., Mohty, M., and Malard, F. (2020). Plasmacytoid dendritic cell biology and its role in immune-mediated diseases. Clin. Transl. Immunol. *9*.
79. Cho, C.H., Yoon, S.Y., Lee, C.K., Lim, C.S., and Cho, Y. (2015). Effect of interleukin-29 on interferon-α secretion by peripheral blood mononuclear cells. Cell J. *16*, 528–537.
80. Rossi, A. (2016). Intracellular fate of AAV particles in human Dendritic Cell and impact on Gene Transfer.
81. Rossi, A., Dupaty, L., Aillot, L., Zhang, L., Gallien, C., Hallek, M., Odenthal, M., Adriouch, S., Salvetti, A., and Büning, H. (2019). Vector uncoating limits adeno-associated viral vector-mediated transduction of human dendritic cells and vector immunogenicity. Sci. Reports 2019 91 *9*, 1–14.
82. Kuznetsova, A. V., Kurinov, A.M., and Aleksandrova, M.A. (2014). Cell Models to Study Regulation of Cell Transformation in Pathologies of Retinal Pigment Epithelium. J. Ophthalmol. *2014*.
83. Hansen, K.A., Sugino, I.K., Yagi, F., Wang, H., Tsukahara, I., Gullapalli, V., Bennett, J., and Zarbin, M.A. (2003). Adeno-Associated Virus Encoding Green Fluorescent Protein as a Label for Retinal Pigment Epithelium. Invest. Ophthalmol. Vis. Sci. *44*, 772–780.
84. Cereso, N., Pequignot, M.O., Robert, L., Becker, F., Luca, V. De, Nabholz, N., Rigau, V., Vos, J. De, Hamel, C.P., and Kalatzis, V. (2014). Proof of concept for AAV2/5-mediated gene therapy in iPSC-derived retinal pigment epithelium of a choroideremia patient. Mol. Ther. - Methods Clin. Dev. *1*, 14011.
85. Auricchio, A., Kobinger, G., Anand, V., Hildinger, M., O'Connor, E., Maguire, A.M., Wilson, J.M., and Bennett, J. (2001). Exchange of surface proteins impacts on viral vector cellular specificity and transduction characteristics: the retina as a model. Hum. Mol. Genet. *10*, 3075–3081.
86. Garita-Hernandez, M., Routet, F., Guibbal, L., Khabou, H., Toualbi, L., Riancho, L., Reichman, S., Duebel, J., Sahel, J.-A., Goureau, O., et al. (2020). AAV-Mediated Gene Delivery to 3D Retinal Organoids Derived from Human Induced Pluripotent Stem Cells. Int. J. Mol. Sci. 2020, Vol. 21, Page 994 *21*, 994.
87. Nagineni, C.N., Pardhasaradhi, K., Martins, M.C., Detrick, B., and Hooks, J.J. (1996). Mechanisms of interferon-induced inhibition of Toxoplasma

gondii replication in human retinal pigment epithelial cells. Infect. Immun. *64*, 4188–4196.
88. Achberger, K., Probst, C., Haderspeck, J.C., Bolz, S., Rogal, J., Chuchuy, J., Nikolova, M., Cora, V., Antkowiak, L., Haq, W., et al. (2019). Merging organoid and organ-on-a-chip technology to generate complex multi-layer tissue models in a human retina-on-a-chip platform. Elife *8*.
89. Cowan, C.S., Renner, M., De Gennaro, M., Gross-Scherf, B., Goldblum, D., Hou, Y., Munz, M., Rodrigues, T.M., Krol, J., Szikra, T., et al. (2020). Cell Types of the Human Retina and Its Organoids at Single-Cell Resolution. Cell *182*, 1623-1640.e34.
90. Gonzalez-CorderoAnai, GohDebbie, KruczekKamil, NaeemArifa, FernandoMilan, HolthausSophia-Martha, kleine, TakaakiMatsuki, I., B.J., KlocMagdalena, AgundezLeticia, et al. (2018). Assessment of AAV Vector Tropisms for Mouse and Human Pluripotent Stem Cell–Derived RPE and Photoreceptor Cells. https://home.liebertpub.com/hum *29*, 1124–1139.
91. Singh, P.K., and Kumar, A. (2015). Retinal Photoreceptor Expresses Toll-Like Receptors (TLRs) and Elicits Innate Responses Following TLR Ligand and Bacterial Challenge. PLoS One *10*, e0119541.
92. Sauter, M.M., Kolb, A.W., and Brandt, C.R. (2018). Toll-like receptors 4, 5, 6 and 7 are constitutively expressed in non-human primate retinal neurons. J. Neuroimmunol. *322*, 26–35.
93. Lin, X., Fang, D., Zhou, H., and Su, S.B. (2013). The expression of Toll-like receptors in murine Müller cells, the glial cells in retina. Neurol. Sci. *34*, 1339–46.
94. Yin, X., Mead, B.E., Safaee, H., Langer, R., Karp, J.M., and Levy, O. (2016). Engineering Stem Cell Organoids. Cell Stem Cell *18*, 25–38.
95. Zhong, X., Gutierrez, C., Xue, T., Hampton, C., Vergara, M.N., Cao, L.-H., Peters, A., Park, T.S., Zambidis, E.T., Meyer, J.S., et al. (2014). Generation of three-dimensional retinal tissue with functional photoreceptors from human iPSCs. Nat. Commun. 2014 51 *5*, 1–14.
96. Achberger, K., Haderspeck, J.C., Kleger, A., and Liebau, S. (2019). Stem cell-based retina models. Adv. Drug Deliv. Rev. *140*, 33–50.
97. Akhtar, T., Xie, H., Khan, M.I., Zhao, H., Bao, J., Zhang, M., and Xue, T. (2019). Accelerated photoreceptor differentiation of hiPSC-derived retinal organoids by contact co-culture with retinal pigment epithelium. Stem Cell Res. *39*, 101491.
98. Chichagova, V., Georgiou, M., Science, B.D.-… & V., and 2020, undefined Enhancing immune function of hiPSC-derived retinal organoids by incorporating microglial cells. iovs.arvojournals.org.
99. Wilsey, L.J., Reynaud, J., Cull, G., Burgoyne, C.F., and Fortune, B. (2016). Macular Structure and Function in Nonhuman Primate Experimental Glaucoma. Invest. Ophthalmol. Vis. Sci. *57*, 1892–1900.
100. Picaud, S., Dalkara, D., Marazova, K., Goureau, O., Roska, B., and Sahel, J.-A. (2019). The primate model for understanding and restoring vision. Proc. Natl. Acad. Sci. *116*, 26280–26287.
101. Ramachandran, P.S., Lee, V., Wei, Z., Song, J.Y., Casal, G., Cronin, T., Willett, K., Huckfeldt, R., Morgan, J.I.W., Aleman, T.S., et al. (2017). Evaluation of Dose and Safety of AAV7m8 and AAV8BP2 in the Non-Human Primate Retina. Hum. Gene Ther. *28*, 154–167.
102. Ye, G., Budzynski, E., Sonnentag, P., Nork, T.M., Miller, P.E., Sharma,

A.K., Ver Hoeve, J.N., Smith, L.M., Arndt, T., Calcedo, R., et al. (2016). Safety and Biodistribution Evaluation in Cynomolgus Macaques of rAAV2tYF-PR1.7-hCNGB3, a Recombinant AAV Vector for Treatment of Achromatopsia. Hum. Gene Ther. Clin. Dev. *27*, 37–48.
103. YeGuo-jie, M., K., ZeissCaroline, CalcedoRoberto, D., H., L., K., A., S., IwabeSimone, A., C., W., H., et al. (2017). Safety and Efficacy of AAV5 Vectors Expressing Human or Canine CNGB3 in CNGB3-Mutant Dogs. https://home.liebertpub.com/humc *28*, 197–207.
104. Moshiri, A., Chen, R., Kim, S., Harris, R.A., Li, Y., Raveendran, M., Davis, S., Liang, Q., Pomerantz, O., Wang, J., et al. (2019). A nonhuman primate model of inherited retinal disease. J. Clin. Invest. *129*, 863–874.
105. Bowdish, D. (2011). Maintenance & culture of THP-1 cells.
106. Timmers, A.M., Newmark, J.A., Turunen, H.T., Farivar, T., Liu, J., Song, C., Ye, G.J., Pennock, S., Gaskin, C., Knop, D.R., et al. (2020). Ocular Inflammatory Response to Intravitreal Injection of Adeno-Associated Virus Vector: Relative Contribution of Genome and Capsid. Hum. Gene Ther. *31*, 80–89.
107. Ran, G., Chen, X., Xie, Y., Zheng, Q., Xie, J., Yu, C., Pittman, N., Qi, S., Yu, F.X., Agbandje-McKenna, M., et al. (2020). Site-Directed Mutagenesis Improves the Transduction Efficiency of Capsid Library-Derived Recombinant AAV Vectors. Mol. Ther. - Methods Clin. Dev. *17*, 545–555.
108. Ebihara, N., Chen, L., Tokura, T., Ushio, H., Iwatsu, M., and Murakami, A. (2007). Distinct functions between toll-like receptors 3 and 9 in retinal pigment epithelial cells. Ophthalmic Res. *39*, 155–163.
109. Lin, X., Fang, D., Zhou, H., and Su, S.B. (2012). The expression of Toll-like receptors in murine Müller cells, the glial cells in retina. Neurol. Sci. 2012 348 *34*, 1339–1346.
110. Paustian, C., Taylor, P., Johnson, T., Xu, M., Ramirez, N., Rosenthal, K.S., Shu, S., Cohen, P.A., Czerniecki, B.J., and Koski, G.K. (2013). Extracellular ATP and Toll-Like Receptor 2 Agonists Trigger in Human Monocytes an Activation Program That Favors T Helper 17. PLoS One *8*, e54804.
111. E, M., T, T., E, V., E, P., R, P., and L, F. (2021). OCT Hyperreflective Retinal Foci in Diabetic Retinopathy: A Semi-Automatic Detection Comparative Study. Front. Immunol. *12*, 613051–613051.
112. Tannenbaum, J., and Bennett, B.T. (2015). Russell and Burch's 3Rs then and now: The need for clarity in definition and purpose. J. Am. Assoc. Lab. Anim. Sci. *54*, 120–132.
113. Yamada, H., Gursel, I., Takeshita, F., Conover, J., Ishii, K.J., Gursel, M., Takeshita, S., and Klinman, D.M. (2002). Effect of Suppressive DNA on CpG-Induced Immune Activation. J. Immunol. *169*, 5590–5594.
114. Zhang, P., Yang, C. lin, Liu, R. tao, Li, H., Zhang, M., Zhang, N., Yue, L. tao, Wang, C. cong, Dou, Y. chun, and Duan, R. sheng (2018). Toll-like receptor 9 antagonist suppresses humoral immunity in experimental autoimmune myasthenia gravis. Mol. Immunol. *94*, 200–208.
115. Chan, Y.K., Wang, S.K., Chu, C.J., Copland, D.A., Letizia, A.J., Verdera, H.C., Chiang, J.J., Sethi, M., Wang, M.K., Neidermyer, W.J., et al. (2021). Engineering adeno-associated viral vectors to evade innate immune and inflammatory responses. Sci. Transl. Med. *13*.

116. Bayik, D., Gursel, I., and Klinman, D.M. (2016). Structure, mechanism and therapeutic utility of immunosuppressive oligonucleotides. Pharmacol. Res. *105*, 216–225.
117. Ohto, U., Ishida, H., Shibata, T., Sato, R., Miyake, K., and Shimizu, T. (2018). Toll-like Receptor 9 Contains Two DNA Binding Sites that Function Cooperatively to Promote Receptor Dimerization and Activation. Immunity *48*, 649-658.e4.
118. Lecomte, E., Tournaire, B., Cogné, B., Dupont, J.-B., Lindenbaum, P., Martin-Fontaine, M., Broucque, F., Robin, C., Hebben, M., Merten, O.-W., et al. (2015). Advanced Characterization of DNA Molecules in rAAV Vector Preparations by Single-stranded Virus Next-generation Sequencing. Mol. Ther. - Nucleic Acids *4*, e260.
119. Penaud-Budloo, M., Lecomte, E., Guy-Duché, A., Saleun, S., Roulet, A., Lopez-Roques, C., Tournaire, B., Cogné, B., Léger, A., Blouin, V., et al. (2017). Accurate Identification and Quantification of DNA Species by Next-Generation Sequencing in Adeno-Associated Viral Vectors Produced in Insect Cells. Hum. Gene Ther. Methods *28*, 148–162.
120. Radford, A.D., Chapman, D., Dixon, L., Chantrey, J., Darby, A.C., and Hall, N. (2012). Application of next-generation sequencing technologies in virology. J. Gen. Virol. *93*, 1853–1868.
121. Penaud-Budloo, M., François, A., Clément, N., and Ayuso, E. (2018). Pharmacology of Recombinant Adeno-associated Virus Production. Mol. Ther. - Methods Clin. Dev. *8*, 166–180.
122. Jawa, V., Joubert, M.K., Zhang, Q., Deshpande, M., Hapuarachchi, S., Hall, M.P., and Flynn, G.C. (2016). Evaluating Immunogenicity Risk Due to Host Cell Protein Impurities in Antibody-Based Biotherapeutics. AAPS J. 2016 186 *18*, 1439–1452.
123. Agency, E.M. (2012). Assessment report: Glybera.
124. Denard, J., Beley, C., Kotin, R., Lai-Kuen, R., Blot, S., Leh, H., Asokan, A., Samulski, R.J., Moullier, P., Voit, T., et al. (2012). Human Galectin 3 Binding Protein Interacts with Recombinant Adeno-Associated Virus Type 6. J. Virol. *86*, 6620–6631.
125. Denard, J., Rouillon, J., Leger, T., Garcia, C., Lambert, M.P., Griffith, G., Jenny, C., Camadro, J.-M., Garcia, L., and Svinartchouk, F. (2018). AAV-8 and AAV-9 Vectors Cooperate with Serum Proteins Differently Than AAV-1 and AAV-6. Mol. Ther. - Methods Clin. Dev. *10*, 291–302.
126. Deierborg, T., and Burguillos, M.A. (2015). A new “sweet” ligand for Toll-like receptor 4. Oncotarget *6*, 19928.
127. Ubanako, P., Xelwa, N., and Ntwasa, M. (2019). LPS induces inflammatory chemokines via TLR-4 signalling and enhances the Warburg Effect in THP-1 cells. PLoS One *14*, e0222614.
128. Lannes, N., Eppler, E., Etemad, S., Yotovski, P., Filgueira, L., Lannes, N., Eppler, E., Etemad, S., Yotovski, P., and Filgueira, L. (2017). Microglia at center stage: a comprehensive review about the versatile and unique residential macrophages of the central nervous system. Oncotarget *8*, 114393–114413.
129. Gosselin, D., Skola, D., Coufal, N.G., Holtman, I.R., Schlachetzki, J.C.M., Sajti, E., Jaeger, B.N., O’Connor, C., Fitzpatrick, C., Pasillas, M.P., et al. (2017). An environment-dependent transcriptional network specifies human microglia identity. Science (80-.). *356*, 1248–1259.

130. Hasselmann, J., and Blurton-Jones, M. (2020). Human iPSC-derived microglia: A growing toolset to study the brain's innate immune cells. Glia *68*, 721–739.
131. Nakazawa, T., Matsubara, A., Noda, K., Hisatomi, T., She, H., Skondra, D., Miyahara, S., Sobrin, L., Thomas, K.L., Chen, D., et al. (2006). Characterization of cytokine responses to retinal detachment in rats. undefined.
132. Zacks, D.N., Hänninen, V., Pantcheva, M., Ezra, E., Grosskreutz, C., and Miller, J.W. (2003). Caspase Activation in an Experimental Model of Retinal Detachment. Invest. Ophthalmol. Vis. Sci. *44*, 1262–1267.
133. Liu, Y., Joo, K.I., and Wang, P. (2013). Endocytic processing of adeno-associated virus type 8 vectors for transduction of target cells. Gene Ther. *20*, 308–317.
134. Hornung, V., Rothenfusser, S., Britsch, S., Krug, A., Jahrsdörfer, B., Giese, T., Endres, S., and Hartmann, G. (2002). Quantitative Expression of Toll-Like Receptor 1–10 mRNA in Cellular Subsets of Human Peripheral Blood Mononuclear Cells and Sensitivity to CpG Oligodeoxynucleotides. J. Immunol. *168*, 4531–4537.
135. Wiser, C., Kim, B., Vincent, J., and Ascano, M. (2020). Small molecule inhibition of human cGAS reduces total cGAMP output and cytokine expression in cells. Sci. Rep. *10*.
136. Vujosevic, S., Bini, S., Torresin, T., Berton, M., Midena, G., Parrozzani, R., Martini, F., Pucci, P., Daniele, A.R., Cavarzeran, F., et al. (2017). HYPERREFLECTIVE RETINAL SPOTS IN NORMAL AND DIABETIC EYES: B-Scan and En Face Spectral Domain Optical Coherence Tomography Evaluation. Retina *37*, 1092–1103.
137. Kon, Y., Iida, T., Maruko, I., and Saito, M. (2008). The optical coherence tomography-ophthalmoscope for examination of central serous chorioretinopathy with precipitates. Retina *28*, 864–869.
138. Turgut, B., and Yildirim, H. (2015). The Causes of Hyperreflective Dots in Optical Coherence Tomography Excluding Diabetic Macular Edema and Retinal Venous Occlusion§§. Open Ophthalmol. J. *9*, 36–40.
139. Berasategui, B., Fonollosa, A., Artaraz, J., Ruiz-Arruza, I., Ríos, J., Matas, J., Llorenç, V., Diaz-Valle, D., Sastre-Ibañez, M., Arriola-Villalobos, P., et al. (2018). Behavior of hyperreflective foci in non-infectious uveitic macular edema, a 12-month follow-up prospective study. In BMC Ophthalmology (BioMed Central Ltd.).
140. Hanumunthadu, D., Rasheed, M., Goud, A., Gupta, A., Vupparaboina, K., and Chhablani, J. (2020). Choroidal hyper-reflective foci and vascularity in retinal dystrophy. Indian J. Ophthalmol. *68*, 130–133.
141. Dimopoulos, I.S., Hoang, S.C., Radziwon, A., Binczyk, N.M., Seabra, M.C., MacLaren, R.E., Somani, R., Tennant, M.T.S., and MacDonald, I.M. (2018). Two-Year Results After AAV2-Mediated Gene Therapy for Choroideremia: The Alberta Experience. Am. J. Ophthalmol. *193*, 130–142.
142. Cehajic-Kapetanovic, J., Xue, K., Martinez-Fernandez de la Camara, C., Nanda, A., Davies, A., Wood, L.J., Salvetti, A.P., Fischer, M.D., Aylward, J.W., Barnard, A.R., et al. (2020). Initial results from a first-in-human gene therapy trial on X-linked retinitis pigmentosa caused by mutations in RPGR. Nat. Med. *26*, 354–359.

143. Fletcher, E.L. (2020). Contribution of microglia and monocytes to the development and progression of age related macular degeneration. Ophthalmic Physiol. Opt. *40*, 128–139.
144. Bolz, M., Schmidt-Erfurth, U., Deak, G., Mylonas, G., Kriechbaum, K., and Scholda, C. (2009). Optical Coherence Tomographic Hyperreflective Foci. A Morphologic Sign of Lipid Extravasation in Diabetic Macular Edema. Ophthalmology *116*, 914–920.
145. Langmann, T. (2007). Microglia activation in retinal degeneration. J. Leukoc. Biol. *81*, 1345–1351.
146. Li, L., Eter, N., and Heiduschka, P. (2015). The microglia in healthy and diseased retina. Exp. Eye Res. *136*, 116–130.
147. Boyd, R.F., Boye, S.L., Conlon, T.J., Erger, K.E., Sledge, D.G., Langohr, I.M., Hauswirth, W.W., Komáromy, A.M., Boye, S.E., Petersen-Jones, S.M., et al. (2016). Reduced retinal transduction and enhanced transgene-directed immunogenicity with intravitreal delivery of rAAV following posterior vitrectomy in dogs. Gene Ther. *23*, 548–556.
148. Arden, E., and Metzger, J. (2016). Inexpensive, serotype-independent protocol for native and bioengineered recombinant adeno-associated virus purification. J. Biol. Methods *3*, e38.
149. Grieger, J.C., Choi, V.W., and Samulski, R.J. (2006). Production and characterization of adeno-associated viral vectors. Nat. Protoc. *1*, 1412–1428.
150. Nony, P., Chadeuf, G., Tessier, J., Moullier, P., and Salvetti, A. (2003). Evidence for Packaging of rep-cap Sequences into Adeno-Associated Virus (AAV) Type 2 Capsids in the Absence of Inverted Terminal Repeats: a Model for Generation of rep -Positive AAV Particles . J. Virol. *77*, 776–781.
151. Tai, P.W.L., Xie, J., Fong, K., Seetin, M., Heiner, C., Su, Q., Weiand, M., Wilmot, D., Zapp, M.L., and Gao, G. (2018). Adeno-associated Virus Genome Population Sequencing Achieves Full Vector Genome Resolution and Reveals Human-Vector Chimeras. Mol. Ther. - Methods Clin. Dev. *9*, 130–141.
152. Gange, W.S., Sisk, R.A., Besirli, C.G., Lee, T.C., Havunjian, M., Schwartz, H., Borchert, M., Sengillo, J.D., Mendoza, C., Berrocal, A.M., et al. (2021). Perifoveal Chorioretinal Atrophy after Subretinal Voretigene Neparvovec-rzyl for RPE65-Mediated Leber Congenital Amaurosis. Ophthalmol. Retin.

8. Declaration of own contribution

The study was conceived by Dominik Fischer.

The work was carried out mainly at the Institute for Ophthalmic Research in Tübingen and also at the Centre for Regenerative Therapies (CRTD) in Dresden, and at the Institute of Neuroanatomy and Developmental Biology (INDB) in Tübingen, always under the supervision of Dominik Fischer.

All experiments were performed and analysed by me (Eduardo David Rodríguez Bocanegra) with the support of my group (Dominik Fischer, Kirsten Bucher, Oksana Faul, Fabian Wozar and Immanuel Seitz), except:

- Flow cytometry assays which were performed with the assistance of Kirsten Bucher (Fischer's group) and Kristin Bieber from the Core Facility Flow Cytometry, Tübingen.
- Droplet digital PCR assays which were performed with the assistance of Luise Luib from the Department of Paediatrics, Tübingen.
- Linear mixed effect models were performed and analysed with the assistance of Torsten Strasser from the Institute for Ophthalmic Research, Tübingen.
- Multiplex-assays which were performed with the assistance of Dorothea Siegel-Axel in the German Centre for Diabetes Research, Tübingen.

I certify that I have written this thesis and all papers derived from it in which I am first author after guidance by Dominik Fischer and Kirsten Bucher and that I have not used any sources other than those indicated by me.

Tübingen, the

Eduardo David Rodríguez Bocanegra

9. Publications

- **Rodríguez-Bocanegra E**, Wozar F, Seitz I, Ochakovski A, Bucher K, Wilhelm B, Bartz-Schmidt KU, Peters T, Fischer MD and the RD-CURE Consortium, (2021) Longitudinal evaluation of hyperreflective foci in the retina following subretinal delivery of adeno-associated virus in non-human primates. *Translational Vision Science & Technology*, 10 (6):15.

- Bucher K, **Rodríguez-Bocanegra E**, Dauletbekov D, Fischer MD, (2020) Immune responses to AAV-mediated retinal gene therapy – implications for treatment success and safety. *Progress in Retinal and Eye Research*, 100915.

10. Acknowledgements

This doctoral thesis has been a great challenge both personally and academically. It has been three years of hard work full of ups and downs, failed attempts, waiting times and stress, along with the occasional moment of transient excitement and joy. But the fact that I am writing these lines means that I am nearing the end, an end that would not have been possible without the support and help of all those who have been there during these years.

First of all, I would like to express my sincere thanks and gratitude to my mentor, Dominik, for giving me the opportunity to carry out my PhD project in his research group in Tübingen, as well as for his continuous support and guidance, which made the completion of this thesis possible. In this context, I would also like to thank my lab colleagues Kirsten and Oksana for their knowledge, advice and their human and professional qualities over the years - my apologies for not having learnt sufficiently your language!

I would also like to thank Soumaya, Alice and Alexandra. You have been a fundamental pillar during my stay in Germany. Thank you for supporting me during these years, for your "group therapy" sessions and for the good times we had in and out of work.

I would also like to thank my friends and colleagues in Spain. To my *sevillanos* Pablo, María, Edu; to my *catalanes* Isa, Marc, María, Anna; to my *canarios* Adri, Diego, Borja, Pedro; to my *sœur,* Lina; and to many others who have given me so much during these last years and who are still there despite the distance.

I would also like to thank my parents Sacramento and Sebastian, and my brother Juan, for their continuous support and care, for being with me in each of my decisions, and for being the reason for who I am today. To my family, for whom I profess great admiration and love, thank you for being my sanctuary and for giving me strength at all times.

Finally, the biggest and warmest thank you goes to you, Vic. Thank you for your dedication, your craziness, your patience and your advice. Thank you for always being there and for believing in me. All this would not have been possible without you. *Merci*.